

A Thesis for the Degree of Ph.D. in Engineering

Self-standing *in vitro* multi-layered blood vessel
model reproducing immunological tissue
deformation

February 2022

Graduate School of Science and Technology
Keio University

Shun Itai

Thesis Abstract

The biochemical reaction of blood vessels plays an essential role in immune response and various diseases. Thus, the construction of *in vitro* blood vessel models mimicking *in vivo* tissues has a high demand for biomedical research and pharmacokinetic testing. However, previously reported models were difficult to mimic the biomedical deformation reaction of blood vessels faithfully because the tissues were fixed to rigid scaffolds. The insufficient flexibility of the scaffold disturbs the contraction of blood vessels and leads to the deviation of the behaviors with *in vivo* tissues.

Here, the author proposes a flexibly deformable self-standing multi-layered blood vessel model to reproduce an inflammatory mediator-induced deformation reaction. A self-standing collagen tube enables the tissue to deform flexibly in biochemical reactions and achieves contraction and relaxation at tissue and cell levels. Also, by constructing a circumferentially aligned smooth muscle layer outside the endothelial layer, the immunological deformation reaction on both endothelial and smooth muscle layers is reproduced.

Chapter 1 introduces the background, the purpose, and the concept of this research.

Chapter 2 describes the fabrication of a double-layered collagen hydrogel tube device. First, a simple repeated molding process precisely and easily fabricates the double-layered collagen tube device. After forming an endothelial layer inside the tube, the tissue formation is confirmed by evaluating the barrier function of the endothelium. Also, the cellular response of the endothelial cells is confirmed by co-culturing with vascular pericytes.

Chapter 3 reproduces the immunological deformation reaction of the endothelium layer with the tube device forming an endothelial layer inside. Exposure to histamine (an inflammatory mediator of allergy) confirms contraction and recovery reactions at both tissue and cell levels. Also, the ability of the device for drug testing is evaluated by exposing olopatadine hydrochloride (an anti-histamine material) and histamine. In addition, the traction force of the endothelial cells under reaction is calculated by numerical analysis with the finite element method.

Chapter 4 proposes a blood vessel model with a circumferentially aligned smooth muscle layer. By rolling up an axially aligned smooth muscle fiber, a circumferential alignment is easily formed in a collagen tube (Rolling up maturation molding (RuM-M) method). The alignment is evaluated by live imaging of actin. An immunological deformation reaction of the co-cultured endothelium and smooth muscle is reproduced with co-cultured tissue under exposure to histamine.

Chapter 5 concludes this dissertation by discussing the value of the proposed self-standing *in vitro* multi-layered blood vessel model and the prospective.

Table of Contents

Table of Contents	i
CHAPTER 1. GENERAL INTRODUCTION	1
1.1 OBJECTIVES IN THIS DISSERTATION.....	1
1.2 FUNDAMENTAL FEATURES OF BLOOD VESSELS.....	2
1.3 STRUCTURE OF BLOOD VESSELS.....	2
1.3.1 Arteries and Veins.....	2
1.3.2 Capillary vessels.....	4
1.4 IMMUNOLOGICAL DEFORMATION REACTION ON BLOOD VESSELS.....	5
1.5 NEEDS FOR <i>IN VITRO</i> BLOOD VESSEL MODELS.....	6
1.6 PREVIOUS RESEARCHES.....	8
1.6.1 Technologies for vascular tissue engineering.....	8
1.6.2 Issues on previous monolayer models.....	13
1.6.3 Issues on previous multi-layered models.....	14
1.7 OBJECTIVES & APPROACHES.....	16
1.8 DISSERTATION OUTLINE.....	18
CHAPTER 2. Double-layered perfusable polymer hydrogel tube device	21
2.1 INTRODUCTION.....	21
2.2 FABRICATION PROCEDURE.....	21
2.2.1 Preparation of solutions & molds.....	21
2.2.2 Fabrication of the tube device.....	22
2.2.3 Cell seeding.....	26
2.3 EXPERIMENTAL METHOD.....	27
2.3.1 Fluorescent staining and observation.....	27
2.3.2 Perfusion set up.....	27
2.3.3 Permeability experiment set up.....	28
2.3.4 Image analysis and calculation of the permeability coefficient.....	29

Table of Contents

2.4	FABRICATION RESULTS	30
2.4.1	Design of collagen tube devices	30
2.4.2	Single-layer tube fabrication	31
2.4.3	Double-layer tube fabrication.....	33
2.5	CELL CULTURE RESULTS	35
2.5.1	Static culture.....	35
2.5.2	Immunostaining analysis.....	35
2.5.3	Permeability evaluation.....	36
2.5.4	Co-culture demonstration	39
2.5.5	Stability of the tube device under cell culture	39
2.6	CONCLUSION	40
CHAPTER 3. Immunological deformation reaction of ECs on flexible collagen tube devices		43
3.1	INTRODUCTION	43
3.2	EXPERIMENTAL METHOD	44
3.2.1	Fabrication method of the vascularized tube device	44
3.2.2	Chemicals used for immunological reaction experiments.....	45
3.2.3	Fluorescent staining and observation	47
3.2.4	Set up for perfusion experiments.....	47
3.2.5	Image analysis	47
3.2.6	Numerical analysis	48
3.2.7	Statistical analysis	48
3.3	THEORETICAL CALCULATION OF THE SHEAR STRESS ON ECS	48
3.4	MEDIATOR-INDUCED DEFORMATION REACTION RESULTS	50
3.4.1	Deformation during vascularization of the tube device.....	50
3.4.2	Mediator-induced deformation reaction on the vessel model.....	50
3.4.3	Difference of the behavior of vessels against various concentrations of histamine	53
3.4.4	Numerical analysis of cell traction force.....	56
3.4.5	Drug testing demonstration with anti-histamine	58
3.5	CONCLUSION	60
CHAPTER 4. Circumferentially aligned and immunologically deformable SMCs by RuM-M		

method	61
4.1 INTRODUCTION	61
4.2 FABRICATION METHOD	62
4.2.1 Design of the mold	62
4.2.2 Preparation of cell suspended pre-gel solution	64
4.2.3 Formation method of the SMC fiber	65
4.2.4 Fabrication of the SMC layer embedded blood vessel model	67
4.3 EXPERIMENTAL METHOD	68
4.3.1 Florescent staining and observation	68
4.3.2 Image analysis of the SMC alignment	68
4.3.3 Contraction demonstration with histamine	70
4.4 FABRICATION RESULTS	71
4.4.1 Formation results of the HUASMC fiber	71
4.4.2 Evaluation of the axial alignment of the SMC fibers	71
4.4.3 Fabrication results of the SMC layer embedded collagen tube	74
4.4.4 Construction of blood vessel model by co-culture with HUVECs	77
4.4.5 Immunological contraction demonstration of the SMC layer	77
4.4.6 Immunological deformation on the blood vessel model	80
4.5 CONCLUSION	83
CHAPTER 5. Concluding remarks	85
5.1 CONCLUSION	85
5.2 FUTURE PERSPECTIVES	86
Acknowledgments	89
References	91
Appendix A License numbers	104
Appendix B Antibody list	105

CHAPTER 1.

GENERAL INTRODUCTION

1.1 Objectives in this dissertation

The objective of this dissertation is to fabricate an *in vitro* blood vessel model reproducing immunological deformation reaction.

Since the biochemical reaction of blood vessels plays an essential role in immune response or various diseases, *in vitro* blood vessel models mimicking *in vivo* tissues have high demand as a platform for biomedical research and pharmacokinetic testing. However, previously reported models were difficult to mimic the biomedical reaction faithfully because of the lack of implementation of the tissue deformation. The insufficient flexibility of the scaffold due to the fixation to rigid surfaces disturbs the tissue contraction and leads to the deviation of the behaviors or functions with *in vivo* tissues.

In this research, a flexibly deformable multi-layered collagen tube device is proposed to reproduce an inflammatory mediator-induced deformation reaction of blood vessels. A self-standing collagen tube enables the flexible deformation of the tissue in biochemical reactions and achieves contraction and relaxation at tissue and cell levels. Also, the smooth muscle layer in the device shows circumferential alignment by rolling up the maturation molding method (RuM-M method), resulting in the reproduction of the immunological deformation reaction on both endothelial and smooth muscle layers.

1.2 Fundamental features of blood vessels

A blood vessel is one of the most vital organs in the human body since no organs can work properly without a supply of blood^[1]. Each one minute, about 5 to 6 L of blood is delivered to the entire body through a hundred thousand kilometer-length of blood vessels^[2]. Transportation is the most common function of blood vessels. Still, not just as a transport pipe, blood vessels play many crucial roles in maintaining a healthy body^[3]. Functions of blood vessels can be roughly divided into five headings as follows:

- (i) Deliver oxygen and nutrients to each tissue.
- (ii) Drain carbon dioxide and metabolic wastes from tissue to lung and excretion organs, respectively.
- (iii) Transport water, electrolytes, and hormones to all over the body.
- (iv) Interact with immune tissue and regulate immune reaction.
- (v) Regulate the temperature of the body.

Since all these roles are closely involved in tissue homeostasis, maintenance of the blood vessel directly relates to the health of the body^[4]. Blood vessels have roughly three classifications in the structure and function to perform these roles: arteries, veins, and capillary vessels^[5] (Figure 1.1).

1.3 Structure of blood vessels

1.3.1 Arteries and Veins

As you know, arteries mainly transport blood from the heart to tissues, while veins return blood to the heart^[6]. The wall of these vessels has a three-layered structure of tunica intima, tunica media, and tunica adventitia^[7].

Tunica intima consists of a monolayer structure of flat endothelial cells (ECs). The endothelial layer forms connection bands to prevent the big molecules from diffusing outside the vessels^[8]. Also, ECs play an essential role in regulating vascular contraction, angiogenesis, permeability, and hemostasis^[9].

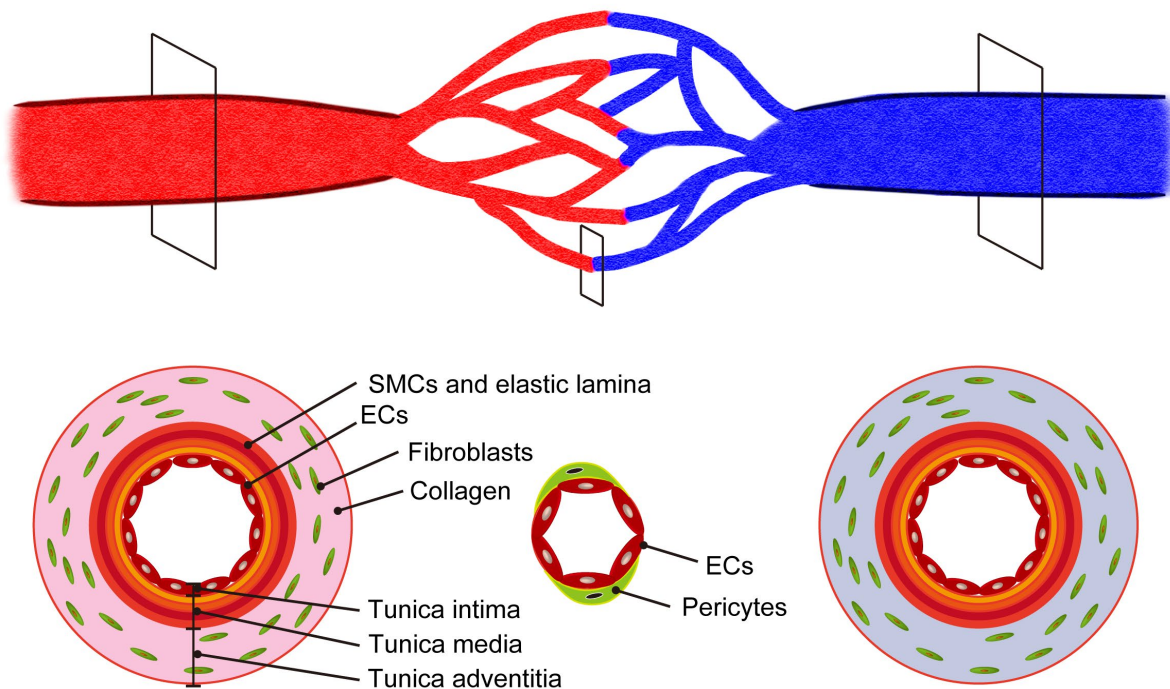


Figure 1.1 The structure of blood vessels. Blood vessels can be classified into three types: arteries, veins, and capillary vessels. Arteries and veins are composed of three layers: tunica intima (ECs and a basal membrane), tunica media (SMCs and elastic laminas), and tunica adventitia (fibroblasts and a connective tissue). Capillary vessels are composed of ECs and a basal membrane surrounded with pericytes.

Tunica media is mainly composed of smooth muscle cells (SMCs) and elastic laminas^[10]. The fenestrated internal elastic lamina and external elastic lamina composed of elastin separate the tunica media from tunica intima and tunica adventitia, respectively^[11]. SMCs are aligned circumferentially surrounded with the extracellular matrix as a helical shape to change the diameter of the blood vessels^{[12]–[14]}. The contraction and relaxation of the SMCs directly link to vasoconstriction and vasodilatation, resulting in control of the blood flow mass^[15].

Tunica adventitia contains fibroblasts and collagen connective tissue. Nerves and capillary vessels pass through in the layer to regulate the contraction behavior of SMCs and supply nutrients to the wall of blood vessels^[16].

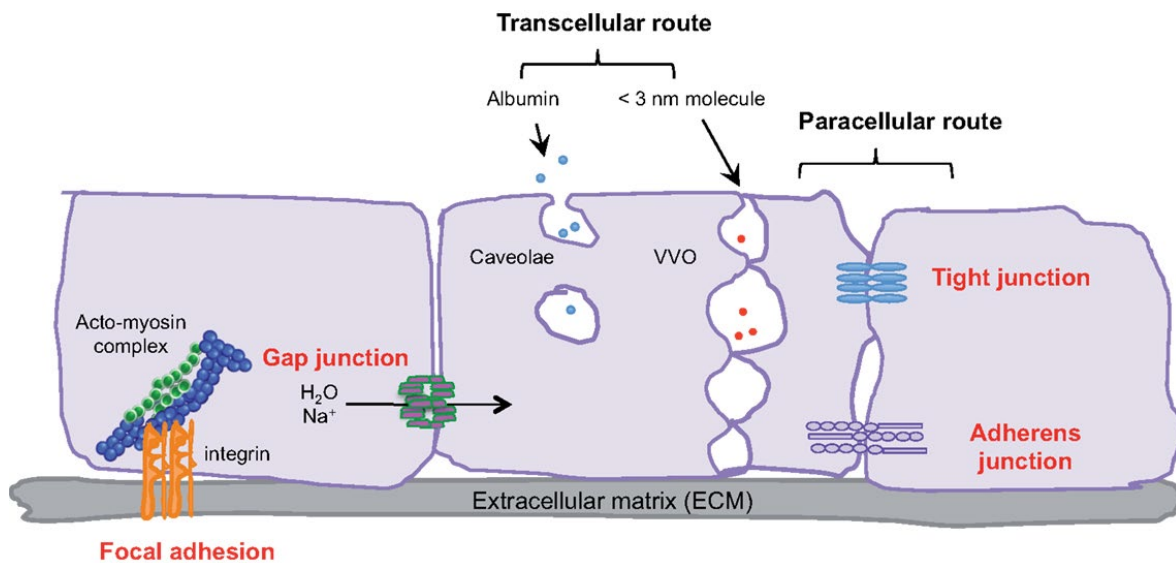


Figure 1.2 The permeation regulation by blood vessels. Transcellular pathway exchanges molecular substances such as oxygen, nutrients, water and wastes. Paracellular pathway is used for immune cells like leukocytes to penetrate into tissue, regulated by adherence and tight junctions^[19]. (Copyright: © 2013 Azzi, Hebda and Gavard., *Frontiers in Oncology*, <http://creativecommons.org/licenses/by/4.0/>)

1.3.2 Capillary vessels

Capillary vessels are formed with a monolayer of ECs surrounded by a basement membrane and some pericytes^[17]. Oxygen, carbon dioxide, metabolic molecules, and immune cells transported through blood vessels are exchanged with each tissue through the surface of the ECs of capillary vessels. ECs regulate permeability to control the concentration of these elements in tissues^[18]. The permeation pathways between a blood vessel and the perivascular tissue are distinguished into two types: a transcellular pathway and a paracellular pathway^[19] (Figure 1.2).

Molecular substances such as oxygen, nutrients, water, and wastes are exchanged by endocytosis of ECs, called transcellular pathways^[20]. Ingested pharmaceuticals are also delivered to the tissue through the transcellular pathway^[21].

Besides, immune cells like leukocytes pass through the junctions of ECs, called paracellular pathways, since immune cells have excess volume to be allowed

endocytosing.^[22] The permeability at the paracellular pathway is regulated by adherence junctions (AJs) and tight junctions (TJs) of ECs.^[23] These junctions are strengthened and weakened by various factors to control the permeability^[24].

1.4 Immunological deformation reaction on blood vessels

In immune reactions, mediator-triggered deformation reactions are key factors to induce the reactions.

At capillary vessels, the permeability of the blood vessels is increased with the contractile deformation of ECs under immunological reaction^[25] (Figure 1.3). As mentioned in subsection 1.3.2, AJs and TJs normally keep the permeability low by strong protein connection. Still, when ECs are exposed to inflammatory mediators such as histamine or thrombin, these junctions are relaxed by the contractile force that occurs on ECs.^{[26], [27]} Then, the relaxation induced by contractile force induces permeability increase to deliver immune cells into tissues.^{[28]–[30]} This is one of the immune reactions to maintain our healthy body.^[31] However, if the balance of inflammatory mediators collapses by disorder or wrong reaction of the body like allergy, the relaxation triggers excess inflammations^[32]. Therefore, the permeate regulation by deformation of ECs strongly relates to the maintenance of our body, including medicinal effects and inflammatory diseases^[33].

At artery and veins, both ECs and SMCs react to inflammatory mediators. The mediators cause direct and indirect reactions on SMCs and induce contraction and relaxation, respectively^[34]. Indirect relaxation of SMCs results in vasodilatation, which is the major phenomenon mediated through immune reactions^[35] (Figure 1.4). Since the vasodilatation is induced by relaxation factors released from ECs, the response is called endothelium dependent vasodilatation (EDV)^[36]. When ECs are exposed to inflammatory mediators, nitric oxide (NO), prostacyclin (PGI₂), and other relaxation factors are released and get into SMCs^[37]. It leads to vasodilatation by the relaxation of the SMCs, resulting in fever, red flare, or eczema as immune phenomena medically^{[38]–[40]}.

 Introduction

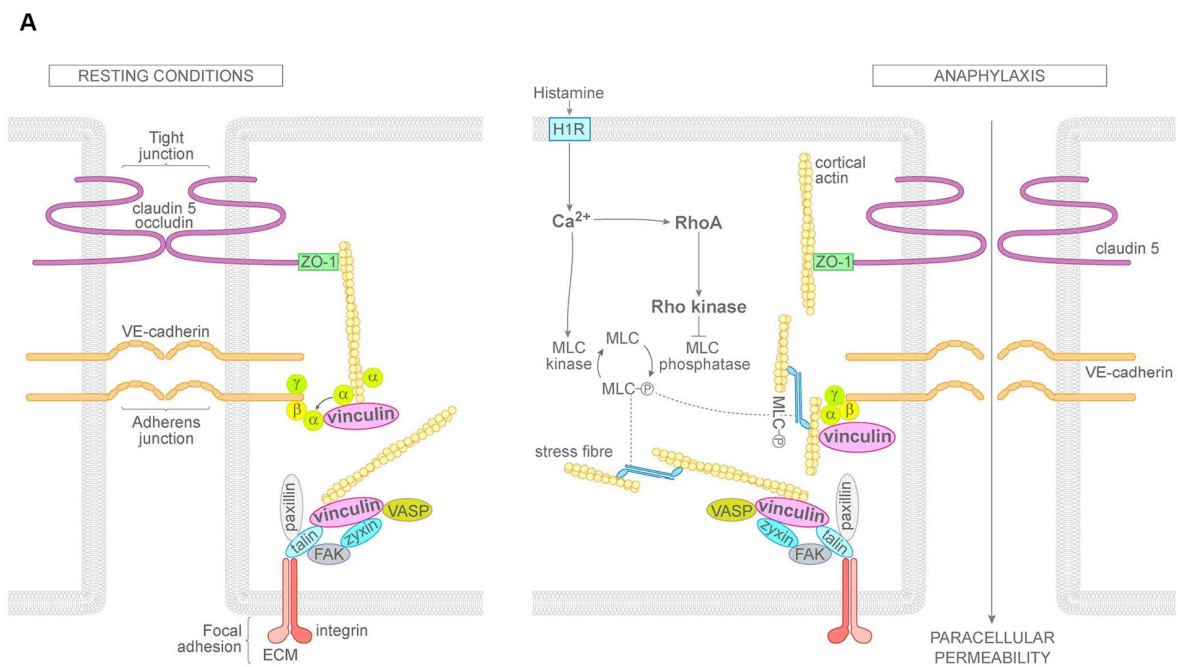


Figure 1.3 The mechanism of immunological reaction of ECs at capillary vessels. Exposed histamine induces a rapid increase of cytoplasmic Ca^{2+} , resulting in the enhancement of the tension on adherence junctions and tight junctions which leads to the increase of permeability. ^[25] (Copyright: © 2018 Kugelmann, D., Rotkopf, L.T., Radeva, M.Y. et al., *Sci Rep*, <http://creativecommons.org/licenses/by/4.0/>.)

1.5 Needs for *in vitro* blood vessel models

Disorders of the blood vessel directly link to the crisis of our life since blood vessels are responsible for many critical functions, as introduced in sections 1.2 to 1.4. For example, cardiovascular diseases (CVD) are the most common cause of mortality worldwide and account for about one-third of death^{[41], [42]}. However, despite the majority of the vascular-related diseases, the mechanism is not well unraveled on lots of diseases^[43]. Thus, detailed analysis on the diseases has been longed to develop effective treatment and medicine.

The most common pre-clinical testing method at present is animal testing^[44]. The main reason to use animals is the high reliability that comes from the similarity between animal bodies and humans^[45]. Animal testing is useful but raises ethical issues around the

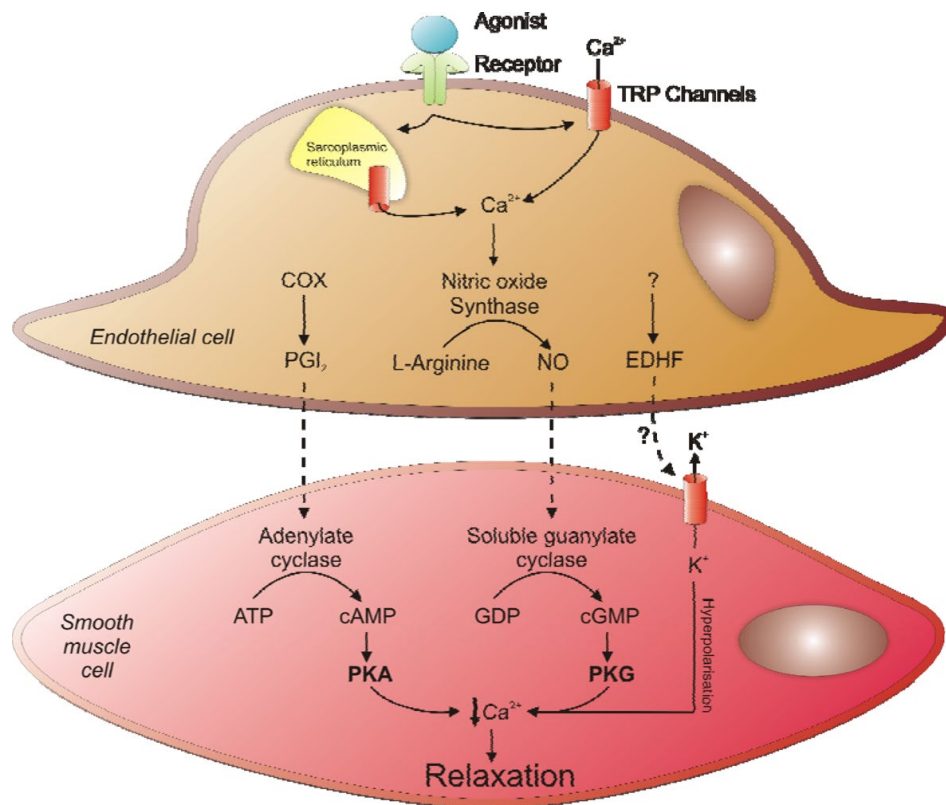


Figure 1.4 The mechanism of indirect immunological deformation reaction of SMCs. ECs exposed to inflammatory mediators release nitric oxide (NO), prostacyclin (PGI₂), and other relaxation factors. The factors get into SMCs lead the vasodilatation by the relaxation of the SMCs.^[35] (Copyright: © 2010 Joseph R. Burgoyne and Philip Eaton; Sensors, <http://creativecommons.org/licenses/by/3.0/>)

exposure of animals to cruel experiences^{[46][47]}. In addition, animal testing requires researchers to be highly skilled and is both expensive and time-consuming^[48]. As an alternative to animal testing, researchers have previously suggested to use simple disease models, such as tissue slices. However, such models did not sufficiently mimic complicated *in vivo* tissues^[49], because human bodies react to chemicals not only in the target cell or tissue but also in the surrounding structures mutually^{[50][51]}.

Among disease models, *in vitro* perfusable 3D tissue models are expected to mimic *in vivo* tissues^[52]. Due to the high demand for vessel models for biomedical research and

pharmacokinetic testing, vascular tissue engineering has been one of the most popular research fields in biomedical engineering over the past couple of decades^{[53], [54]}. A blood vessel tissue model comprises cells, scaffolds, and vascular-like structures^[55]. *In vitro* vessel models have lots of advantages for investigating tissues since blood vessels formed *in vitro* can control various factors, including cell types and concentrations, the material of scaffold, the diffusion gradient of the material, and mechanical stimulation^{[56], [57]}. The mechanisms behind how these factors affect the construction, maintenance, and biochemical reactions of vascular tissues still remain unknown^[58]. Therefore, the *in vitro* blood vessel models are required for analytical experiments on the behavior of cells and tissues, in which the parameters listed above can be varied^[59].

1.6 Previous researches

1.6.1 Technologies for vascular tissue engineering

Over the past decades, a variety of fabrication techniques have been developed to construct *in vitro* vascular models such as soft lithography, 3D printing, laser processing, electrospinning, self-organization, and decellularization.

Soft lithography

Soft lithography is a fabrication technique of soft material with micro structures by transferring a mold pattern. Polydimethylsiloxane (PDMS), a silicone elastomer, was traditionally used as a material for the scaffold. The molds for the PDMS lithography were fabricated by photolithography^{[60], [61]} or mechanical milling^[62], and microchannel structures were fabricated as a vascular lumen (Figure 1.5(a,b)). These devices achieved the formation of an endothelial layer, along with a microfluidic perfusion system. However, the difference in the material and stiffness of the scaffold with *in vivo* extracellular matrix (ECM) tissue resulted in the morphology deviation of cells. Thus, fabrication of microchannel with ECM-

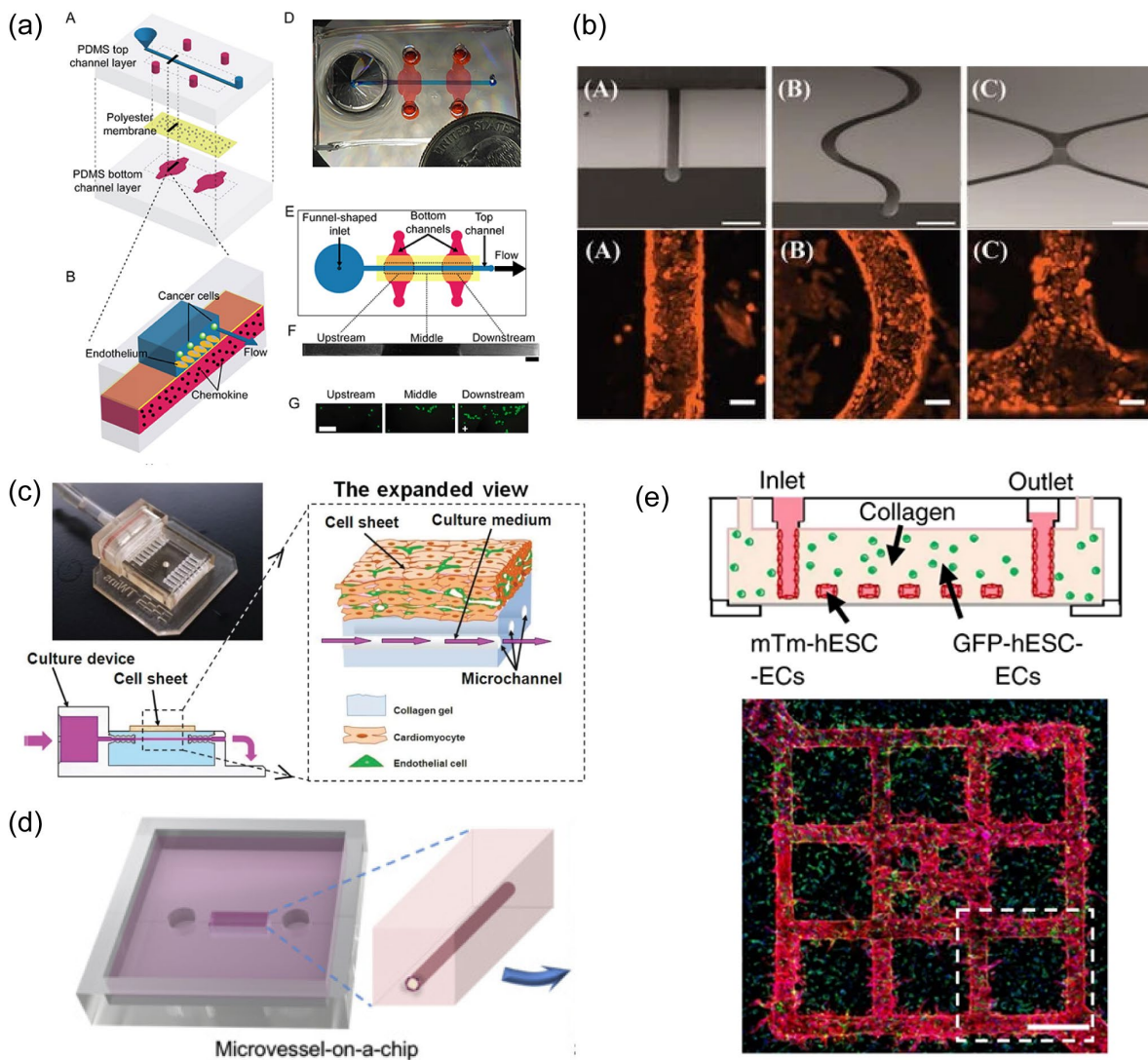


Figure 1.5 *In vitro* blood vessel models fabricated by soft lithography. (a) A multi-layered PDMS microchannel for a co-culture of Endothelium and cancer cells^[61]. (Copyright: © 2009 J. Song et al.; *PLOS ONE*, <http://creativecommons.org/licenses/by/3.0/>) (b) A circular PDMS microchannel for an endothelial layer fabrication^[60]. (Copyright: © 2013 *Bioprocess Biosyst. Eng.*, License number is shown in Appendix A) (c) A collagen vascularized microchannel co-culturing with a myocardial cell sheet^[63]. (Copyright: © 2013 K. Sakaguchi et al.; *Sci. Rep.*, <http://creativecommons.org/licenses/by/3.0/>) (d) A collagen microvessel model on a PDMS chip^[65]. (Copyright: © 2017 J. Pauty. et al., *EBioMedicine* <http://creativecommons.org/licenses/by/4.0/>) (e) A bulk seeded collagen-based microchannel model fabricated by injection molding and soft lithography techniques^[64]. (Copyright: © 2019 Redd, M.A., Zeinstra, N., Qin, W. et al., *Nat Commun* <http://creativecommons.org/licenses/by/4.0/>)

based material, such as collagen, has been pursued recently^{[7], [63]–[65]} (Figure 1.5(c-e)). Since the ECM hydrogel is quite soft for manufacturing, most researchers cover the ECM with stiffer material like PDMS^[66]. Other than photolithography and mechanical milling, simple molding with steel, glass, and acrylic molds were proposed to form a cylindrical lumen structure. These methods achieved a simple fabrication of ECM-based blood vessel models with a perfusion system.

3D printing

Along with the rapid development of the 3D printing technique, blood vessel models fabricated with the printing of molds, scaffolds, or even cells have been reported^[3].

As a mold, polycaprolactone (PCL), polyethylene glycol (PEG), carbohydrate glass, and other various materials were used^{[67], [68]}. By using these water-soluble materials as a sacrificial layer, the models achieved to construct complicated hollow structures for vascular networks^{[69], [70]} (Figure 1.6(a,b)). Also, these materials are used as a scaffold by directly printing a cylindrical structure.

3D Printing of cells, which is called 3D bioprinting, is another notable technique^[71]. By printing the mixture of cells and hydrogel (bioink), a well-defined spatial pattern of a blood vessel can be formed. The flexibility of the vascular network design helps the construction of *in vivo*-like structure. Some co-culture models of SMCs and ECs have been reported by bioprinting and achieved co-axial structure of these cells^{[72], [73]} (Figure 1.6(c,d)).

Laser processing

Laser processing is another approach to construct a luminal structure of blood vessels. Laser energy is used to degrade the desired position of the bulk of hydrogel for vascular network formation^[74]. A wide range of materials from ECM to synthetic polymers are known to be cut by laser. The high resolution of laser has benefits on fabricating the controlled structure of blood vessels, and many vascular models such as capillary scale model^[75] (Figure 1.7(a)) and mimicking model of *in vitro* architecture^[76] (Figure 1.7(b)) have been reported.

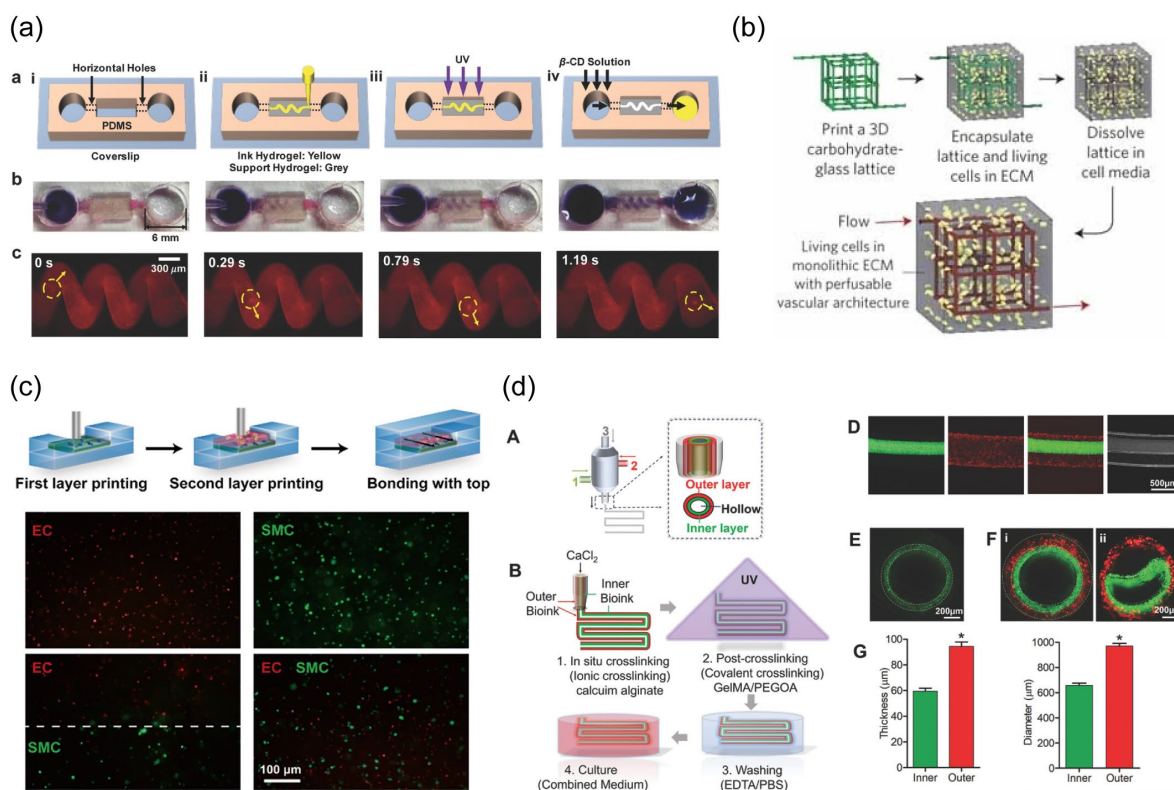


Figure 1.6 *In vitro* blood vessel models fabricated by 3D printing. (All license numbers are shown in Appendix A) (a) A spring-shaped microchannel fabricated by printing of hydrogel into supporting hydrogel^[69] (Copyright: © 2018 *Adv. Funct. Mater.*). (b) A vascular network fabricated by sacrificial molding process of carbohydrate in ECM^[70] (Copyright: © 2012 *Nat. Mater.*). (c) Bioprinting of SMCs and ECs to form a bi-layer co-culture model^[72] (Copyright: © 2018 *Biomed. Microdevices*). (d) 3D co-axial bioprinting for SMC and EC layer formation with a lumen structure inside^[73] (Copyright: © 2018 *Adv. Mater.*).

Electrospinning

Electrospinning is used to construct a tubular structure mimicking blood vessels^[77]. Nano-scale polymer fibers are firstly formed from dissolved polymer solutions by an electrical force. Then, a rotating mandrel is used to collect the fibers to form a tubular scaffold^[78]. Various synthetic polymers or a mixture of synthetic and natural polymers can be used as a material^{[79], [80]}, and achieved the culture of vascular cells on the scaffold^[81] (Figure 1.7(c,d)).

Introduction

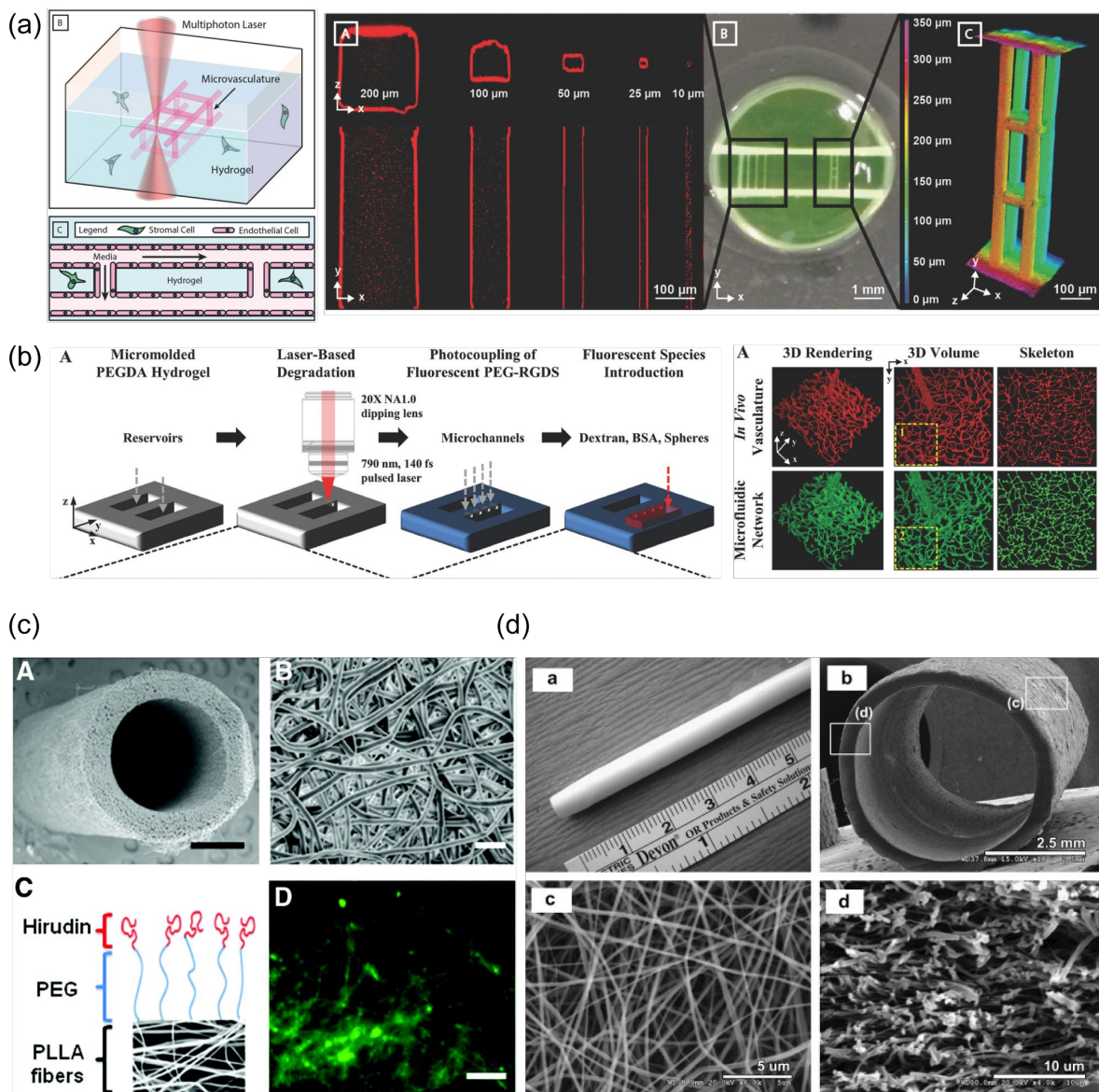


Figure 1.7 *In vitro* blood vessel models fabricated by laser processing and electrospinning. (All license numbers are shown in Appendix A) (a) A capillary vessel model by a microvessels fabricated by laser processing of hydrogel^[75] (Copyright: © 2018 *Adv. Mater.*). (b) A 3D vascular-derived microfluidic network by laser processing generated from an *in vivo* vascular network image^[76] (Copyright: © 2018 *Adv. Healthc. Mater.*). (c) A PLLA microfibrillar vascular model by electrospinning^[79] (Copyright: © 2018 *Arterioscler. Thromb. Vasc. Biol.*). (d) A PCL/collagen scaffold for a vascular model by electrospinning^[80] (Copyright: © 2018 *Adv. Drug Deliv. Rev.*).

Other techniques

Besides the development of constructing techniques for lumen structure, a self-organization-based fabrication of blood vessels has been attracting attention recently. ECs have a function to form a vascular network by themselves. The mechanism is called vasculogenesis (An initial formation process of a blood vessel during embryonic development) and angiogenesis (A growth of new capillaries from existing blood vessels). By inducing these functions with microfluidic devices, perfusable vascular networks were self-organized^[82] (Figure 1.8(a)). The interesting point of the method is the uncontrolled complicated network formation like *in vivo*^[83].

On the other hand, some researchers use the real *in vivo* structure of blood vessels as a scaffold for *in vitro* model, known as the decellularization method. Decellularized tissue has a vacant vascular tree network with remained ECM as a scaffold^[84]. By seeding cultured cells to the blank tissue, a vascular network with seeded ECs was easily formed^{[85], [86]} (Figure 1.8(b)).

1.6.2 Issues on previous monolayer models

In vitro vessel models are roughly classified into monolayer models (mimicking capillary vessels) and multi-layered models (mimicking arteries and veins).

As capillary models, many monolayer models have been fabricated by various techniques as described in section 1.6.1 (Figure 1.5(a-e), Figure 1.6(a,b), Figure 1.7(a,b), Figure 1.8(a,b)). Especially in terms of the ability as a platform for biomedical research, shape-controlled vessel structures serve as a quantitatively analytical vessel model (Figure 1.5(a-e), Figure 1.6(a,b), Figure 1.7(a)).

However, these models could not reproduce the immunological contractile reaction of blood vessels correctly because the models are not capable of implementing macro-scale tissue deformation. When the permeability of the vessels *in vivo* increases by the contractile force that occurs on ECs, the force also induces macro-scale deformation of vessel tissues.

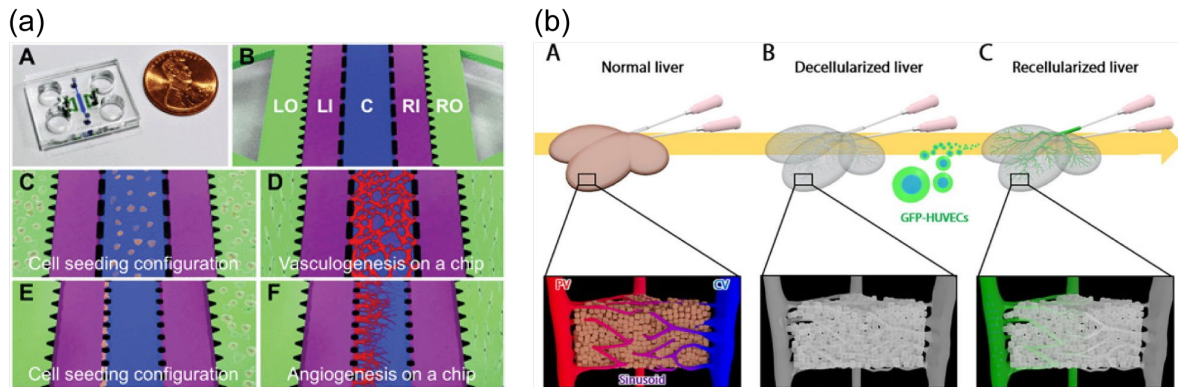


Figure 1.8 *In vitro* blood vessel models fabricated by self-organization and decellularization. (All license numbers are shown in Appendix A) (a) Self-organization of a vascular network on a chip by inducing vasculogenesis and angiogenesis^[82] (Copyright: © 2018 *Lab Chip*). (b) Vascular network formation in a decellularized liver tissue as a scaffold for ECs^[85] (Copyright: © 2018 *Acta Biomater.*).

The tissue deformation relieves the stress between ECs, resulting in the maintenance of the junctions between cells even though the property of TJs gets weaker^[87]. On the contrary, ECs on fixed or rigid scaffolds, often used in previous models, detach each other entirely through the biochemical reaction because the materials stiffer than native tissues obstruct the tissue deformation. This difference of junction conditions leads to the difference in the control mechanism of permeability with *in vivo*^{[88], [89]}. To achieve the reproduction of immunological contraction reactions *in vitro*, both macro-scale (tissue level) and micro-scale (cellular level) deformation are indispensable.

Since the immunological reaction of blood vessels plays a crucial role in medical effects or inflammatory diseases, as mentioned in section 1.4, contraction behavior on permeation regulation has to be precisely reproduced on *in vitro* capillary vessel models. Thus, a flexibly deformable model is required to be developed as a biomedically applicable platform for pharmacokinetic and biomedical researches^[90].

1.6.3 Issues on previous multi-layered models

About artery and vein models, simple co-culture models of ECs and SMCs were

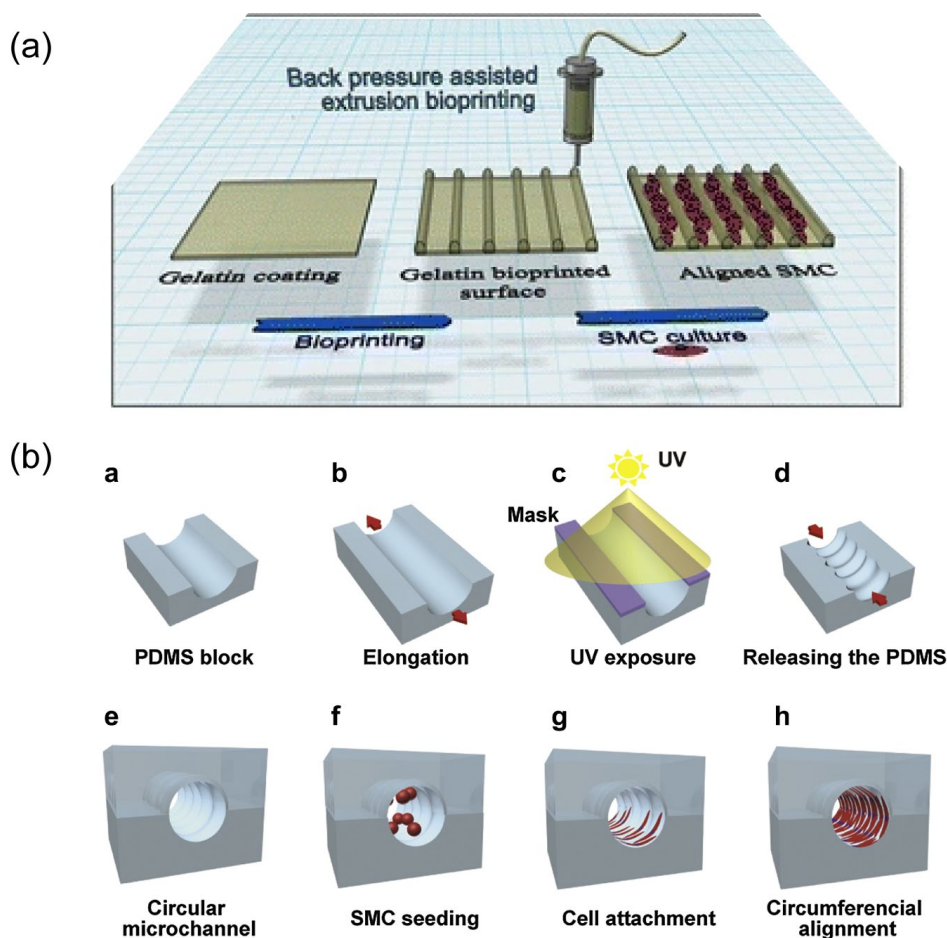


Figure 1.9 Previous alignment methods of smooth muscle cells. (All license numbers are shown in Appendix A) (a) A gelatin hydrogel microchanneled platform^[94] (Copyright: © 2018 *Biomed. Microdevices*). (b) Aorthogonal microwrinkle structure inside the circular microchannel to guide a circumferential SMC alignment^[93] (Copyright: © 2018 *Biomaterials*).

reported (Figure 1.6 (c,d)), but the direction of the cells in the models was random. As mentioned in sections 1.3 and 1.4, the formation of the circumferential alignment of the smooth muscle layer is required to mimic the contraction behavior of SMCs under biochemical reactions^{[91], [92]}.

To mimic the circumferentially aligned structure of *in vivo* smooth muscles, scaffolds with microwrinkle patterns^[93] or microchannels^[94] were previously reported (Figure 1.9(a,b)). These physically parcellated grooves achieved the self-alignment of SMCs

along with the patterns. However, these models could not reproduce the contraction behavior of the SMCs under biological reactions because the tissues are fixed to a rigid surface. The insufficient flexibility of the scaffold disturbs the tissue contraction and leads to the deviation of the behaviors with *in vivo* tissues in biological reaction, including immunological reaction^[95]. Thus, as same as capillary models, a flexibly deformable multi-layered model is required to develop as biomedically applicable artery/vein models.

1.7 Objectives & Approaches

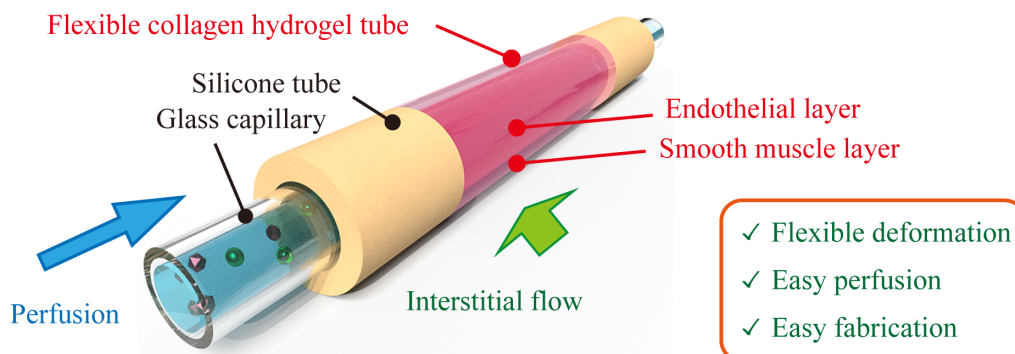
To achieve the immunological deformation reaction of blood vessels, the author proposes a self-standing multi-layered *in vitro* blood vessel model with a flexibly deformable collagen hydrogel tube device^[96] (Figure 1.10(a)).

A self-standing collagen tube enables the tissue to deform flexibly in immunological reaction and achieves contraction both at tissue and cell levels^[97]. The tissue contraction relieves the stress between ECs under reaction to maintain cellular junction even tight junctions are broken, resulting in the reproduction of immunological phenomena of ECs similar to *in vivo* (Figure 1.10(b)). Moreover, the drug screening can easily be performed on the device due to the connector part.

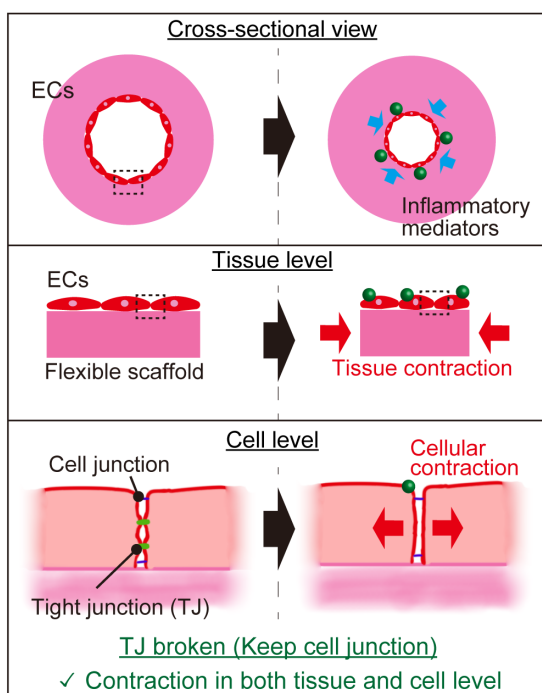
Also, a circumferentially aligned SMC layer is formed by rolling up an axially aligned fiber-shaped SMC tissue (rolling up maturation molding method (RuM-M method)) (Figure 1.10(c)). The spiral-shaped SMC layer is embedded into an unfixed collagen hydrogel tube to construct a blood vessel model by co-culturing with ECs. The unfixed scaffold enables the flexible deformation of a multi-layered blood vessel model by contraction of ECs and SMCs in immunological reactions.

First, the self-standing tube is proposed to construct a flexibly deformable endothelial layer. Then the ability of the device for the reproduction of immunological deformation reaction and drug testing is evaluated by exposure to an inflammatory mediator

(a) Chapter 2 (Basic concept)



(b) Chapter 3
(Immunological deformation on ECs)



(c) Chapter 4
(Immunological deformation on ECs & SMCs)

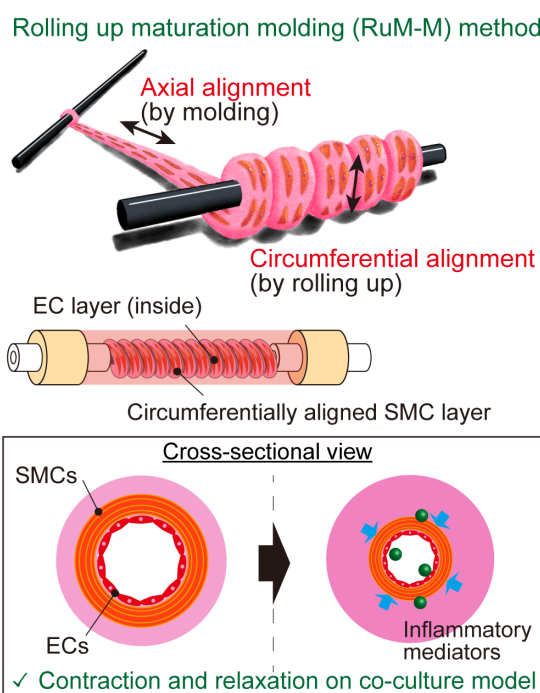


Figure 1.10 A flexibly deformable collagen hydrogel tube device for a self-standing multi-layered *in vitro* blood vessel model, the proposing device of this research. (a) The basic concept of the model. Chapter 2 describes the fabrication method and confirms the ability for cell culture. (b) Immunological deformation reaction of ECs is reproduced on the tube device in chapter 3. (c) Rolling up maturation molding method (Rum-M method) is proposed in chapter 4 to achieve the circumferential alignment of SMCs. Immunological deformation reaction of the co-cultured ECs and SMCs is reproduced on the tube device.

and a pharmaceutical chemical. Finally, the rolling up maturation molding method (RuM-M method) is proposed to fabricate circumferentially aligned SMC layer in a co-cultured blood vessel model, and achieve the immunological deformation reaction of the co-cultured endothelium and smooth muscle.

1.8 Dissertation outline

This dissertation is composed of 5 chapters as below:

Chapter 1 introduces the background, the purpose, and the concept of this research.

Chapter 2 describes the basic fabrication of a double-layered collagen hydrogel tube device. First, a simple repeated molding process precisely and easily fabricates the double-layered collagen tube device. Then, after forming an endothelial layer inside the tube, the tissue formation is confirmed by evaluating the barrier function of the endothelium. Also, the cellular response of the endothelial cells is confirmed by co-culturing with vascular pericytes.

Chapter 3 reproduces the immunological deformation reaction of the endothelium layer with the tube device forming an endothelial layer inside. Exposure to histamine (an inflammatory mediator of allergy) confirms contraction and recovery reactions at both tissue and cell levels. Also, the ability of the device for drug testing is evaluated by exposing olopatadine hydrochloride (an anti-histamine material) and histamine. In addition, the traction force of the endothelial cells under reaction is calculated by numerical analysis with the finite element method.

Chapter 4 proposes a blood vessel model with a circumferentially aligned smooth muscle layer. By rolling up an axially aligned smooth muscle fiber, a circumferential alignment is easily formed in a collagen tube (Rolling up maturation molding (RuM-M) method). The alignment is evaluated by live imaging of actin. An immunological deformation reaction of the co-cultured endothelium and smooth muscle is reproduced with co-cultured tissue under exposure to histamine.

Chapter 5 concludes this dissertation by discussing the value of the proposed self-

standing *in vitro* multi-layered blood vessel model and the prospective.

CHAPTER 2.

Double-layered perfusable polymer hydrogel tube device

2.1 Introduction

In this chapter, the double-layered ECM-based polymer hydrogel tube device is developed to form a flexibly deformable scaffold for the blood vessel model.

First, a simple repeated molding process is described to precisely and easily fabricate a double-layered collagen hydrogel tube device. Then, endothelial cells are seeded on the inner surface of the tube to form an endothelial layer. The tissue formation is confirmed by evaluating the barrier function of the endothelium with immunostaining and a permeability experiment. Also, the cellular response of the endothelial cells is confirmed by co-culturing with vascular pericytes.

2.2 Fabrication procedure

2.2.1 Preparation of solutions & molds

Collagen hydrogel was used as the ECM of the tube device. Collagen consists of

30% of amino acids in the body of animals^[98]. For example, Dermis, bones, cartilages, or Ligaments are mainly composed of collagen. Also, in multicellular organisms, organs are formed by tissues composed of cells and ECM, which of the main component is collagen^[99]. Collagen as an ECM not only works as a supporting structure of the tissue but also plays essential roles in transportation, cell migration, and cellular interaction^[100]. In this research, type-I collagen gel, which occupies 80 to 90% of the collagen in our body, was used as the scaffold of the device.

For the reconstitution of a pre-gel collagen solution, HEPES (200 mM), sodium hydrogen carbonate (260 mM), and sodium hydroxide (50 mM) were mixed to prepare a reconstitution buffer. Then, 10X HANKS balanced salt solution, the reconstitution buffer, and acid-solubilized Type-I collagen solution (Type-I collagen, KOKEN, 5 mg/mL) were mixed on the ice at a volume ratio of 1:1:8 for reconstituting the collagen pre-gel solution.

A glucose film was coated on a tungsten wire before assembling the mold for fabrication as a sacrificial layer to reduce friction between the wire and silicone tubes when removing the mold. Glucose is known to be caramelized by heating an aqueous solution over 160°C^[101]. The caramelized melt has a high viscosity and is immediately solidified by cooling at room temperature. The coating was formed by taking advantage of these characteristics.

First, glucose was dissolved in DI water at 0.4 wt%. Then, the solution was warmed to 160°C to remove most of the water. After the solution formed a viscous melt liquid, a tungsten wire was dipped into the liquid. Then, the wire was pulled up at constant speed by a Z-axis stage to coat a glucose film on the tungsten wire (Figure 2.1 (a-c)).

2.2.2 Fabrication of the tube device

The fabrication process of the double-layered collagen tube device was divided into seven steps as below:

- (i) A glass capillary, silicone tubes, and a glucose-coated tungsten wire were assembled for the mold (Figure 2.2(a)).

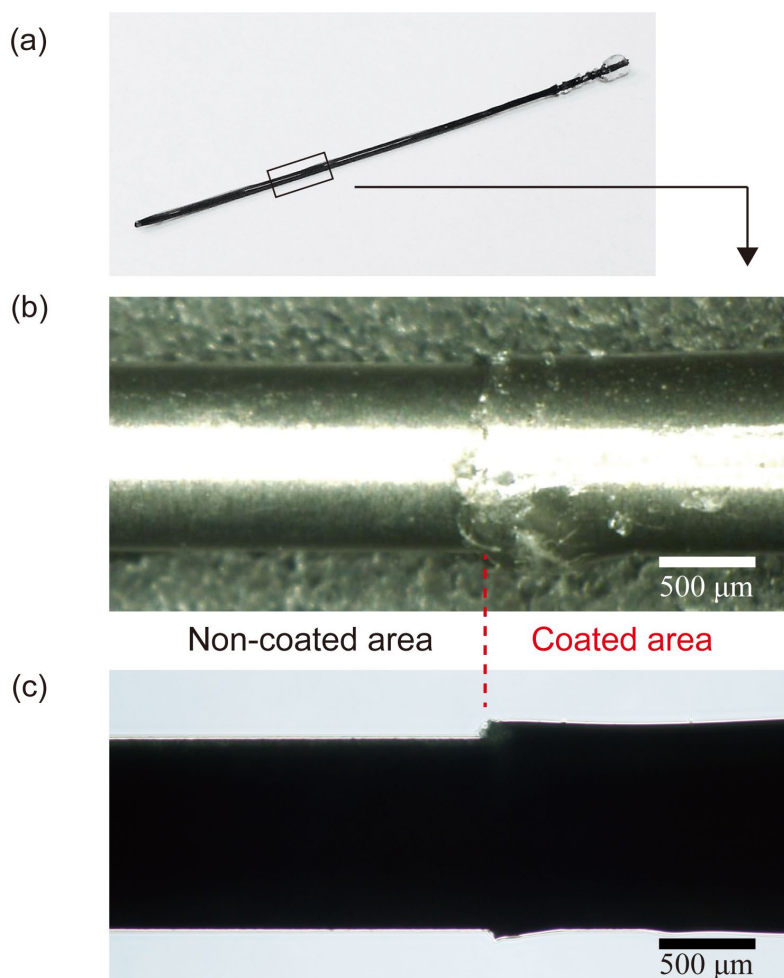
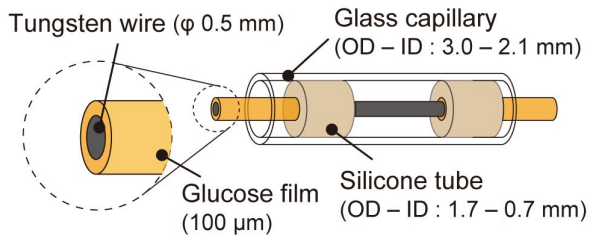


Figure 2.1 A glucose film coated on a tungsten wire. (a) An overall image. (b) An enlarged view. (c) A phase-contrast microscopic image.

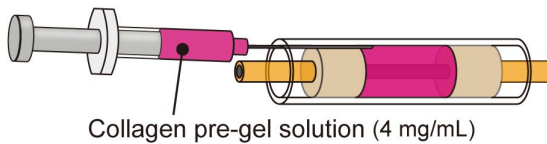
- (ii) A collagen pre-gel solution was injected into the inner space of the mold by an injection needle (Figure 2.2(b)). Note that the injection needle was inserted through the tiny space between the glass capillary and the silicone tubes.
- (iii) The mold was put into Endothelial Growth Medium 2 (EGM-2) and incubated at 37°C to solidify the collagen (Figure 2.2(c)).
- (iv) The mold was removed to obtain a single-layer collagen tube (Figure 2.2(d)).
- (v) A thinner tungsten wire was inserted into the single-layer collagen tube to form a

Single-layer fabrication

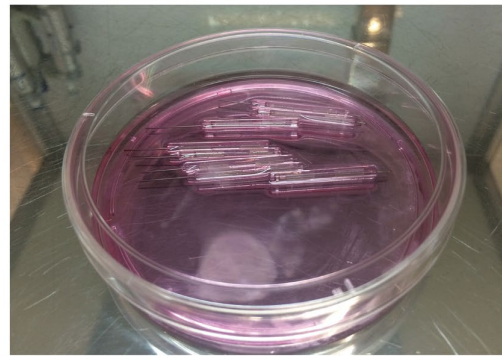
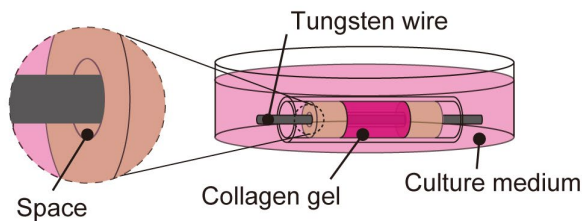
(a) Assemble the mold



(b) Inject collagen pre-gel solution



(c) Incubate to solidify collagen



(d) Remove the mold



Single-layer collagen tube device

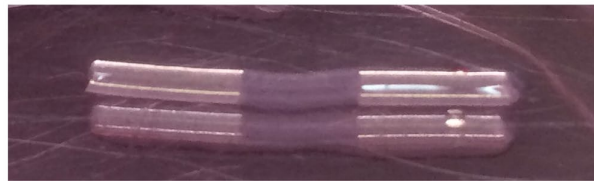
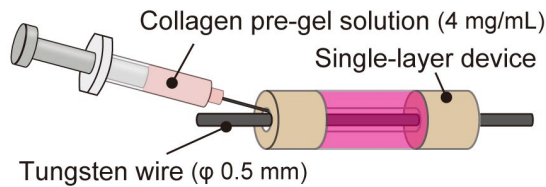


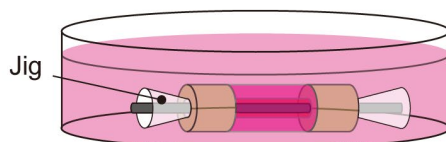
Figure 2.2 Fabrication process of the device (Part 1). (a) A glass capillary, a glucose coated tungsten wire, and two silicone tubes were assembled for the mold. (b) A collagen pre-gel solution was injected and the mold was put into the medium. (c) The mold was incubated to solidify the collagen and melt the glucose film. (d) The glass capillary and the tungsten wire were removed to obtain a single-layer collagen tube. (OD : Outer diameter, ID : Inner diameter)

Double-layer fabrication

- (a) Insert a thinner tungsten wire and inject collagen solution



- (b) Incubate to solidify collagen



- (c) Remove the mold



Figure 2.3 Fabrication process of the device (Part 2). (a) A thinner tungsten wire was inserted into the single-layer tube and the collagen pre-gel solution was injected. (b) Plastic jigs were inserted to fix the wire to the center, and the device was incubated to solidify the collagen of the second layer. (c) The tungsten wire was removed to obtain a double-layered collagen tube.

mold composed of the inner inserted tungsten wire and an outer solidified collagen tube (Figure 2.3(a)).

- (vi) A collagen pre-gel solution was injected into the mold. After that, plastic jigs were inserted into both sides of the silicone tubes to fix the wire to the center, followed by incubation at 37°C while soaking in the medium to solidify the collagen (Figure 2.3(b)).
- (vii) The tungsten wire was removed to obtain a double-layered collagen tube (Figure 2.3(c)).

2.2.3 Cell seeding

Cell culture demonstrations were performed using two types of cells: Human Umbilical Vein Endothelial Cells (HUVECs, Lonza) and Human Brain Vascular Pericytes (HBVPs, Sciencell).

HUVECs are one of the most popular EC models used for *in vitro* experiments because human umbilical veins are relatively more available than other types of human blood vessels^[102]. HUVECs are isolated from the umbilical veins of donors and cryopreserved to make the cells commercially available^[103]. Although umbilical veins specifically appear in our body, HUVECs are known to express various essential endothelial markers, signaling molecules, and biochemical responses, ensuring the ability to use as a general EC model for vascular tissue engineering^[104].

HBVPs are isolated from the brain tissue of donors and cryopreserved to make the cells commercially available. The cells have been confirmed to regulate the function of blood vessels by interacting with ECs^[105]. In detail, the pericytes located far from the vessel release vascular endothelial growth factor (VEGF) to enhance angiogenesis, while the cells attached around the vessels make stable the vessel to stop the proliferation and angiogenesis of ECs^[106], ^[107]. Thus, HBVPs are used for a demonstration experiment to confirm the ability of the vessel model to perform cell-cell interaction.

The culture medium was EGM-2 supplemented with a bullet kit for the HUVECs, and Pericyte Medium (PM) supplemented with a complete kit for the HBVPs. Prior to cell seeding, cells were incubated in dishes at 37°C in a humid atmosphere with 5 % CO₂, and the medium was replaced every three days.

For cell seeding in collagen devices, cells were first dissociated from the dishes by trypsinization with trypsin EDTA. For cells being seeded to the surface of collagen, the trypsinized cells were suspended in the medium, and the cell suspension (2.0×10^6 cells/mL) was directly injected into the lumen of the device (Figure 2.4). For cells being seeded into the collagen layer, the trypsinized cells were suspended in a collagen pre-gel solution prior to the fabrication process.

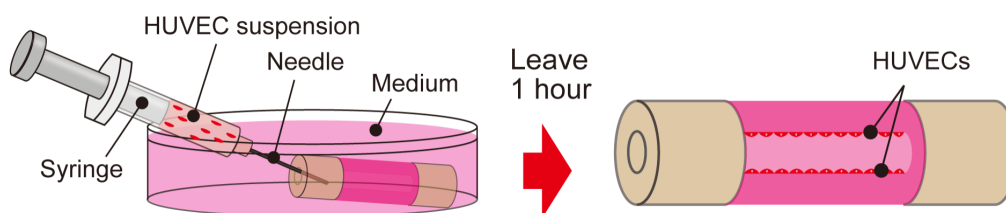


Figure 2.4 Seeding of HUVECs onto the inner surface of the collagen tube device. First, the cell suspension of HUVECs was injected into the tube device with an injection needle and a syringe. Then, the tube was left still for an hour to adhere HUVECs.

2.3 Experimental method

2.3.1 Fluorescent staining and observation

An inverted fluorescence/phase-contrast microscope (Olympus, IX73P1-22FL/PH, JAPAN) was the main instrument used to observe the device and cells.

To distinguish the borders between the polymer gel layers and seeded cells, the cells and gels were stained with fluorescence. To stain the polymer gel, a NHS-labeled fluorescent dye (NHS-Alexa) were mixed to the reconstituted collagen pre-gel solution at a volume ratio of 1:200.

For immunostaining of cells, the device was immersed in a 4% paraformaldehyde solution for 15 minutes at room temperature for fixation. After that, the fixed cells were permeabilized with 0.1% Triton-X in 1% bovine serum albumin (BSA) in phosphate buffered saline (PBS) for 1 hour, and reacted with the primary antibody in 1% BSA in PBS at 4°C for overnight. Finally, the cells were stained with secondary antibody in PBS for 2 hours at room temperature. (Details of antibodies are shown in Appendix B)

2.3.2 Perfusion set up

The perfusion culture was performed by infusing the culture medium into the collagen tube using a syringe pump. To construct the flow route of the medium, two holes

 Double-layered perfusable polymer hydrogel tube device

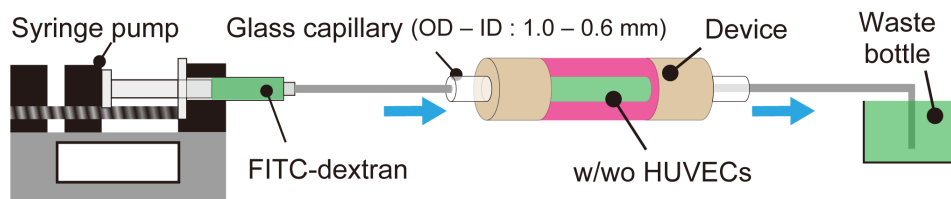


Figure 2.5 Set up for the perfusion experiment. Each side of the silicone tube of the collagen tube device was connected to syringe pump and waste bottle, respectively.

were formed on the side wall of a culture dish by a soldering iron. Then, glass capillaries (φ 1.0 mm) were inserted into the holes and fixed with an adhesive bond. One glass capillary was connected to the syringe pump through a silicone tube, while the other glass capillary was connected to a waste bottle. After that, each side of the silicone tube of the collagen device was connected to each glass capillary from the inside of the dish (Figure 2.5). The culture medium was perfused into the collagen device with a flow mass of $40 \mu\text{L}/\text{min}$ by the syringe pump.

2.3.3 Permeability experiment set up

Fluorescein isothiocyanate dextran (FITC-dextran, 70kDa (6.6 nm)), which is commonly used for permeability experiments^[108], was flowed into the vessel model to check the formation and function of the tight junction of HUVECs. Since the size of the TJ is normally ranged from 0.5 to 1.0 nm, the 70kDa dextran cannot pass through the junction^[109]. The procedure for the permeability experiment is as follows:

- (i) Air bubbles in the flow route were removed by flow in PBS.
- (ii) FITC-dextran was solved in PBS at $10 \mu\text{mol}/\text{L}$.
- (iii) The dextran solution was flowed into the tube device with HUVECs at the flow rate of $40 \mu\text{L}/\text{min}$ for 3 minutes with a syringe pump.
- (iv) The fluorescent image was taken by the fluorescence microscope, and fluorescent intensity profiles were analyzed by image analysis.

2.3.4 Image analysis and calculation of the permeability coefficient

The permeability of the endothelial tissue on the tube device was measured by image analysis and a theoretical calculation.

An image analysis software (ImageJ, NIH) was used to measure the permeability. First, the obtained fluorescent images were opened in ImageJ, and the desired line to extract the fluorescent intensity was written on the images. Then, the brightness values for red, green, and blue were shown by “RGB Profile plot”. The green color values were recorded to use for the calculation.

When the concentration of a substance is heterogeneous in a certain area, the concentration is uniformed because the entropy becomes large by the second law of thermodynamics. The permeability coefficient (P) of the substance across an area of the blood vessel wall is described as follows using Fick’s first law:

$$P = \frac{J_s/S}{\Delta c} \quad (2.1)$$

where J_s is the initial flux of the solute, S is an area of the blood vessel wall, and Δc is the concentration difference. In the case of immediately after the lumen of the vessel is filled with the dextran solution, J_s is calculated as follows:

$$J_s = \left(\frac{dN}{dt} \right)_0 \quad (2.2)$$

where N is the number of molecules in the tissue. Since the concentration difference Δc is equal to the solute concentration in the lumen at the beginning, Δc is calculated as follows:

$$\Delta c = \frac{N_0}{V} \quad (2.3)$$

where N_0 is the number of molecules initially filled the lumen, and V is the volume of the lumen of the vessel. By substituting equations (2.2) and (2.3) into the equation (2.1), P is described as follows:

$$P = \frac{V}{S} \times \left(\frac{dN}{dt} \right)_0 \times \frac{1}{N_0} \quad (2.4)$$

In the experiment, the number of molecules (N) can be replaced by fluorescent intensity

because whole dextran molecules are modified by fluorescence. By replacing it, the equation changes as follows:

$$P = \frac{V}{S} \times \left(\frac{dI}{dt} \right)_0 \times \frac{1}{I_0} \quad (2.5)$$

where I_0 is the fluorescent intensity inside the lumen, and dI/dt is the change in the fluorescent intensity at the surface. In addition, V and S are calculated as follows:

$$V = \pi r^2 l \quad (2.6)$$

$$S = 2\pi r l \quad (2.7)$$

where r and l are the radius and the length of the vessel model, respectively. By substituting equations (2.6) and (2.7) into the equation (2.5), P is described as follows:

$$P = \frac{r}{2} \times \left(\frac{dI}{dt} \right)_0 \times \frac{1}{I_0} \quad (2.5)$$

The permeability coefficient was calculated by substituting the obtained fluorescent intensity into this equation^[110].

2.4 Fabrication results

2.4.1 Design of collagen tube devices

The size and structure of a collagen tube device should be designed in consideration of the target vessel model since blood vessels *in vivo* vary in diameter from 30 mm (aorta and vena cava) to 5 μm (capillary vessels)^[111]. This research aims to reproduce the blood vessel deformation occurring on the SMC and EC layers. Thus, the author chose a medium-sized blood vessel with a multi-layered structure with inner diameters of approximately 100–1000 μm (similar to arteries and veins).

The size of the collagen tube device can be designed by changing the dimensions

Double-layered perfusable polymer hydrogel tube device

Table 2.1 Design of single-layer collagen devices and their mold dimensions

Device type	Aimed single-layer collagen tube ID _c /OD _c	Glass capillary (Outer mold) ID _g /OD _g	Tungsten wire (Inner mold) OD _t	Silicone tube ID _s /OD _s	Thickness of glucose film
A	1000/2400	2400/4000	1000	1200/2000	100
B	500/2100	2100/3000	500	700/1700	100
C	300/1800	1800/3000	300	500/1500	100

(ID = inner diameter, OD = outer diameter)

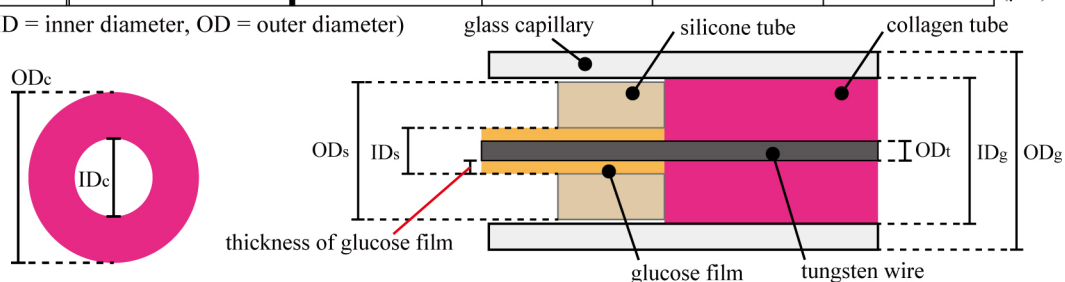
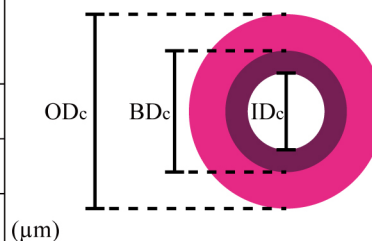


Table 2.2 Design of double-layer collagen devices and their mold dimensions

Device type	Aimed double-layer collagen tube ID _c /BD _c /OD _c	Single-layer type	Tungsten wire (inner mold) OD _t
D	300/1000/2400	A	300
E	400/1000/2400	A	400
F	500/1000/2400	A	500

(ID = inner diameter, BD = border diameter of 2 layers, OD = outer diameter)



of the mold. To demonstrate the flexibility of the design, several sizes of molds were prepared for fabricating single or double-layer collagen devices having inner diameters of 300–1000 μm (Table 2.1 and Table 2.2).

2.4.2 Single-layer tube fabrication

A monolayer collagen tube device was easily fabricated (Figure 2.6(a)). Phase-contrast observation of three types of single-layer tube devices (Type A-C) showed that the collagen gel formed a clear tube shape and was firmly connected to the silicone tubes

 Double-layered perfusable polymer hydrogel tube device

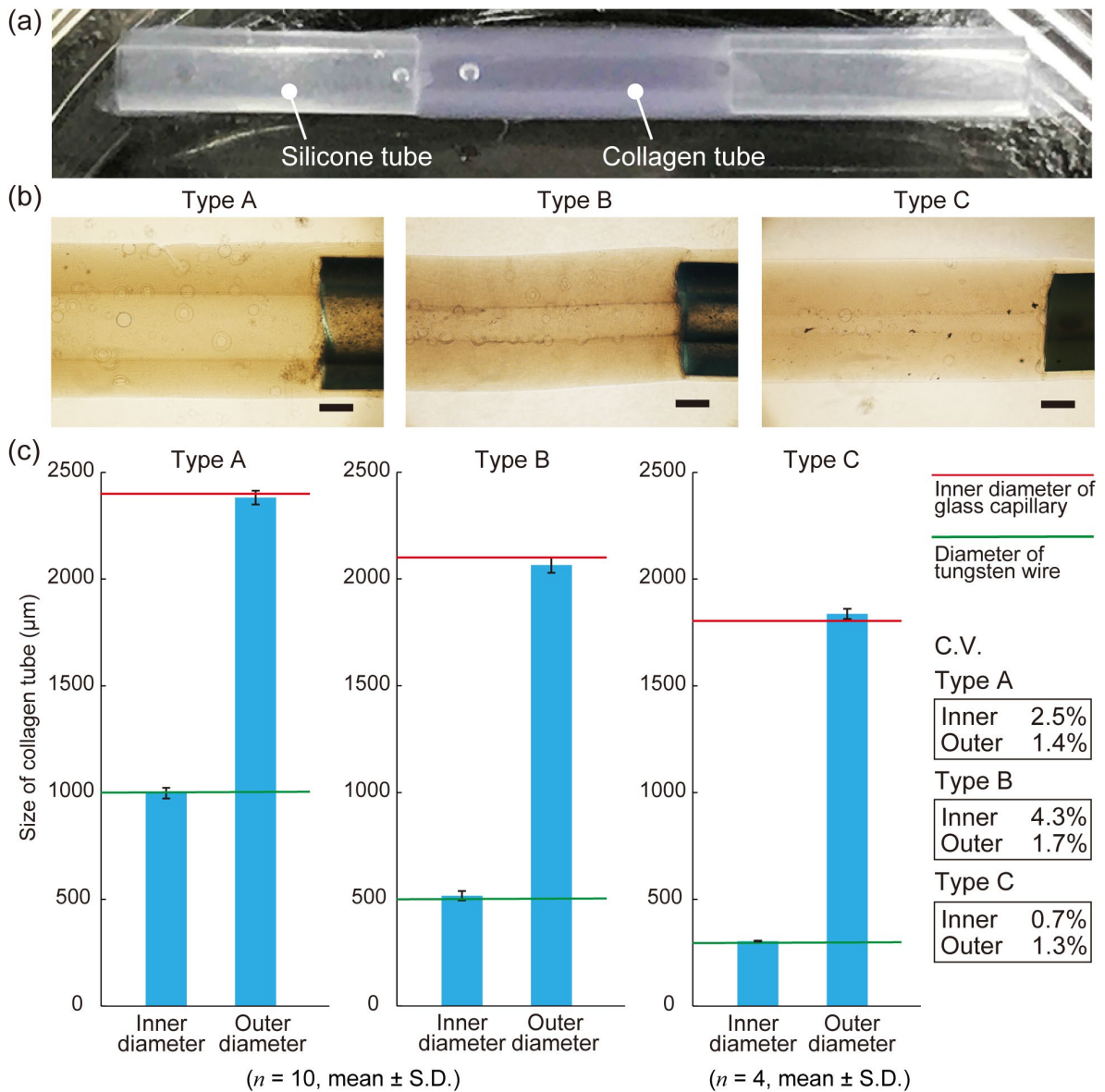


Figure 2.6 Fabrication results of a single-layer collagen device. (a) An overall picture of the device. (b) Phase-contrast microscopic images of devices. Three sizes of single-layer collagen tube devices were fabricated, and the collagen gel formed a clear tube shape and was firmly connected to the silicone tubes. (c) Diameters of collagen devices. All collagen tube devices had high uniformity in the diameter along the tube, and the coefficients of variation (C.V.) for the diameter fluctuations between each device were less than 5% for both the inner and outer diameters of all types of collagen devices. (Scale bars: 500 µm).

at both ends for all types of devices (Figure 2.6(b)). The silicone tubes were covered by a thin collagen layer, enhancing the bonding force between the silicone and collagen strong enough to maintain the structure, even when the structure was manipulated with tweezers. The structure was stable for more than six months in the medium.

Next, the author evaluated the diameters of the fabricated collagen tube devices (Figure 2.6(c)). The inner diameters for device Types A, B, and C were $304 \pm 2 \mu\text{m}$, $516 \pm 22 \mu\text{m}$, and $997 \pm 25 \mu\text{m}$, respectively. The outer molds defined the outer diameters: $1837 \pm 23 \mu\text{m}$, $2065 \pm 36 \mu\text{m}$, and $2381 \pm 32 \mu\text{m}$ for Types A, B, and C, respectively. All devices were approximately 10 mm in length. All collagen tubes exhibited high uniformity in the diameter along the tube. The coefficients of variation (C.V.) for the fluctuations in diameters were less than 5% for both inner and outer diameters in all types of collagen devices. These results indicate that the collagen tube devices, which have inner diameters range from approximately 300 μm to 1000 μm , can be stably fabricated by a simple molding process.

2.4.3 Double-layer tube fabrication

Next, a layer was added inside the single-layer collagen tube device to form a double-layered device. Since blood vessels have some polymer layers like basal membrane or elastic plate inside the collagen layer, the device with double-layered polymer gel have the benefits to mimic *in vivo* structure. A type D collagen tube device was observed by a phase-contrast microscope (Table 2) (Figure 2.7(a)). To help visualize the additional collagen layer, the outer and inner collagen layers were stained with red and green fluorescence, respectively (Figure 2.7(b,c)). The fluorescence microscopic observations revealed that an additional layer was fabricated inside the first collagen layer.

Next, the diameters and thicknesses of the layers in the fabricated double-layer collagen tube devices were evaluated (Figure 2.7(d)). The same types of single-layer collagen tubes were used for fabrication, in which the inner and outer diameters were $997 \pm 25 \mu\text{m}$ and $2381 \pm 32 \mu\text{m}$. The thicknesses of the additional layers in device Types D, E, and F were $685 \pm 6 \mu\text{m}$, $590 \pm 12 \mu\text{m}$, and $498 \pm 7 \mu\text{m}$, respectively. The C.V. for the thickness fluctuations between devices was lower than 4% for all types of devices. The value indicates

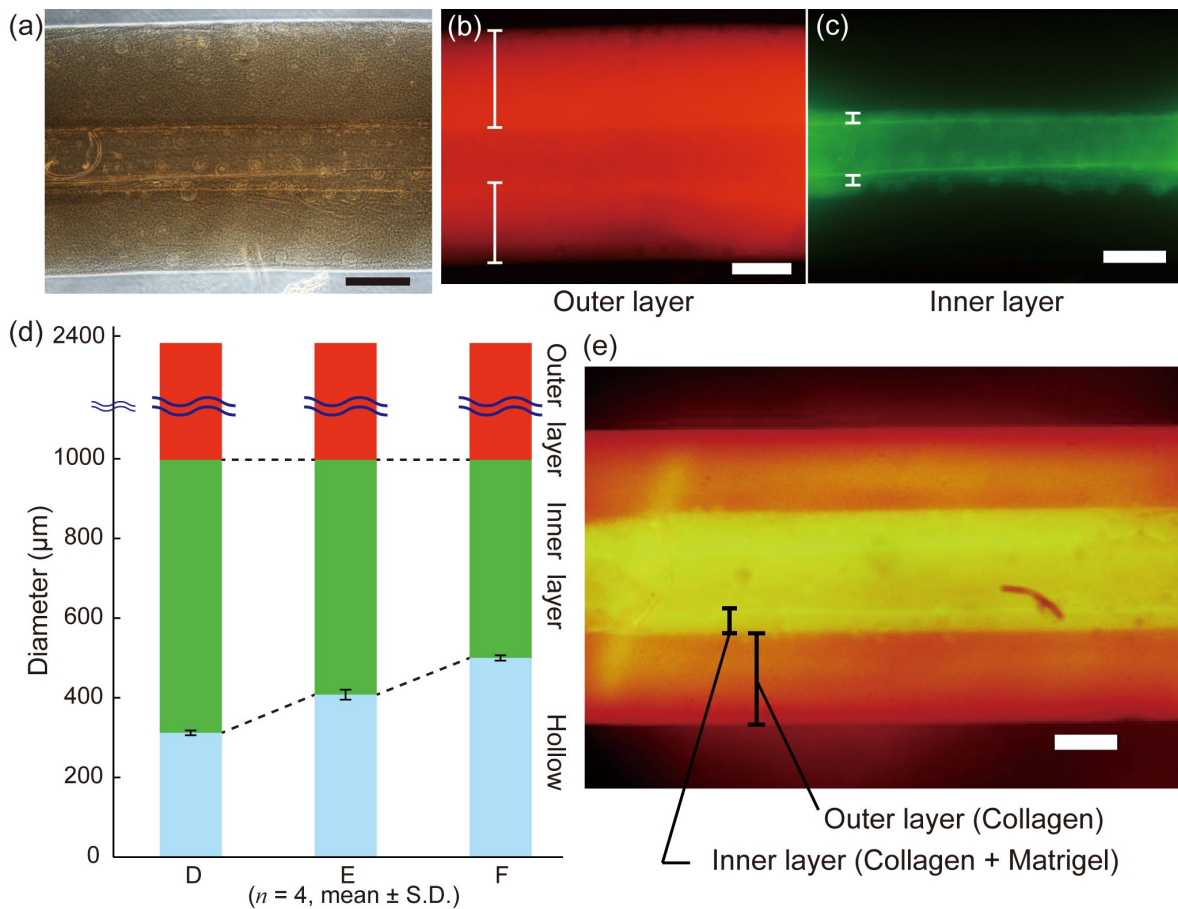


Figure 2.7 Fabrication results of a double-layer collagen tube device. (a) A phase-contrast microscopic image. (b) A fluorescent image of the outer collagen layer stained with red fluorescence. (c) A fluorescent image of the inner collagen layer stained with green fluorescence. Additional collagen layer was formed inside the first layer. (d) Diameters and thicknesses of collagen layers. (e) A double-layer heterogeneous collagen tube composed of 4 mg/mL bovine skin-derived type-I collagen for the outer layer, and mixture of 2 mg/mL bovine skin-derived type-I collagen and 4 mg/mL mouse sarcoma derived Matrigel for the inner layer. (Scale bars: 500 μm)

that the thicknesses of the layers in the double-layer collagen devices were precisely controlled.

Using the developed layer addition process, a heterogeneous double-layer tube device composed of two different layers mimicking basal membrane and collagen connective

tissue was fabricated. The material of the layers was 4 mg/mL type-I collagen for the outer layer (stained with red fluorescence), and a mixture of 2 mg/mL type-I collagen and mouse sarcoma derived Matrigel (Corning®, 4 mg/mL) for the inner layer (stained with green fluorescence) (Figure 2.7(e)). The result shows that the method can be used to fabricate a heterogeneous multilayer scaffold with various polymer gel layers.

2.5 Cell culture results

2.5.1 Static culture

The culturing capability of the fabricated devices was firstly investigated by a static culture of HUVECs on the inner surface of the single-layer tube. The cells were seeded by cell suspension injection into the collagen tube (Figure 2.8(a)). Day by day, sparsely seeded cells gradually adhered and proliferated along the inner collagen surface (Figure 2.8(b)). After a week of culture, the inner surface of the single-layer tube was filled with proliferated HUVECs (Figure 2.8(c)).

2.5.2 Immunostaining analysis

To examine the monolayer formation of HUVECs, immunostaining analysis was performed on the proliferated cells (Details of antibodies are shown in Appendix B). As mentioned in section 1.3.2, endothelial cells are known to form tight junctions at the connection between cells. The author stained CD31 (junction marker) by human CD31 antibody with red fluorescence (Alexa 568), and nuclei by DAPI (Figure 2.8(d)) to check the existence of cellular junctions. From the fluorescent image, the cultured HUVECs expressed CD31 at the region of cell-cell contacts, indicating the formation of cellular junctions.

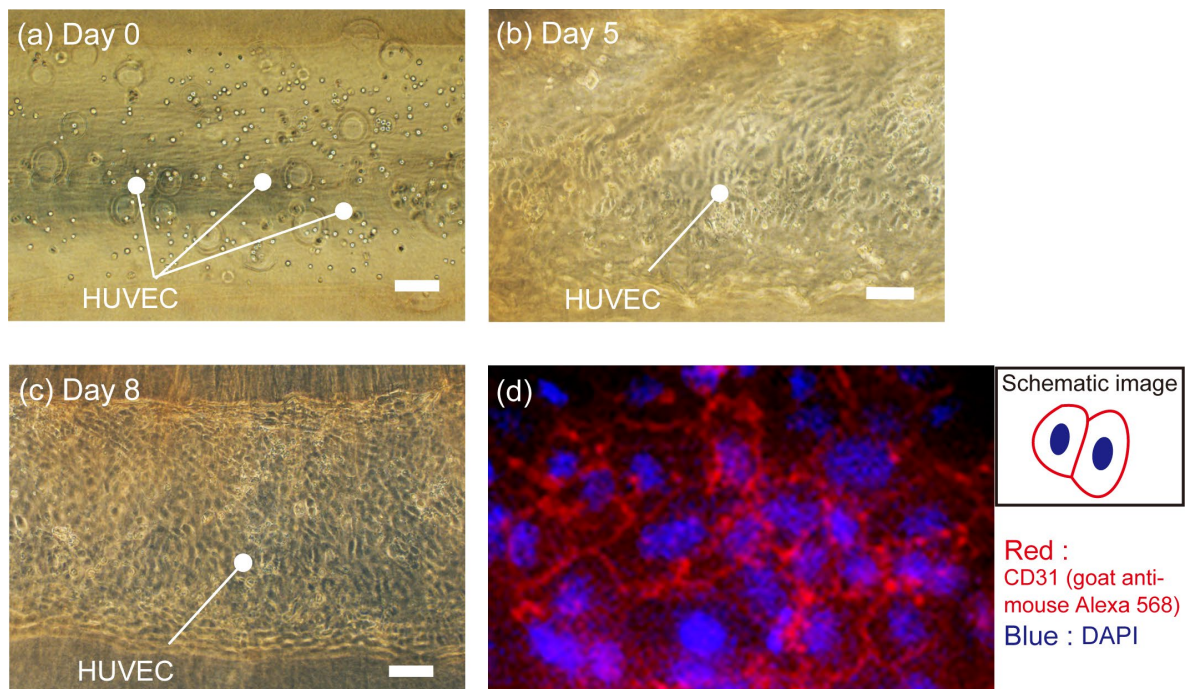


Figure 2.8 Mono-culture of HUVECs at the inner surface of the device. (a) A phase-contrast microscopic image on Day 0. (b) A phase-contrast microscopic image on Day 5. Sparsely seeded cells gradually adhered and proliferated along the surface. (c) A phase-contrast microscopic image on Day 8. After a week of culture, the inner surface was filled with proliferated HUVECs (Scale bars: 100 μm). (d) Immunostaining analysis of proliferated HUVECs. CD31 of HUVECs and nuclei were stained with red and blue fluorescence, respectively. CD31 was observed, indicating the proper maturation of ECs.

2.5.3 Permeability evaluation

Next, a permeability experiment was performed to confirm the function of tight junctions. FITC-dextran solution (MW: 70 kDa) was flowed into the device by a syringe pump, and the leakage was observed by fluorescent image after 180 seconds of the flow. The result of the device with proliferated HUVECs at the inner surface showed almost no leakage to the outside of the lumen (Figure 2.9(a)), while that of the device with no cells as a control showed diffusion of dextran to the collagen layer (Figure 2.9(b)). Fluorescent intensity measurement by an image analysis software also revealed that the amount of dextran at the

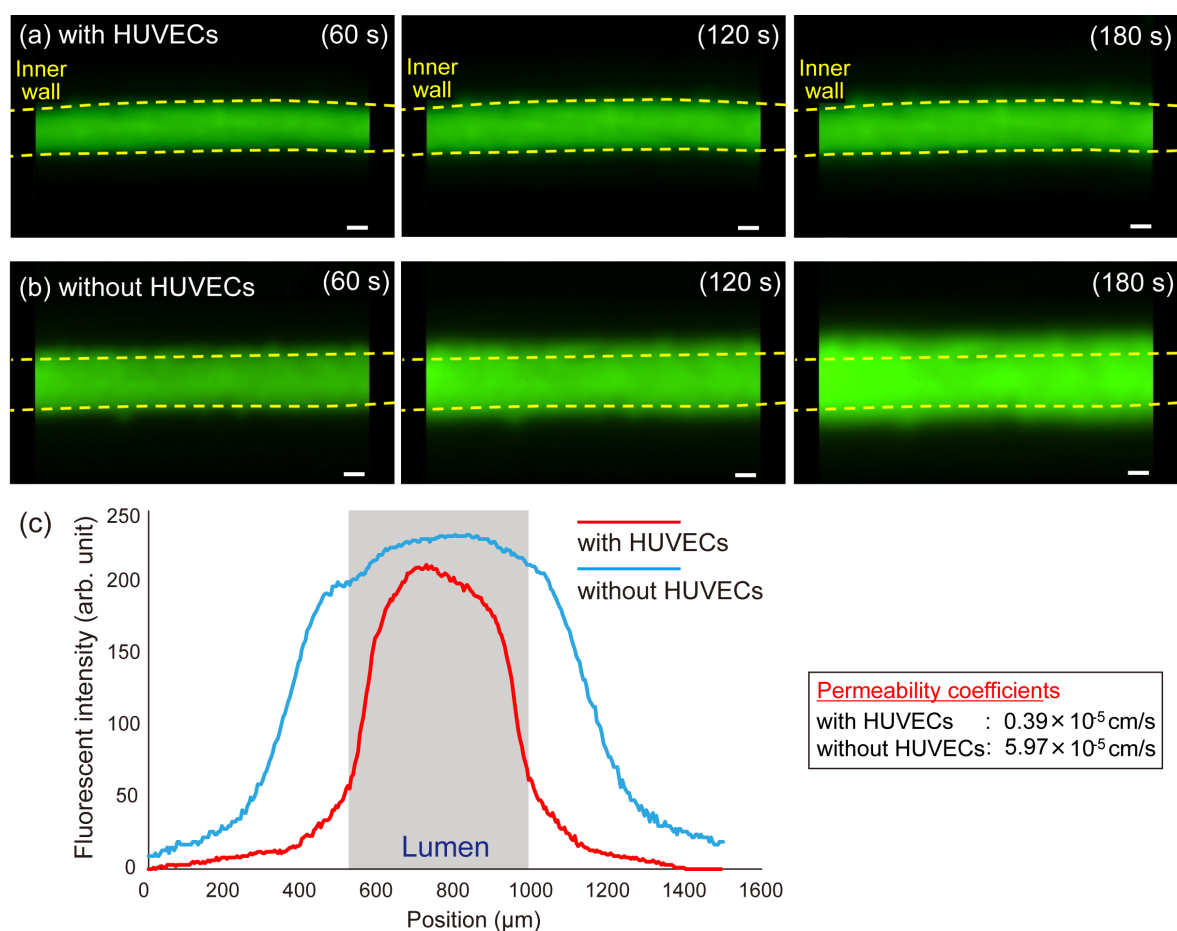


Figure 2.9 Permeability experiment with flowed FITC-dextran solution (a) Fluorescent images of the tube device with a HUVEC layer inside (Scale bars: 200 μm). (b) Fluorescent images of the tube device with no HUVEC layer (Scale bars: 200 μm). (c) Fluorescent intensity profiles of (a) and (b) at 180 s. The fluorescent intensity at the outside of the hollow of the tube with HUVECs is lower than no-cell tube, indicating the functionalization of the tight junction of HUVECs.

outside of the lumen was lower in the device with HUVECs than the device without HUVECs (Figure 2.9(c)). The permeability coefficient of the tube device with and without HUVECs was calculated as $0.39 \times 10^{-5} \text{ cm/s}$ and $5.97 \times 10^{-5} \text{ cm/s}$, respectively, by theoretical calculation with obtained intensity values.

The difference was caused by tight junctions of HUVECs at the inner surface regulating the dextran to permeate into the gel layer. The result indicates the proper

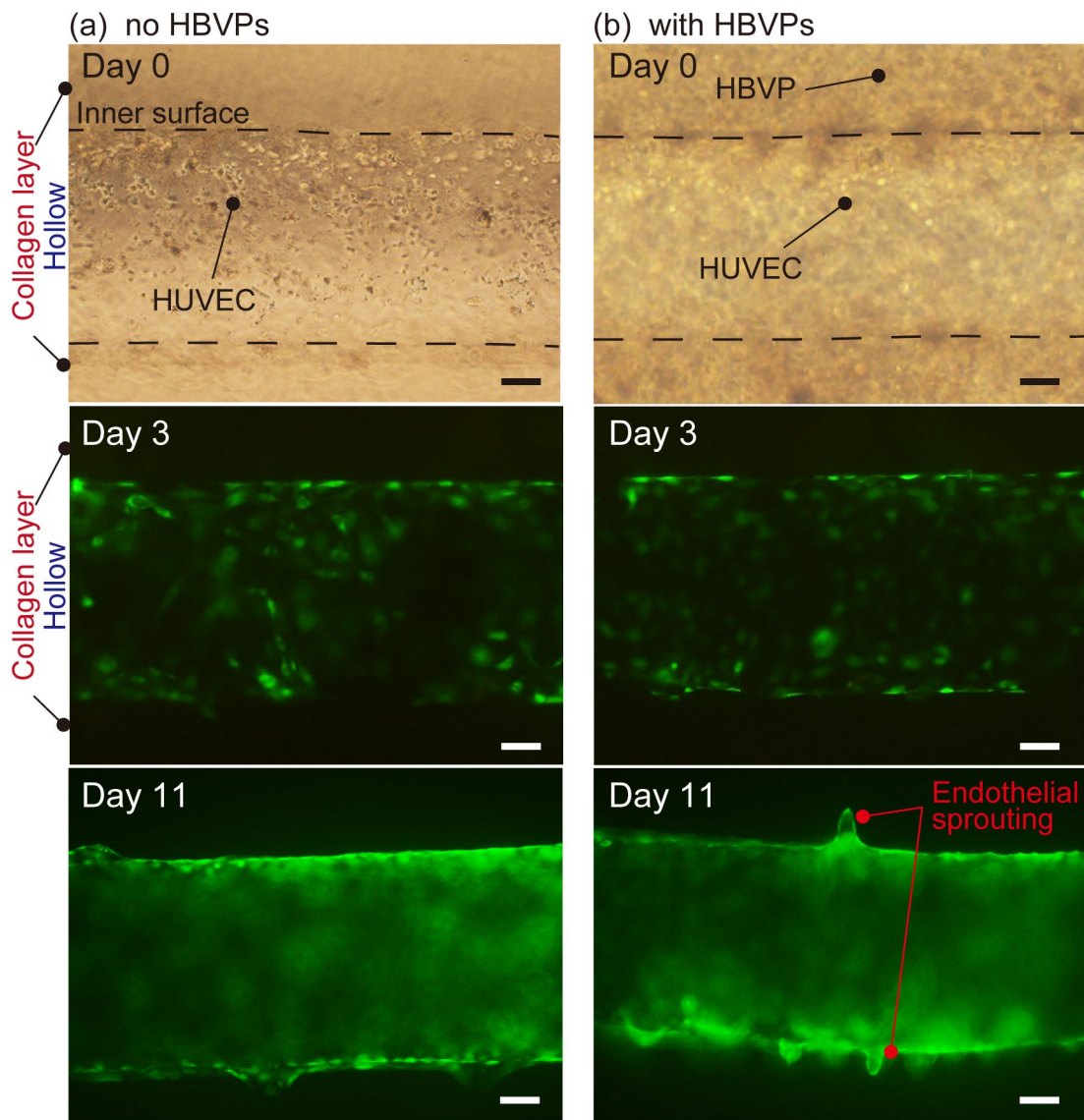


Figure 2.10 Co-culture demonstration in the devices. (a) A mono-culture HUVECs at the inner surface. No endothelial sprouting was found after culturing. (b) A co-culture with HUVECs at the inner surface and HBVPs in the collagen layer. After 11 days of culture, endothelial sprouting into the collagen layer was frequently observed (Scale bars: 100 μm).

functionalization of HUVECs and ensures the culturing and maturing ability of the device.

2.5.4 Co-culture demonstration

Next, co-culture was tested by seeding cells simultaneously inside the collagen layer and on the inner collagen surface. HUVECs were seeded on the inner surface by cell suspension injection into the collagen tube, and HBVPs were suspended in collagen pre-gel solution and encapsulated in the collagen layer. GFP-labeled HUVECs were used for observation. Two types of tubes were prepared, one was only with HUVECs as a control experiment, and the other was with of HUVECs and HBVPs (Figure 2.10(a,b)). Fluorescent images of 3 days after cell seeding show no difference between the two culture types. However, on day 11, the HUVECs of the device co-cultured with HBVPs generated endothelial sprouting (Figure 2.10(b)). The sprouts frequently occurred and penetrated into the collagen gel layer, though no-HBVP tube did not make any sprouts. The result indicates that the interaction between different types of cells was performed adequately in the device, and the device was also useful for cell co-culturing, as was the one type of cell culture.

2.5.5 Stability of the tube device under cell culture

The stability of the device for cell culture was also investigated. HUVECs and HBVPs were cultured for 12 days by both mono-culture and co-culture (Figure 2.11(a,b)), and measured the diameter to compare the size before and after culturing (Figure 2.11(c,d)). From the microscopic images, no crack or deformation was found. The inner and outer diameters of the device before culturing cells were $516 \pm 22 \mu\text{m}$ and $2065 \pm 36 \mu\text{m}$, respectively. As for the device after 12 days of single-layer culturing were $572 \pm 18 \mu\text{m}$ and $2102 \pm 17 \mu\text{m}$, and for the device after 12 days of double-layer culturing were $515 \pm 18 \mu\text{m}$ and $2087 \pm 20 \mu\text{m}$, respectively. The differences in the diameter between before and after culturing are pretty slight, indicating the device is stable for culturing. The results ensure the capability of the device for long-term cell culture.

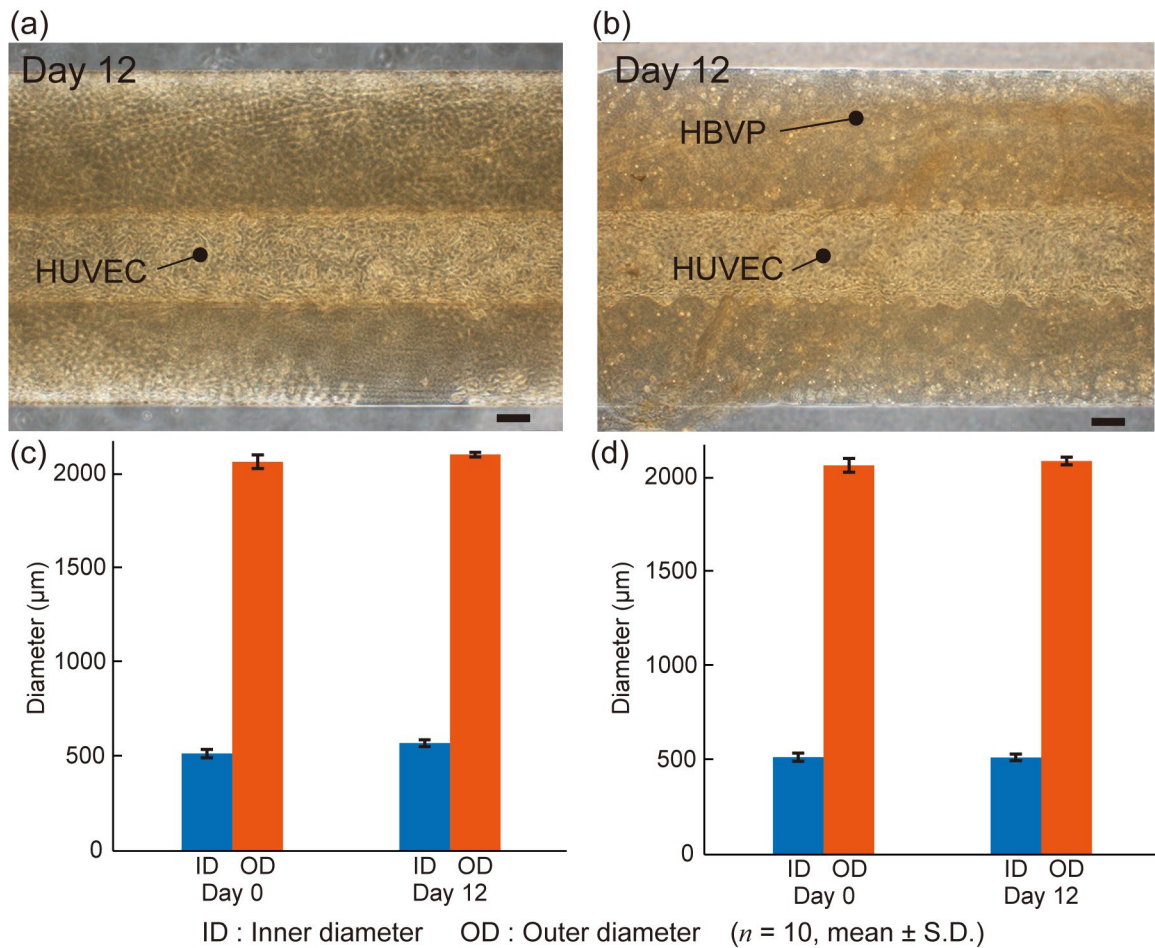


Figure 2.11 The diameter of the devices after 12 days of cell culture. (a) A cell culture with only HUVECs at the inner surface. No cracks were founded. (b) A cell co-culture with HUVECs at the inner surface and HBVPs in the collagen layer. Also, no cracks were founded. (c) The diameter of the tube before and after the mono-culture. The change of the size of the tubes is small. (d) The diameter of the tube before and after the co-culture. Again, the change of the size of the tubes is quite small. (Scale bars: 200 μm)

2.6 Conclusion

In this chapter, a double-layered collagen hydrogel tube device was developed to

construct a flexibly deformable scaffold for blood vessel formation. The device was simply made by the repetition of a molding process. The thicknesses of the collagen layers in the tube device could be flexibly designed, and heterogeneous cell types were able to be co-cultured in/on each collagen layer. Moreover, while the collagen tube was directly attached to silicone tubes, the collagen tube could easily be connected to an external pump system for perfusion culture.

The author fabricated six different sizes of collagen devices (inner diameter approximately 300–1000 μm) using different molds and successfully controlled the coefficients of variation (C.V.) to be below 5% for the diameters of each layer for all six device sizes. The device was strong enough to manipulate with tweezers, and could remain stable for more than three months in a medium. About the EC layer formation, HUVECs seeded on the inner layer properly migrated, and the immunostaining and permeability experiment revealed the formation of tight junctions with the permeability coefficient of $0.39 \times 10^5 \text{ cm/s}$. Also, the ECs interacted with vascular pericytes by co-culture, resulting in the angiogenesis of the endothelial layer. These results indicate that the EC layer constructed on the tube device has the capability to use as a functional blood vessel model.

CHAPTER 3.

Immunological deformation reaction of ECs on flexible collagen tube devices

3.1 Introduction

In this chapter, an inflammatory mediator-induced deformation reaction is reproduced with the fabricated blood vessel on a flexibly deformable collagen hydrogel tube device.

As mentioned in section 1.6.1, previously reported monolayer blood vessel models could not properly reproduce the biochemical contraction reaction of blood vessels because the models are not capable of implementing macro-scale tissue deformation. Therefore, this chapter aims to achieve the reproduction of immunological deformation reactions of ECs *in vitro* both at macro-scale (tissue level) and micro-scale (cellular level) (Figure 3.1).

First, the contraction and recovery behavior of the HUVECs at both tissue and cell levels is confirmed by exposure to histamine (an inflammatory mediator of allergy). Then, the relationship between the behavior and the concentration of histamine is investigated. After that, the ability of the device for drug testing is evaluated by exposing olopatadine hydrochloride (an anti-histamine material) and histamine. In addition, the traction force of the ECs is calculated by numerical analysis with the finite element method.

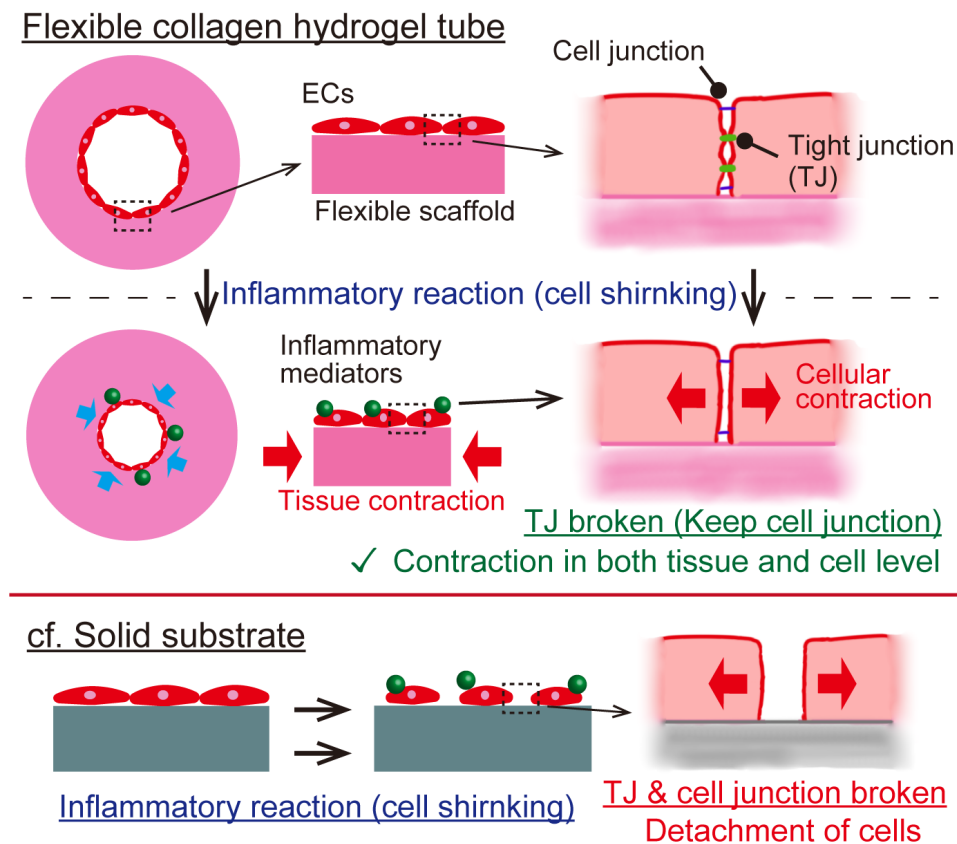


Figure 3.1 The scheme of immunological deformation of ECs. An inflammatory mediator-induced contraction reaction is reproduced with the fabricated blood vessel on a flexibly deformable collagen hydrogel tube device. The cellular deformation of ECs can deform the collagen tube and achieve the contraction behavior both at tissue and cell levels under inflammatory reactions such as allergy. The tissue contraction relieves the stress between cells under reaction to maintain the cellular junction even tight junctions are broken.

3.2 Experimental method

3.2.1 Fabrication method of the vascularized tube device

The fabrication method of the flexible collagen tube was slightly improved from chapter 2. By inserting glass capillaries inside silicone tubes, the glucose coating process was

deleted to simplify the fabrication. Also, since only the endothelial layer is required for experiments in this chapter, a monolayer tube device was used.

Preparation of the reconstituted collagen pre-gel solution (0.4 wt%) was referred to in section 2.2.1. To reduce the concentration of collagen gel to change the stiffness, type-I collagen solution was diluted with hydrochloric acid at pH 3.0 before the reconstitution. The cell culture and harvesting protocols for HUVECs were the same as in section 2.2.3. The detailed fabrication and vascularization processes are as below:

- (i) Before the fabrication, glass capillaries were inserted into silicone tubes. Then, two glass-inserted silicone tubes, a glass tube, and a tungsten wire were prepared as a set of a mold (Figure 3.2(a)).
- (ii) The tungsten wire was inserted into two glass-inserted silicone tubes with 10 mm length of space and covered with a glass tube (Figure 3.2(b)).
- (iii) The collagen pre-gel solution was injected into the inner space of the mold (Figure 3.2(c)).
- (iv) The mold was incubated at (37°C, 5% CO₂) in the culture medium to solidify collagen hydrogel (Figure 3.2(d)).
- (v) The tungsten wire and the glass tube were removed to obtain the collagen hydrogel tube device (Figure 3.2(e)).
- (vi) The cell suspension of HUVECs was injected into the lumen of the collagen layer by a syringe (Figure 3.2(f)).
- (vii) The device was cultured for four days in the medium statically to form a HUVEC layer on the inner surface (Figure 3.2(g)).

3.2.2 Chemicals used for immunological reaction experiments

Histamine, known as the inflammatory mediator in allergy^[112], was used in the biochemical reaction experiments of the blood vessel model. In allergic diseases, histamine is mainly released from mast cells by activation of the receptor of the cells by allergen^[113]. The barrier function of TJs of ECs is broken by histamine reaction through the contraction of

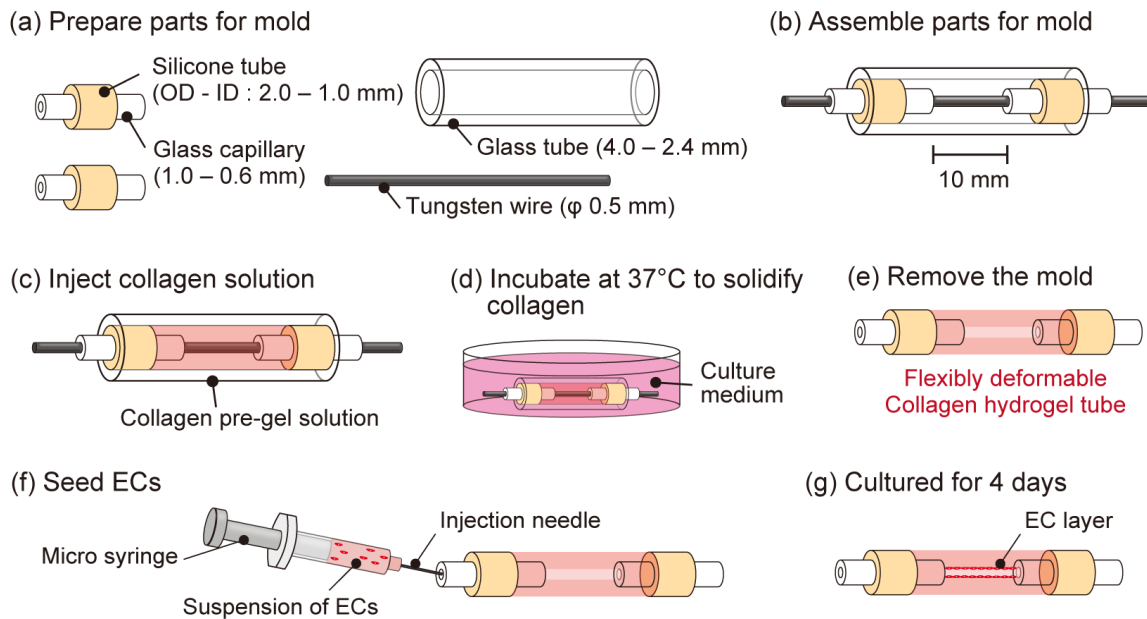


Figure 3.2 The fabrication process of the device. (a) Glass capillaries were inserted into silicone tubes. Two glass-inserted silicone tubes, a glass tube, and a tungsten wire was prepared as a set of a mold. (b) The tungsten wire was inserted into two glass-inserted silicone tubes and covered with a glass tube. (c) A collagen pre-gel solution was injected into the mold. (d) The mold was dipped into a culture medium and incubated to solidify collagen. (e) The tungsten wire and the glass tube were removed to obtain the collagen tube. (f) The cell suspension of ECs was injected into the lumen of the collagen tube. (g) The device was cultured for four days to form a EC layer on the inner surface. (OD : Outer diameter, ID : Inner diameter)

ECs^[114].

Olopatadine hydrochloride, which is known as an ingredient of anti-histamine pharmaceuticals, was used for the drug test demonstration^[115]. Olopatadine is a selective histamine receptor antagonist, blocking the binding of histamine to the receptor to avoid the immune reaction of ECs^[116]. By adding olopatadine hydrochloride simultaneously with histamine, the drug effect of inhibiting the histamine-induced immunological reaction was performed.

3.2.3 Fluorescent staining and observation

The immunostaining, the fluorescent staining, and the observation with the inverted fluorescence/phase-contrast microscope were proceeded as same as the protocol in chapter 2 (Details of antibodies are shown in Appendix B). On the time-lapse imaging, the top edges of the HUVEC layer of trimmed images were aligned while generating the time-lapse sequence image to compare the shrinking behavior easily.

3.2.4 Set up for perfusion experiments

The perfusion experiments with olopatadine were performed by infusing a culture medium including these chemicals into the collagen tube device using a syringe pump. First, the tube device was set on a self-made glass-based culture dish with two connecting tubes embedded. Then one side of the connecting tube was connected to the syringe pump, while the other side was connected to a waste bottle. Finally, the medium including olopatadine was filled into a microsyringe and perfused by a syringe pump. The flow mass was set to 158 $\mu\text{L}/\text{min}$ by the syringe pump.

Note that the flow was generated with two syringe pumps (Infusion & Withdraw) located at the same length from the tube device. Thus, the fluid pressure at the center of collagen (observation point) becomes 0 Pa, and no deformation occurs with the perfusion.

3.2.5 Image analysis

For the analysis of cellular contraction of HUVECs, the occupation area of GFP-HUVECs at the inner surface of the tube device was calculated by ImageJ software (NIH).

First, the fluorescent image was converted into a grayscale image by ImageJ. Then, the grayscale image was binarized by the image thresholding of ImageJ. Finally, the area of the cells was measured by ImageJ.

3.2.6 Numerical analysis

The traction forces of ECs generated by the immunological deformation reaction were calculated by the finite-element method (FEM) analysis software (COMSOL Multiphysics®, COMSOL Inc.). The collagen hydrogel tube was constructed on the software. The young's modulus of the collagen gel was measured by indentation method as 0.59 kPa and 0.24 kPa for 4 mg/mL and 2 mg/mL collagen, respectively. Poisson's ratio of the collagen was set to 0.475, referring to the reported values. Then, triangular meshes were formed on the model at the extra fine scale, which has a side length of 24 to 0.048 μm .

For the boundary condition, the measured deformation value of the inner surface was applied to the model. In detail, the change of the radius at the inner surface was set as the known displacement in polar coordinates. The stress that occurred on the ECs could be calculated with numerical analysis without any fixation condition because the model has no degree of freedom due to the central-axis-symmetry of the known displacement.

3.2.7 Statistical analysis

Student *t*-tests were used for data comparison. The calculated *p*-values were stated in the figures.

3.3 Theoretical calculation of the shear stress on ECs

The fluid shear stress on the cultured cells inside the collagen tube (from perfusion flow) was calculated as shown below^[117]. Because the flow area has a micro-scale (typically 500 μm to 1000 μm in diameter), the flow can be considered a fully developed laminar pipe flow. Therefore the flow was presumed as the laminar flow for calculation described as follows:

$$v_z = \left(-\frac{dp}{dz} \right) \frac{1}{4\mu} (R^2 - r^2), \quad (3.1)$$

where v_z (m/s) is the flow velocity in the axial direction, p (Pa) is the cross-sectional fluid pressure, μ (Pa·s) is the viscosity, R (m) is the radius of the inner surface of the collagen tube, and r (m) is the radius of the fluid cylinder under consideration. The flow mass Q (m³/s) is calculated by the integration of v_z ,

$$Q = \int v_z dA = \frac{\pi R^4}{8\mu} \left(-\frac{dp}{dz} \right) = \frac{\pi R^4 \Delta p}{8\mu L}, \quad (3.2)$$

where L (m) is the length of the collagen tube, and A (m²) is the sectional area of the hollow in the collagen tube. Δp is calculated by the balance of force below,

$$\pi R^2 \Delta p = 2\pi R L \tau, \quad (3.3)$$

where τ (Pa) is the shear stress at the inner surface. From equations (3.2) and (3.3), the relative equation of τ (Pa) and Q (m³/s) is derived as follows:

$$Q = \frac{\pi R^3}{4\mu} \tau. \quad (3.4)$$

Previous research reported that actin filaments in HUVECs were aligned to flow direction when 0.2 Pa fluid shear stress was inflicted on the cell surface for two hours^[118]. Therefore, the shear stress τ (Pa) was set to be 0.2 Pa. The viscosity of the medium was $\mu = 9.3 \times 10^{-4}$ Pa·s and the radius of the inner surface of the collagen tube used for the perfusion culture was $R = 2.5 \times 10^{-4}$ m. By substituting these values into the equation (3.4), the required flow mass is calculated as $Q = 2.64 \times 10^{-9}$ m³/s. The Reynolds number of the flow is calculated as $Re = 2\rho Q / \mu \pi R = 7.08$ by using the calculated flow mass and the density of the medium ($\rho = 980$ kg/m³), proving the flow as laminar flow.

3.4 Mediator-induced deformation reaction results

3.4.1 Deformation during vascularization of the tube device

Green-Fluorescent-Protein-expressed Human Umbilical Vein Endothelial Cells (GFP-HUVECs) were seeded on a fabricated collagen hydrogel tube (Figure 3.3(a,b)) to observe the behavior easily (Figure 3.3(c)). After four days of culture from seeding, GFP-HUVECs formed a confluent endothelial layer on the inner surface of the device (Figure 3.3(d)).

Next, the diameters of the fabricated vessel model were evaluated (Figure 3.3(e)). Before the vascularization of the device, the outer and inner diameters of the collagen gel layer were $2.39 \text{ mm} \pm 0.07 \text{ mm}$, $0.53 \text{ mm} \pm 0.02 \text{ mm}$, while those after vascularization were $2.38 \text{ mm} \pm 0.08 \text{ mm}$, $0.50 \text{ mm} \pm 0.02 \text{ mm}$, respectively (average \pm S.D., $n = 12$). Since the collagen tube was flexible, the inner diameter slightly shrank with vascularization. The lengths of the collagen layer in all devices were approximately 10 mm. All devices showed high uniformity in the diameter along with the collagen layer, and all coefficients of variations (C.V.) for the fluctuations in outer and inner diameters were less than 5%. The results indicate that the vessel model can be precisely fabricated by a simple molding process and culture.

3.4.2 Mediator-induced deformation reaction on the vessel model

Histamine (inflammatory mediator in allergy) was used in the immunological reaction experiments of the blood vessel model. GFP-HUVECs cultured in collagen tubes were exposed to 0.2 mg/mL of histamine four days after seeding. The behavior of the GFP-HUVECs under inflammatory reaction was observed by one-minute time-lapse imaging with a fluorescence microscope.

A time-lapse sequence image was generated to clearly observe the deformation

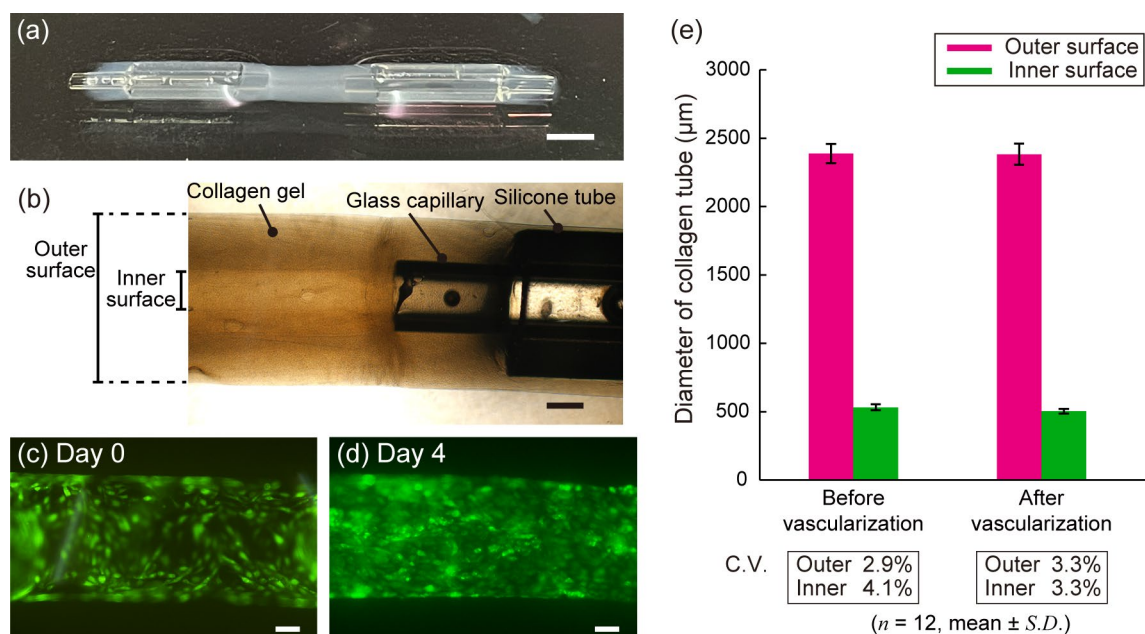


Figure 3.3 Results of fabrication and vascularization. (a) An overall picture of a tube device. The device had high uniformity in the diameter along the tube. (Scale bar: 5 mm) (b) A phase-contrast microscopic image of the tube. The direct connection of the collagen hydrogel to a glass capillary and a silicone tube was revealed. (Scale bar: 500 μm) (c) A fluorescence microscopic image of the GFP-HUVECs seeded on the inner surface of the collagen layer on Day 1. (Scale bar: 100 μm) (d) Proliferated GFP-HUVECs on Day 4. The ECs properly formed a confluent endothelial layer on the inner surface of the tube. (Scale bar: 100 μm) (e) The diameters of the device. The coefficients of variation (C.V.) for the diameter fluctuations were less than 5% on outer and inner diameters in both before and after fabrication.

(Figure 3.4(a)). The relative diameter (Dr) of the vascular model showed shrinking ($Dr = 0.974 \pm 0.005$ (average \pm S.D., $n = 3$)) and recovering behavior in tissue level (Figure 3.4(b)). Note that the diameter at 0 min was determined as the initial diameter to calculate Dr . The deformation is thought to be induced by ECs exposed to histamine because the control tube with no HUVECs showed no deformation under exposure.

Also, the deformation behavior of the collagen substrate was confirmed by time-lapse imaging of the blue-stained collagen layer and GFP-HUVECs (Figure 3.4(c)). The shrinkage of collagen substrate coincides with HUVECs on another time-lapse sequence

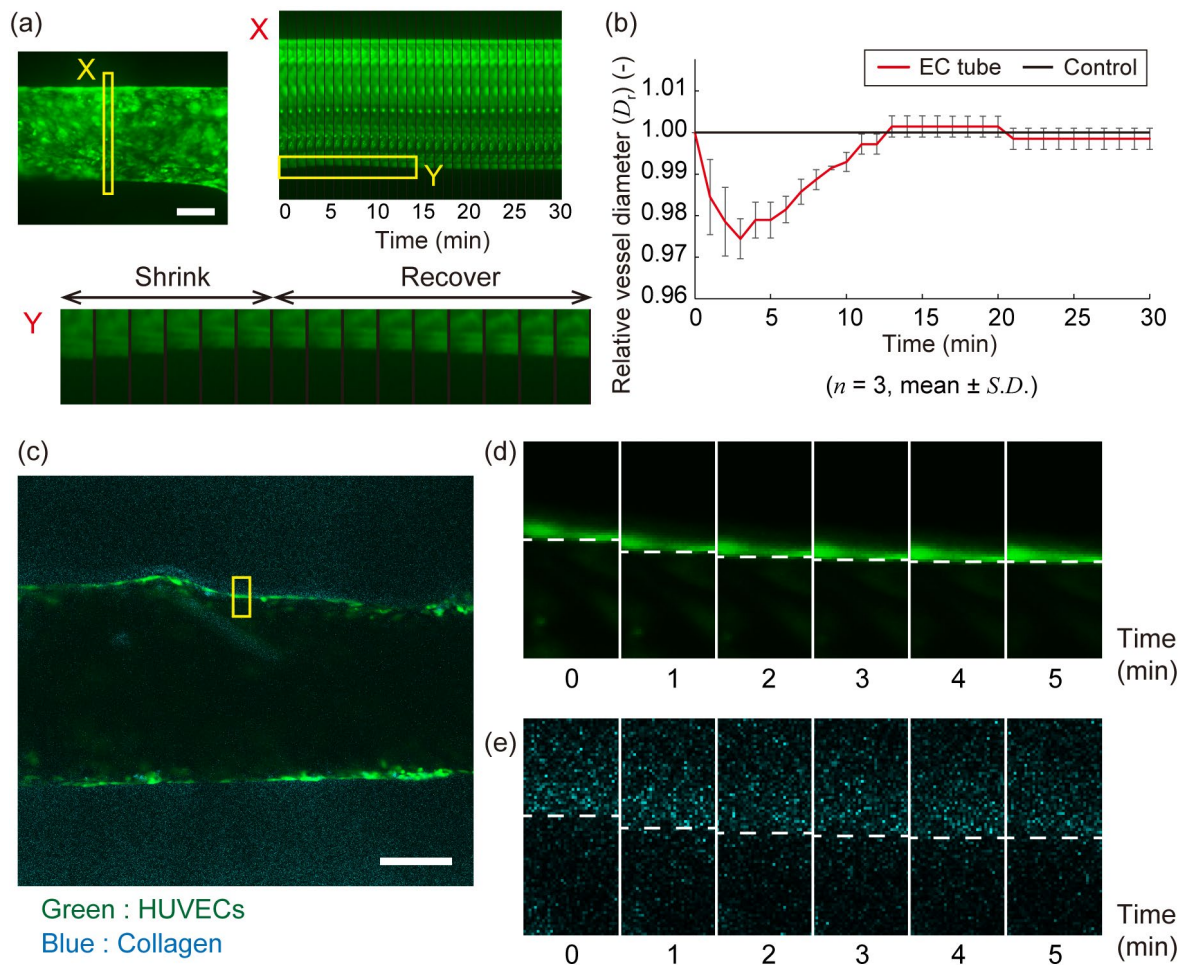


Figure 3.4 Immunological deformation reaction of the vessel model by histamine. (a) Fluorescent images of the EC layer exposed to histamine. (Scale bar: 200 μm) (b) The relative vessel diameter after adding 0.2 mg/mL of histamine. Shrinking and recovering behavior of the vessel in tissue scale was confirmed. (c) Deformation behavior of the collagen scaffold along with the shrinkage of GFP-HUVECs. The collagen layer was stained with the blue fluorescence by mixed with a NHS-labeled blue fluorescent dye (Scale bar: 200 μm) (d) An enlarged time-lapse sequence image of GFP-HUVECs inside the yellow frame. (e) An enlarged time-lapse sequence image of the inner edge of the collagen layer inside the yellow frame. The shrinkage behavior of HUVECs and collagen layer was completely the same.

image, denying the delamination of HUVECs from the substrate (Figure 3.4(d,e)).

Next, the shrinkage of the ECs at the cell level was investigated by image analysis. The cell area was measured using an image analysis software with the fluorescent images of GFP-HUVECs. The measured cell area was divided by the area of the inner surface of the collagen tube to calculate the cellular occupation ratio on the inner surface. The occupation ratio at 0 min was determined as the initial occupation rate to calculate the relative cell area (Ar) (Figure 3.5(a)). On the flexible vessel model, the relative cell area almost maintained $Ar = 1.0$, while cells on a rigid substrate (dish) as a control experiment could not maintain the same relative cell area (Figure 3.5(b)). The minimum Ar of the model and the rigid scaffold after reaction were 0.987 ± 0.009 and 0.769 ± 0.018 , respectively (average \pm S.D., $n = 3$). A Student t-test revealed the significant difference between the vessel models and the rigid substrates. ($p < 0.01$) (Figure 3.5(c)). Moreover, CD31 (junction marker) was stained by a human CD31 antibody with red fluorescence (Alexa 568) to check the behavior of junctions (Details of antibodies are shown in Appendix B). The immunostaining fluorescent images revealed that cadherin expressions were maintained at cell-cell junctions through the reaction on the vessel model (Figure 3.5(d)), while ECs on the rigid substrate lost cadherin expression at junctions of cells due to the detachment between cells (Figure 3.5(e)). The difference seems to be led by the tissue level deformation of the model, ensuring the high ability of the proposed model to reproduce biochemical reactions.

3.4.3 Difference of the behavior of vessels against various concentrations of histamine

The blood vessel models were exposed to various concentrations of histamine (0.1 to 6.4 mg/mL) to analyze the difference in the reaction of ECs. When the concentration of histamine was 0.4 mg/mL, the vessel shrank and recovered at the tissue level, and almost no change was observed in the cell shape (Figure 3.6(a)). On the contrary, under 6.4 mg/mL of histamine, the vessel could not contract much like 0.4 mg/mL, and the cells shrank visibly (Figure 3.6(b)). For a more detailed analysis of the difference, the relative vessel diameters were measured from time-lapse images (Figure 3.7(a)). The minimum diameter of the vessel

 Immunological deformation reaction of ECs on flexible collagen tube devices

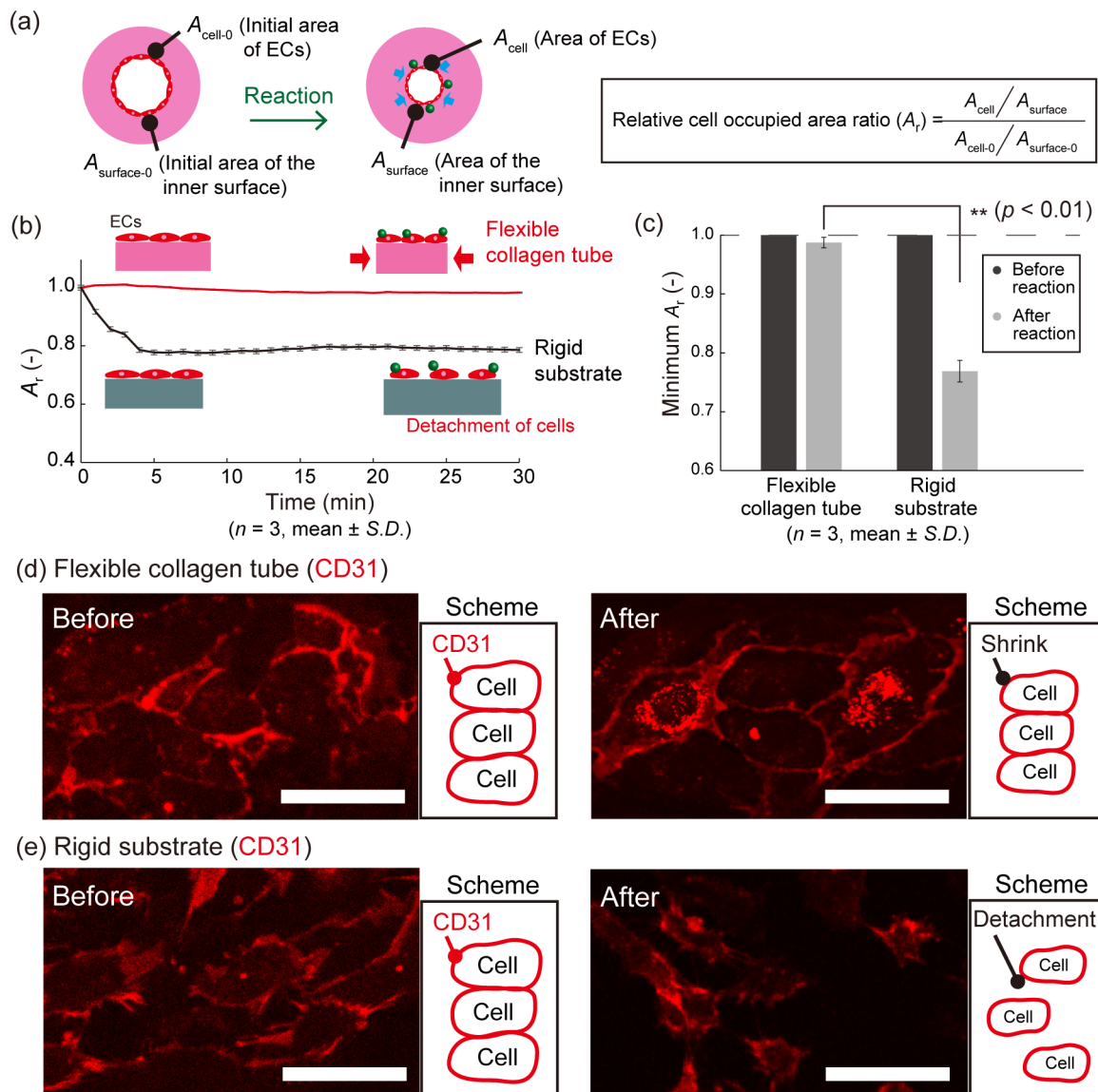


Figure 3.5 Cellular reaction of the vessel model to histamine. (a) A scheme of the tube deformation. (b) The relative cell area against the area of the inner surface after adding 0.2 mg/mL of histamine. The ECs of the vessel models occupied almost the same percentage during the exposure, while of the rigid scaffold are detached from each other and the occupation ratio decreased. (c) Comparison with rigid scaffolds in decreasing ratio of the cell area. The Student t-test revealed the significant difference between the vessel models and fixed scaffolds. ($p < 0.01$) (d,e) Immunostaining fluorescent images of CD31 expressed on the model and the rigid substrate. Even after the exposure of histamine, CD31 expressions were maintained at cell-cell junctions of ECs on the flexible collagen tube, while that of the rigid substrate were lost due to the cell shrinkage. (Scale bar: 50 μm)

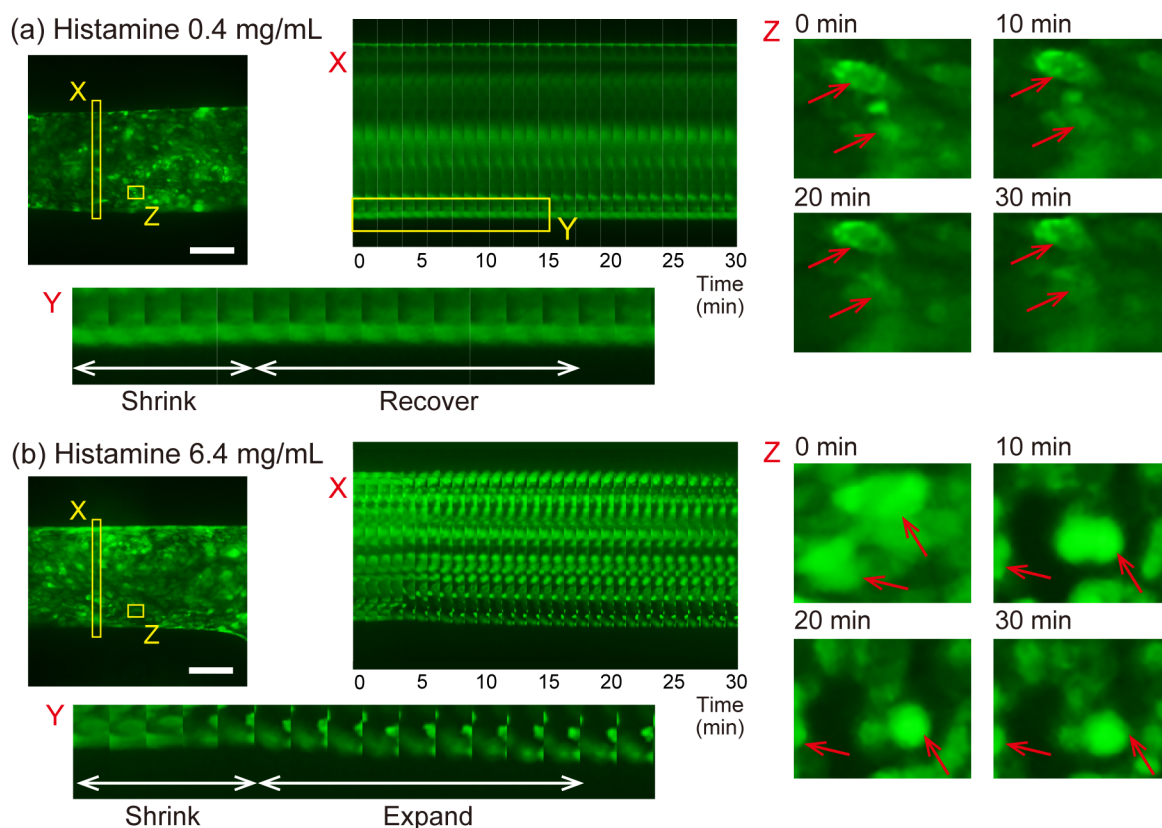


Figure 3.6 Effect of the concentration of histamine on the immunological reaction of blood vessel models. (a) Fluorescent images of the EC layer exposed to 0.4 mg/mL of histamine. (b) Fluorescent images of the EC layer exposed to 6.4 mg/mL of histamine. (Scale bars: 200 μm)

decreases along with the concentration in low value, but in the case of high concentration, the vessel could not contract well (Figure 3.7(b)). The relative cell occupation ratio was also measured and calculated from the time-lapse images (Figure 3.7(c,d)). ECs kept almost the same occupation ratio through the reaction under low histamine concentrations, while ECs under high concentrations could not maintain the initial occupation ratio. The results revealed that ECs under low concentration are connected even under reaction, while ECs under high concentration lost the junction by the excess contractile force generated on the cells. Moreover, since the vessels which lost cell-cell adhesion could not contract at the tissue level, the vessel shrinkage was concluded to be actuated by the contractile force between cells.

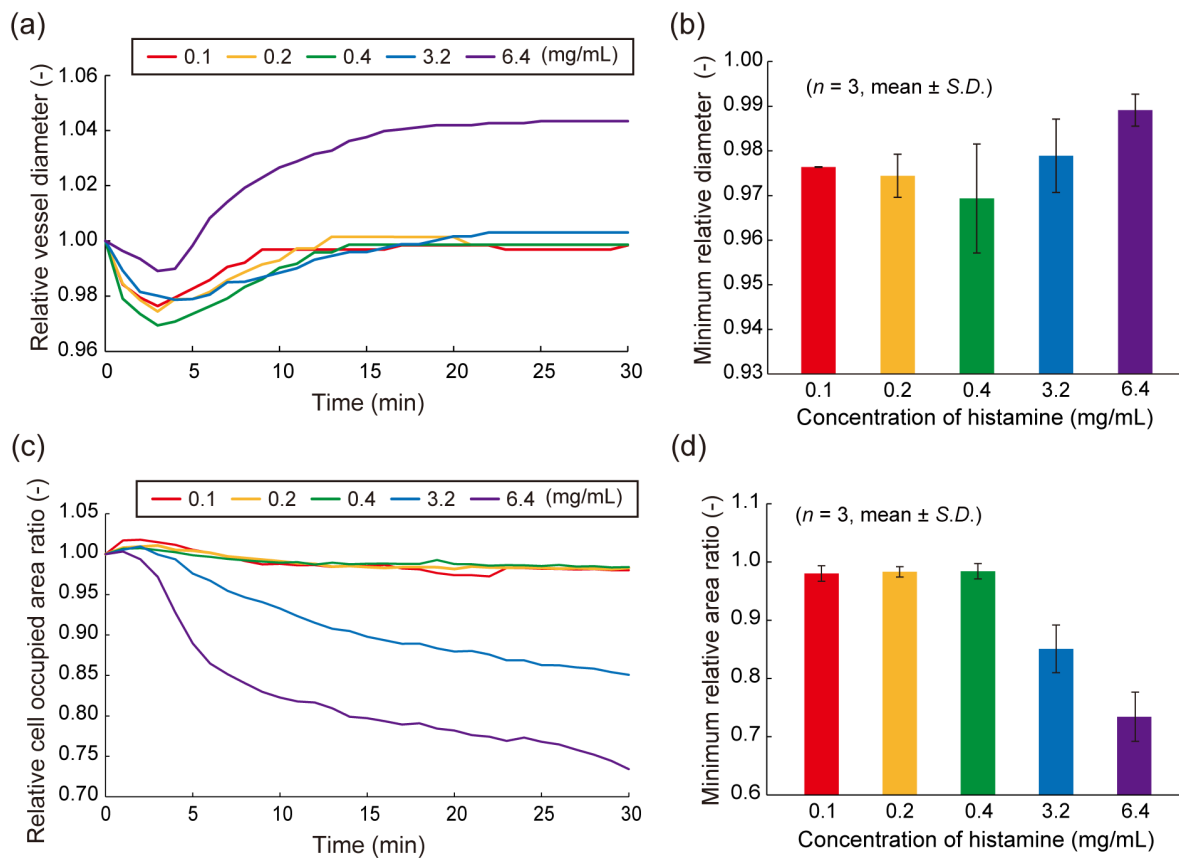


Figure 3.7 Relationship between the concentration of histamine and the deformation of vessel models. (a) The behavior of the relative diameters of the vessels. The shrinking and recovering behavior could not be observed in high concentration. (b) The minimum relative diameter of the vessel in different concentrations. The shrinking ratio increased along with the concentration in low value and decreased in high value. (c) The behavior of the relative cell area of the vessel. (d) The minimum cell area of the vessel in different concentrations. The cells occupied almost the whole inner surface in low concentration, while the cell area decreased in high concentration.

3.4.4 Numerical analysis of cell traction force

As indicated in the above experiments, the deformation behavior of the vessel model both in tissue and cell levels was observed. Recently, mechanical force is revealed to

be a critical factor in various biochemical phenomena in tissues^[30]. Also, the information on the force that occurred at the tissues could be used to design tissue models to mimic the environments of native tissues in high similarity. Therefore, the traction force of the ECs on the vessel model was evaluated by numerical analysis.

First, vascular models with different stiffness of collagen ($E = 0.59$ kPa and 0.24 kPa) were prepared and exposed to 2 mg/mL of histamine. Then, the deformation of the vessel models was measured from fluorescent images in the same way as the above experiments (Figure 3.8(a)). The shrinking ratio of the vessel was larger on a softer vessel in the same concentration of histamine (Figure 3.8(b)). After that, the initial tube shape, property of the material, and deformation values were reconstructed in the finite-element method (FEM) analysis software to analyze the traction force generated on the vessel model.

From the cross-sectional view, the gradient of the stress value along the radial direction was observed (Figure 3.8(c,d)). Note that the hue shows the stress value at each point after deformation. Since the stress and traction force could be approximate as uniform along the tube, the traction force generated by each cell was calculated as follows:

$$F = \sigma \times d_{cell} \times d_{tube} \pi \quad (3.5)$$

where F (N) is the traction force of each cell, σ (Pa) is the stress, d_{cell} (m) is the diameter of a cell, and d_{tube} (m) is the inner diameter of a vessel model.

The traction forces of the cells on the vascular models of 0.4 wt% and 0.2 wt% collagen gel were calculated as 0.849 μ N and 0.889 μ N, respectively. Even though the shrinking amount of the vessel diameter was more than two times higher in 0.2 wt% collagen gel than 0.4 wt%, the difference in the traction force was less than 5 %. The results indicate that the traction force is not changed by the stiffness of the scaffold, and the deformation could be designed by the property of the scaffolds.

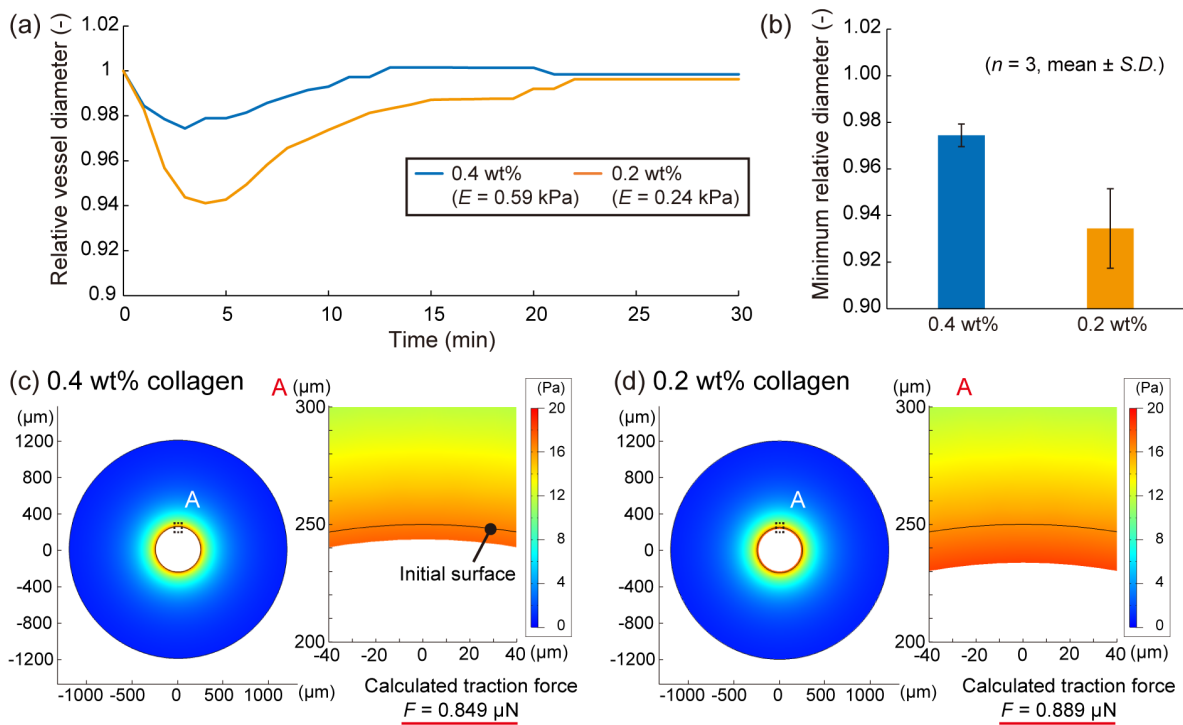


Figure 3.8 Contraction force analysis of the blood vessel model. All models were exposed to 0.2 mg/mL of histamine. (a) The behavior of the relative vessel diameter of two types of stiffness. (b) The minimum relative diameter of the vessel with vessels of different stiffness. (c) The calculation of the cellular traction force on 0.4 wt% collagen tube through numerical analysis. The color bar shows the stress value. (d) Calculation of the cell traction force on 0.2 wt% collagen tube. Almost the same traction forces (less than 5 % difference) were derived from collagen tubes of different stiffness.

3.4.5 Drug testing demonstration with anti-histamine

Finally, a drug test was demonstrated to prove the capability of the proposed blood vessel model for pharmacokinetic testing with olopatadine hydrochloride (an ingredient of anti-histamine pharmaceuticals). The vascular models were exposed to 0.2 mg/mL of histamine along with 0.1 mg/mL olopatadine four days after seeding. To mimic *in vivo* situation, histamine was exposed to the model from the culture medium on a dish by

 Immunological deformation reaction of ECs on flexible collagen tube devices

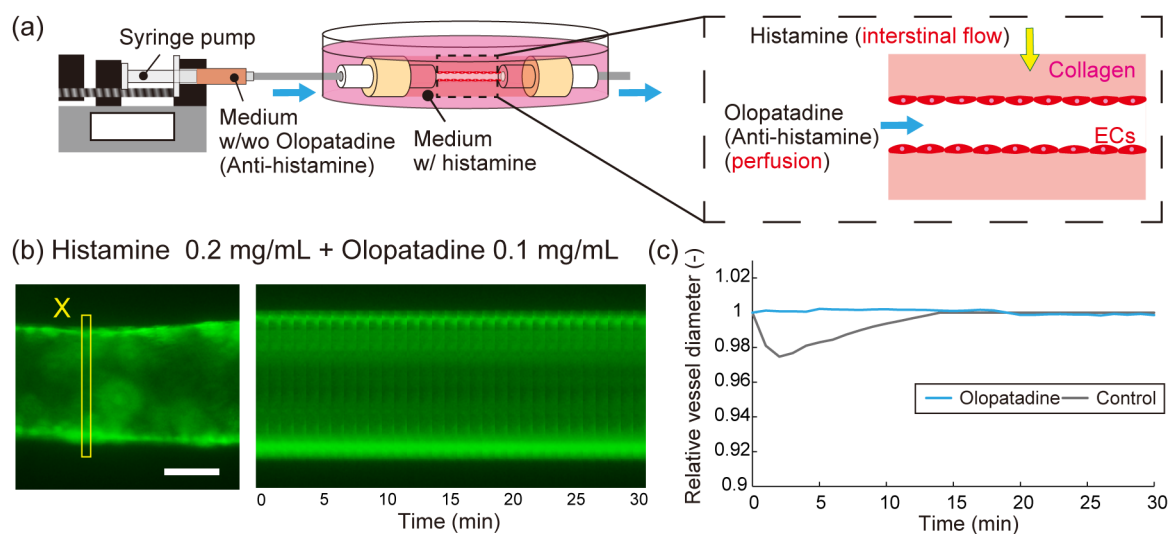


Figure 3.9 Drug test demonstration with olopatadine hydrochloride (an anti-histamine). (a) A schematic image of the perfusion set up. The collagen tube was connected with a syringe pump containing a medium with olopatadine. In control experiments, a medium without olopatadine was flowed into vessel models. (b) Fluorescent images of the EC layer exposed in 0.2 mg/mL of histamine and 0.1 mg/mL of olopatadine. (Scale bar: 100 μm) (c) The behavior of the relative vessel diameter under reaction. The vessel model treated with the flow including olopatadine showed no shrinkage, ensuring that olopatadine properly worked as an anti-histamine drug model.

interstitial flow, and olopatadine was flowed inside the lumen by perfusion from a syringe pump (Figure 3.9(a)). As a control experiment, a culture medium without olopatadine was flowed into the vascular models. The behavior of the GFP-HUVECs under inflammatory reaction was observed by one-minute time-lapse imaging with a fluorescence microscope.

Same as the experiments of histamine reaction, a time-lapse sequence image was generated from the observation, and the behavior of the relative diameter was measured (Figure 3.9(b,c)). The vessel exposed to olopatadine showed no contraction in tissue level and maintained almost the same relative diameter, while the control model showed contraction by the exposure. The result proved that olopatadine properly inhibits the histamine reaction in the same form that simulates blood flow and interstitial flow *in vivo*,

ensuring the capability of the device for pharmacokinetic testing focusing on the evaluation of whole tissue reaction.

3.5 Conclusion

In this chapter, an inflammatory mediator-induced deformation reaction is reproduced with the fabricated blood vessel on a flexibly deformable collagen hydrogel tube device.

A self-standing collagen tube enabled the tissue to deform flexibly in biochemical reaction and achieved contraction both at tissue and cell levels. The contraction of tissue relieved the stress between cells under reaction to maintain cellular junction. Also, the drug perfusion test with the anti-histamine chemical was easily performed due to the connector part and properly inhibited the inflammatory reaction. Moreover, the traction force on ECs was analyzed as about 0.9 μN on two types of scaffolds with different stiffness. These results indicate that the EC layer constructed on the proposed device can react to immunological stimulation flexibly as a platform for biomedical research.

CHAPTER 4.

Circumferentially aligned and immunologically deformable SMCs by RuM-M method

4.1 Introduction

In this chapter, a blood vessel model with a circumferentially aligned smooth muscle layer is proposed. By rolling up an axially aligned smooth muscle fiber, a circumferential alignment is easily formed in a self-standing collagen tube to construct a flexible blood vessel model (Rolling up maturation molding (RuM-M) method) (Figure 4.1).

First, the formation of the axially aligned SMC fiber is confirmed by microscopic observation, fluorescent observation, and image analysis. Then, the dense fiber is rolled up to form a circumferentially aligned SMC layer in a collagen tube and confirmed the alignment in the same way. After that, ECs are seeded into the tube to form a self-standing *in vitro* blood vessel model with the co-culture of the circumferentially aligned SMC layer and EC layer. Finally, the immunological deformation reaction of the co-cultured endothelium and smooth muscle is reproduced by exposure to histamine.

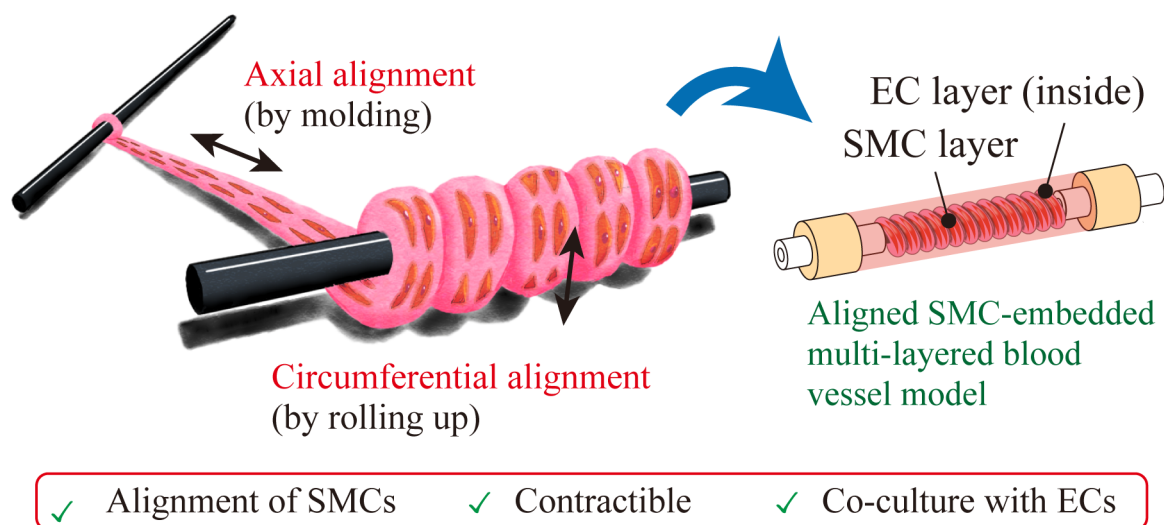


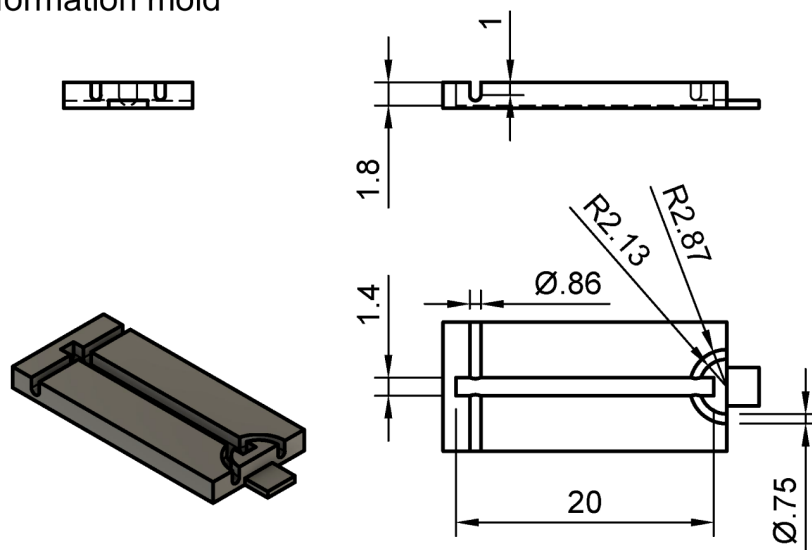
Figure 4.1 Circumferentially aligned and contractive SMC layer fabrication by rolling up maturation molding method (RuM-M method). By rolling up an axially aligned smooth muscle fiber, a circumferential alignment is easily formed in a self-standing collagen tube to construct a flexible blood vessel model. The circumferentially aligned SMCs can contract the blood vessels in immunological reactions as same as *in vivo*. Also, the flexibility of the collagen tube enables the tissue deformation induced by contraction of SMCs. Moreover, the co-culture with endothelium and perfusion culture can be easily achieved.

4.2 Fabrication method

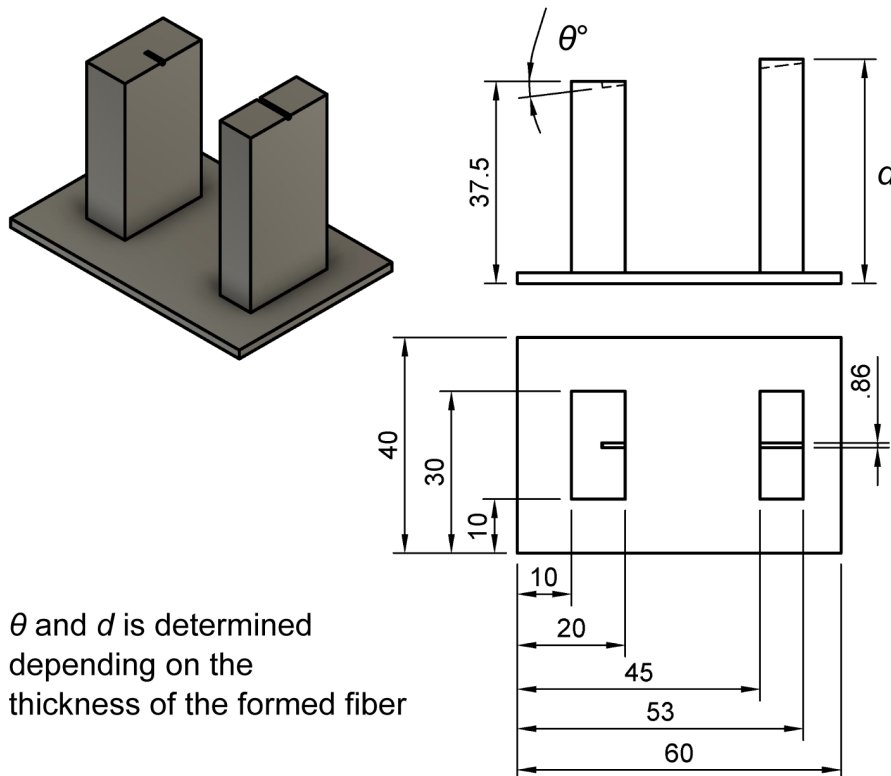
4.2.1 Design of the mold

A fiber formation mold (Figure 4.2(a)), a rolling up mold (Figure 4.2(b)), and an embedding mold (Figure 4.3) were prepared for the fabrication. The molds were composed of polydimethylsiloxane (PDMS) or polylactic acid (PLA). The PDMS mold was fabricated by soft lithography using an acrylic mold. The PLA mold was fabricated by fused deposition modeling (FDM) 3D printing. Note that the slope angle of the rolling up mold was determined depending on the thickness of the formed fiber in each condition.

(a) Fiber formation mold



(b) Rolling up mold



* θ and d is determined depending on the thickness of the formed fiber

Figure 4.2 Drawings of the molds for SMC layer construction (Only important lengths are written). (a) A fiber formation mold. (b) A rolling up mold for circumferential alignment.

Embedding mold (for 4 device fabrication)

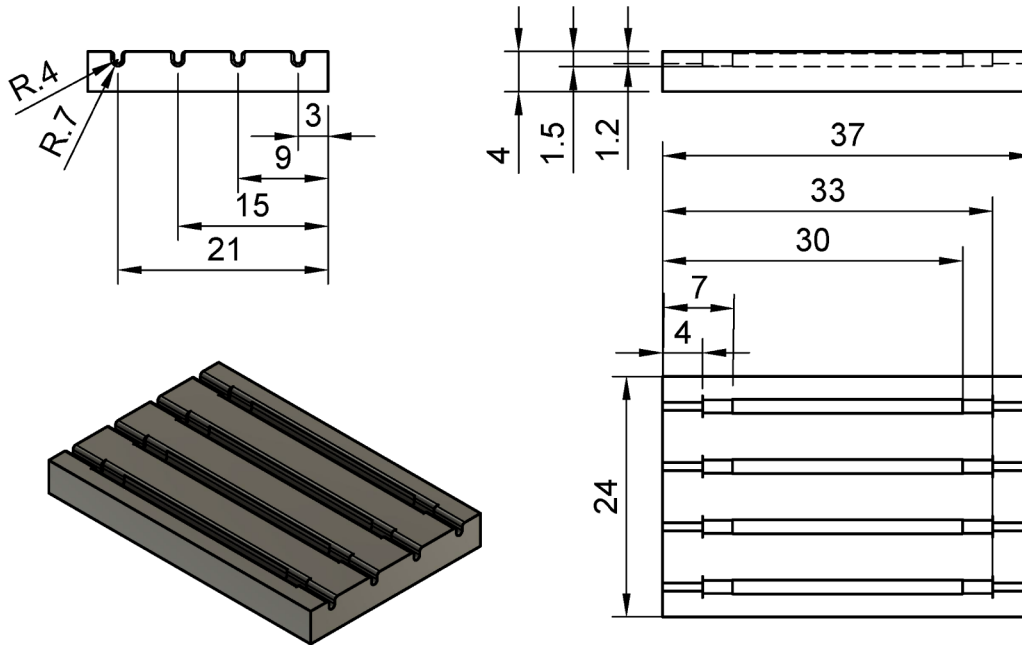


Figure 4.3 A drawing of the embedding mold for fabrication of 4 devices. (Only important lengths are written).

4.2.2 Preparation of cell suspended pre-gel solution

Human umbilical artery smooth muscle cells (HUASMCs) were used as an SMC model for the experiments.

HUASMCs are one of the most popular SMC models used for *in vitro* experiments for the same reason as HUVECs because human umbilical veins are relatively more available than other human blood vessels. As mentioned in section 1.3.1, SMCs construct the tunica media and regulate the blood flow mass by contraction and relaxation^[15]. HUASMCs are isolated from the umbilical veins of donors and cryopreserved to make the cells commercially available.

The culture medium was Smooth Muscle Cell Growth Medium (SMCGM) supplemented with a bullet kit for the HUASMCs, and Endothelial Growth Medium (EGM-

2) supplemented with a bullet kit for the HUVECs. To co-culture HUASMCs and HUVECs, the mixture of the SMCGM and EGM-2 at the volume ratio of 1:1 was used. Prior to cell seeding, cells were incubated in dishes at 37°C in a humid atmosphere with 5 % CO₂, and the medium was replaced every three days.

To suspend HUASMCs into the collagen pre-gel solution, cells were first dissociated from the dishes by trypsinization with trypsin EDTA. Then, the trypsinized HUASMCs were suspended in a collagen pre-gel solution prior to the fabrication process.

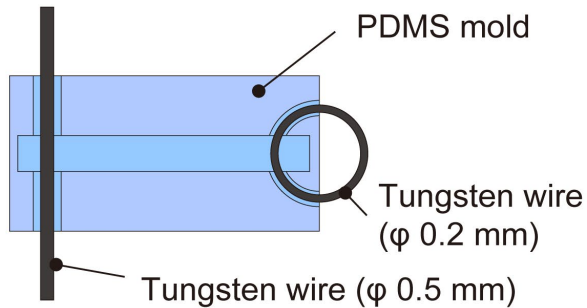
To seed HUVECs onto the surface of collagen, the trypsinized HUVECs were suspended in the medium, and the cell suspension was directly injected into the hollow of the device.

4.2.3 Formation method of the SMC fiber

The fabrication method of the HUASMC tube was divided into two steps: unfixed molding for the formation of SMC fiber, and rolling up and covering with collagen to obtain an SMC layer embedded collagen tube. The detailed formation method of the SMC fiber is as below:

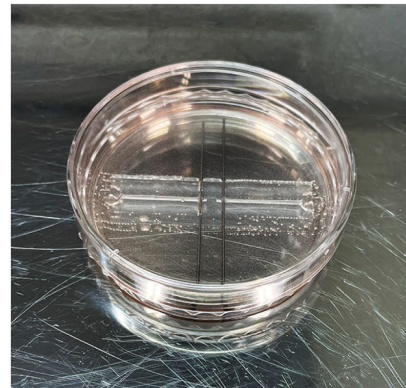
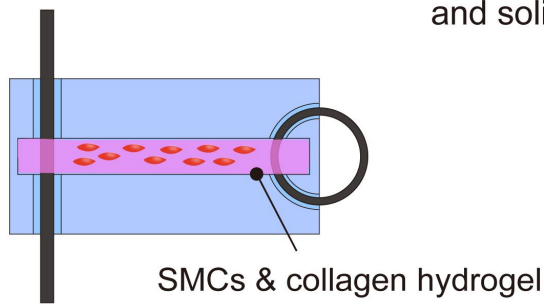
- (i) A straight-shaped tungsten wire and a circle-shaped tungsten wire were embedded into a fiber formation mold (Figure 4.4(a))
- (ii) The HUASMC-suspended (0.8 or 1.0×10^6 cells/mL) collagen pre-gel solution (1.0 or 2.0 mg/mL) was poured into the mold and solidified by incubation at 37°C (Figure 4.4(b)).
- (iii) The tissue was cultured 24 h in the medium (SMCGM) to induce contraction and axial alignment by the cells themselves to form a dense fiber (Figure 4.4(c)).

(a) Assemble the molds



(2 molds are connected in line symmetric)

(b) Pour cell-suspended collagen solution and solidify



(c) Culture 24h to form aligned SMC fiber

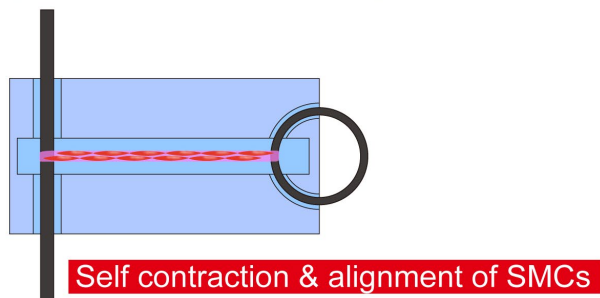


Figure 4.4 Formation method of a SMC fiber. (a) A straight-shaped tungsten wire and a circle-shaped tungsten wire were embedded into a PDMS mold (b) A SMC-suspended collagen pre-gel solution was poured into the mold and solidified by incubation at 37°C. (c) The tissue was cultured 24 h to induce contraction and axial alignment by the cells themselves to form a dense fiber.

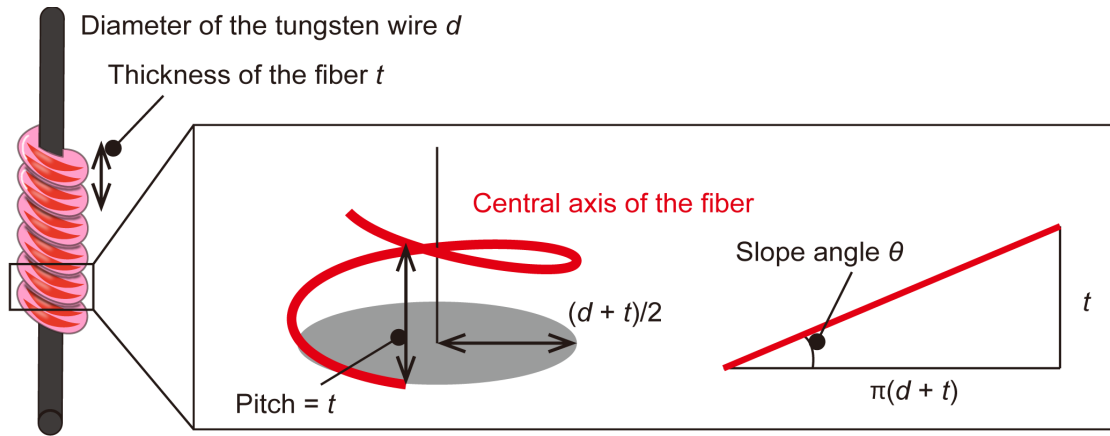


Figure 4.5 A geometric scheme of the rolled-up fiber. The slope angle of the rolling up mold depends on the thickness of the fiber and the diameter of the tungsten wire.

4.2.4 Fabrication of the SMC layer embedded blood vessel model

The formed dense SMC fiber was rolled up and embedded with collagen gel to fabricate a flexibly deformable collagen tube device with a circumferentially aligned SMC layer. Before the fabrication, the slope angle of the rolling up mold was designed with the formed fiber. The pitch of the spiral of the rolled-up fiber has to be the same as the thickness of the fiber to roll up the fiber with no gaps (Figure 4.5). Thus, the slope angle θ ($^{\circ}$) is calculated as follows:

$$\theta = \tan^{-1} \left(\frac{t}{\pi(t + d)} \right) \quad (4.1)$$

where t (mm) is the thickness of the fiber and d (mm) is the diameter of the tungsten wire. The detailed fabrication method of the tube device with the rolling up mold designed with the equation (4.1) is as below:

- (i) The formed aligned HUASMC fiber was removed and fixed on a rolling up mold with covers (Figure 4.6(a)).
- (ii) The tungsten wire was rotated to roll up the SMC fiber around the wire (Figure 4.6(b)).

- (iii) Connectors composed of silicone tubes and glass capillaries were inserted into the tungsten wire from both sides (Figure 4.6(c)).
- (iv) A collagen pre-gel solution (4 mg/mL) was poured around the SMC layer and connectors using the embedding mold to cover by collagen tube. Then, collagen was solidified by incubation at 37°C (Figure 4.6(d)).
- (v) The mold was removed to obtain the collagen tube with a circumferentially aligned SMC layer inside (Figure 4.6(e)).
- (vi) By seeding ECs inside the tube, an arterial tissue model was obtained (Figure 4.6(e)).

4.3 Experimental method

4.3.1 Florescent staining and observation

For the evaluation of the alignment of the actin fibers were stained by a live-cell actin probe (SPY-555 actin, Spirochorme). The fabricated tissue was immersed into a diluted SPY-555 actin solution (1/1000000) and incubated for 1 hour to stain the actin of the HUASMCs. The observation with the inverted fluorescence/phase-contrast microscope and the immunostaining were the same protocol as in chapter 2 (Details of antibodies are shown in Appendix B). On the time-lapse imaging, the top edges of the HUASMC layer of trimmed images were aligned while generating the time-lapse sequence image to compare the shrinking behavior easily.

4.3.2 Image analysis of the SMC alignment

The alignment of the HUASMCs was analyzed by measuring the direction of the actin filaments in HUASMCs with an image analysis software (ImageJ) with LPixel ImageJ plugins (LPixel)^[119]. First, the fluorescent images of actin filaments of SMCs stained by a live cell actin probe were obtained by fluorescence microscope. After that, the image was

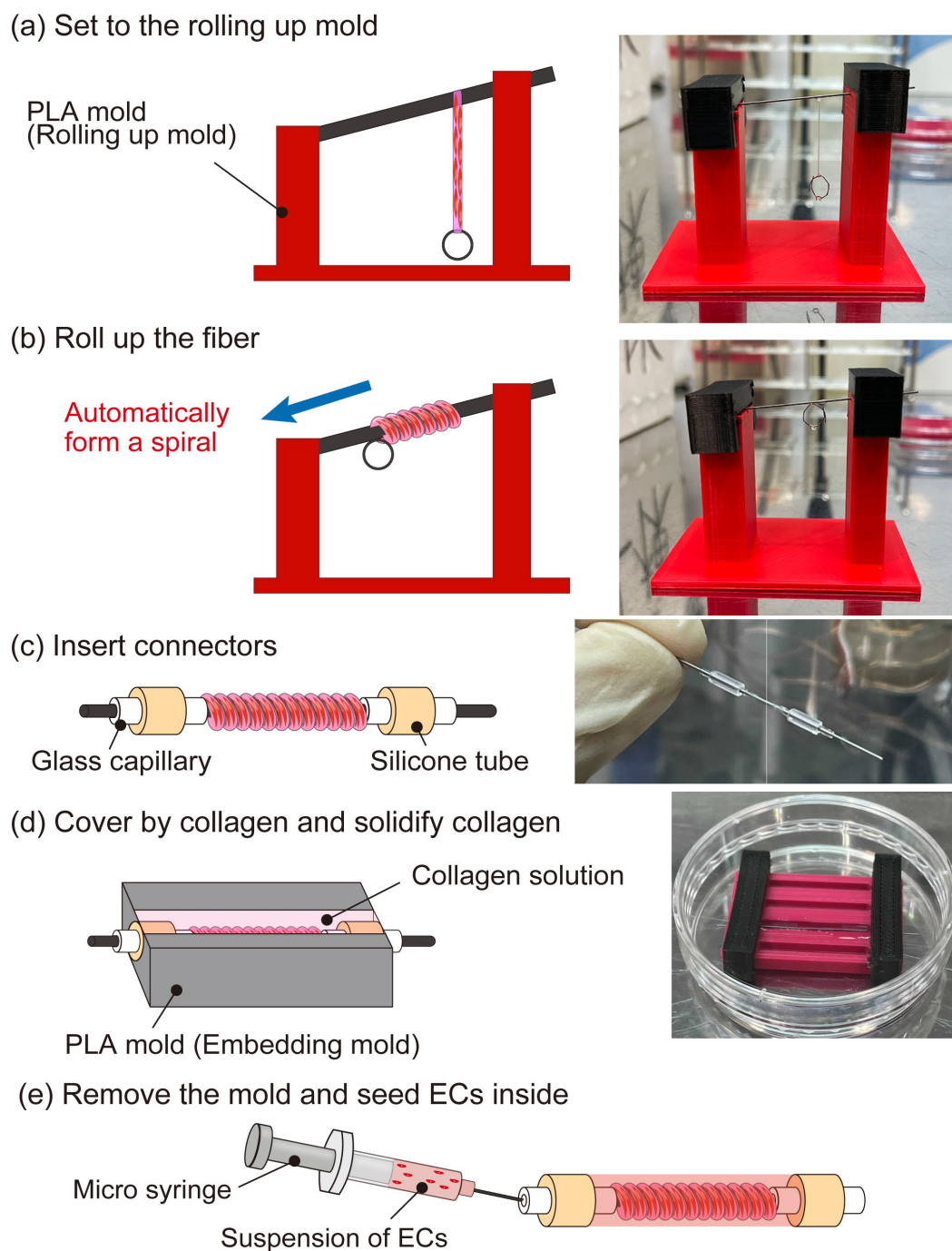


Figure 4.6 Fabrication of a SMC layer embedded blood vessel model. (a) Set the fiber to the rolling up mold. (b) Roll up the fiber to spiral shape. (c) Insert glass capillaries and silicone tubes as connectors. (d) Pour a collagen pre-gel solution and solidify by incubation at 37°C. (d) Remove the mold and seed ECs inside.

binarized by the image thresholding of ImageJ. Then, LPixel was used to extract the morphologies of actin filaments as skeleton images. This was done in line extract mode by using a multidirectional non-maximum suppression algorithm. Finally, the parallelness of each skeleton image was calculated from the line angle measurements in LPixel.

4.3.3 Contraction demonstration with histamine

Same as chapter 3, histamine, an inflammatory mediator, was used to demonstrate the biochemical contractile reaction. The SMC embedded collagen tube was exposed to 0.2 mg/mL histamine in the medium, and the deformation was observed with a microscope in real-time. Note that a collagen tube encapsulating SMCs directly with no alignment was prepared as a control. The contraction rate of the tissue for the axial and circumferential direction was measured from fluorescent images.

The co-culture model of SMCs and ECs was also exposed to histamine to demonstrate cellular interaction. The concentration of histamine was 0.2 mg/mL. Moreover, *N* ω -nitro-L-arginine methyl ester hydrochloride (L-NAME) was added to the co-culture model to prove the cellular interaction between SMCs and ECs. The relaxation reaction (indirect reaction) of SMCs is induced by NO released from ECs under exposure to histamine. L-NAME is a nitric oxide synthase inhibitor (NOS inhibitor), which prevents the generation and release of NO from the ECs^[120]. Thus, 300 μ M of L-NAME and 0.2 mg/mL of histamine were exposed to the co-cultured blood vessel model to prove the NO-related interaction between SMCs and ECs.

The contraction and recovering behavior were observed for 180 min, and the relative diameter of the model was calculated by dividing by the initial diameter (0 min).

4.4 Fabrication results

4.4.1 Formation results of the HUASMC fiber

First, the axially aligned HUASMC fiber was formed with a fiber formation mold of 1.6 mm width. The concentration of the cell suspension was 1.0×10^6 cells/mL. The encapsulated SMCs in the collagen hydrogel (Figure 4.7(a)) aggregated and formed a dense fiber shape within 24 hours (Figure 4.7(b)). There was no significant difference in the observed images between 24 and 48 hours of culture (Figure 4.7(c)). The diameters of the fibers were measured from the microscopic images, and the shrinking ratios were calculated as 73.5% and 74.9% for the fibers cultured 24 hours and 48 hours, respectively (Figure 4.7(d)). The result revealed that the cells aggregate to about one-fourth diameter, indicating the high-dense SMC fiber formation.

Next, the width of the fiber formation mold was varied to check the behavior of the formation of the SMC fibers. With a mold of 1.4 mm width, the SMC fiber was formed at a similar time scale as a mold with 1.6 mm width, while the thickness of the fiber was decreased (Figure 4.8(a,b)). The shrinking ratio was also about 75% for 1.4 mm mold. When the width of the mold was set under 1.0 mm, HUASMCs could not form a fiber and were scattered in the mold (Figure 4.8(c)). The cause may be the tissue could not endure the tension between cells due to the thinness of the fiber.

The concentration of the cells in the suspension and collagen gel was also varied to check the behavior of the fiber formation (Figure 4.8(d)). The thickness was changed by controlling both the concentration of HUASMCs and collagen from approximately 200 to 400 μm (Figure 4.8(e,f)).

4.4.2 Evaluation of the axial alignment of the SMC fibers

To evaluate the alignment of the SMC fibers, actin filaments in SMCs were stained with a live-cell actin probe (Figure 4.9(a)). From the enlarged fluorescence microscopic

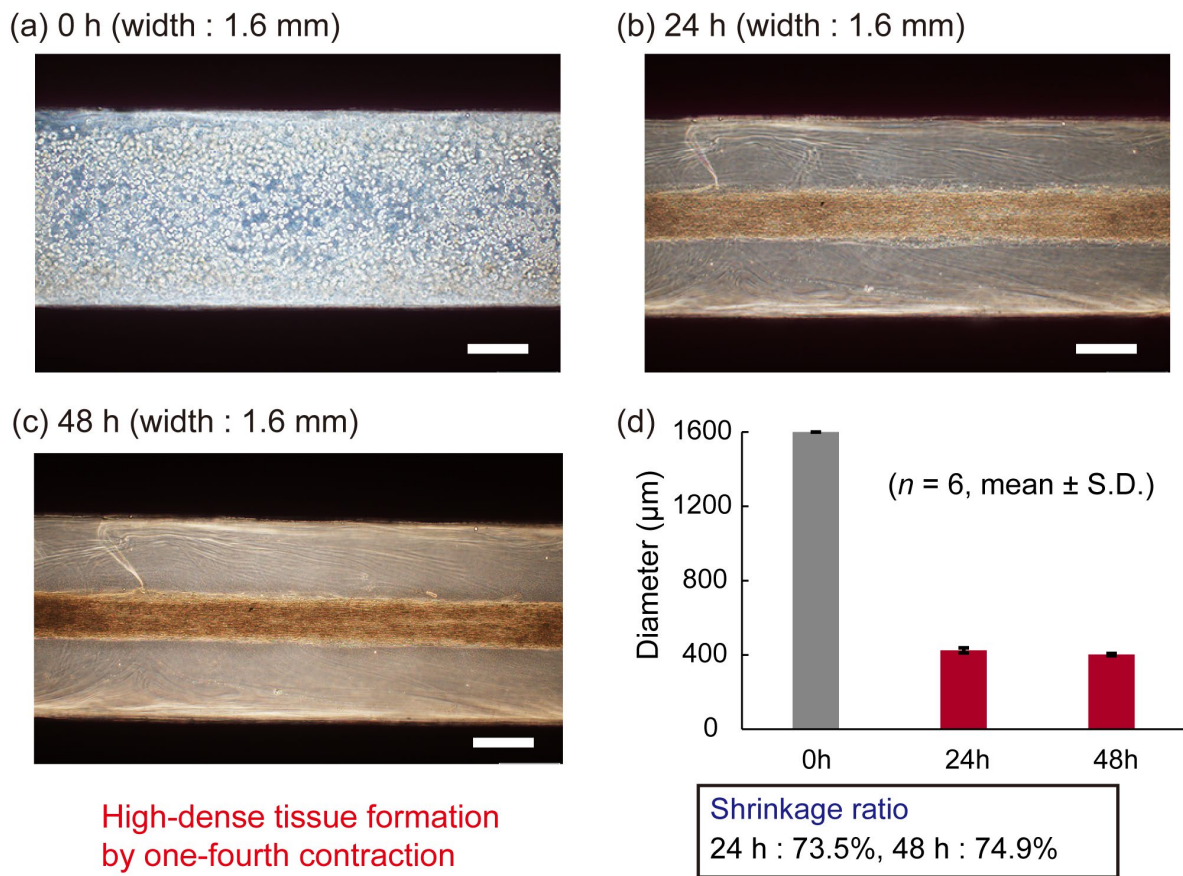


Figure 4.7 Formation results of the HUASMC fiber in a typical condition. (a) A phase-contrast image of the HUASMCs just after seeding. (b) A phase-contrast image of the HUASMCs cultured 24 hours. The cells aggregated and form a dense fiber shape. (c) A phase-contrast image of the HUASMCs cultured 48 hours. No significant difference was observed with the 24-hour culture. (d) Diameter behavior of the HUASMC fiber. The shrinking ratio was calculated as about 75%. (Scale bars: 500 μm)

image, the axial alignment of the actin of SMCs was visibly observed (Figure 4.9(b)). The directionality of the actin filaments was analyzed by extracting the lines of actin from the fluorescent images with image analysis software. The histogram of the ratio of the actin filaments for each direction showed alignment of HUASMCs for the fiber direction. Note that 0° was defined as the fiber direction. The average direction and dispersion were 0.21°

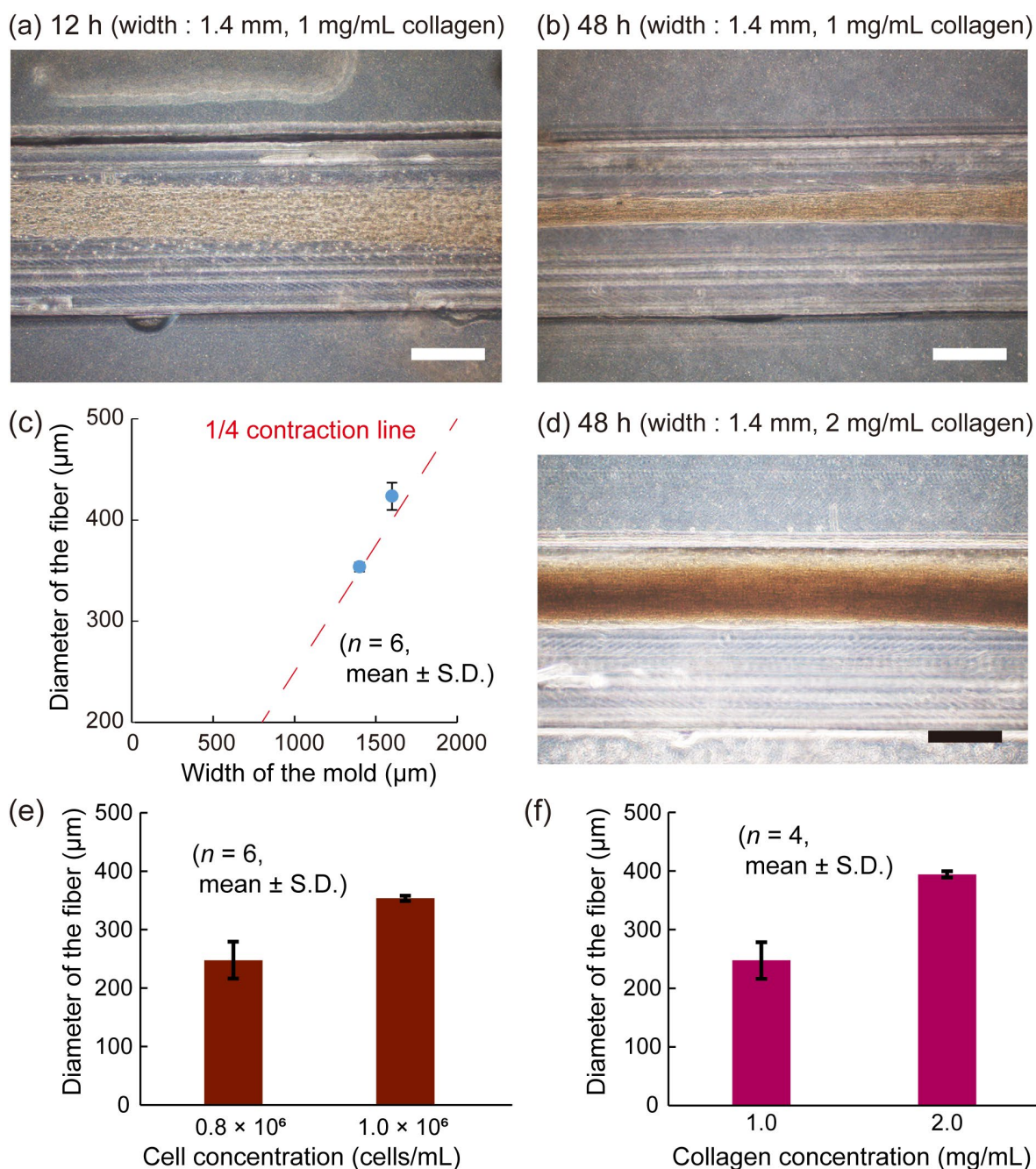


Figure 4.8 Behavior of the formation of HUASMC fibers under various conditions. (a,b) Phase-contrast images of the HUASMCs cultured 12 and 48 hours in a mold with 1.4 mm width. (c) Diameters of the formed dense fibers in different width of the fiber formation mold. The diameter almost followed the one-fourth contraction line. (d) A phase-contrast image of HUASMCs with 2 mg/mL of collagen. (e,f) The effect of the cell concentration and collagen concentration on the diameter of the HUASMC fiber. (Scale bars: 500 μm)

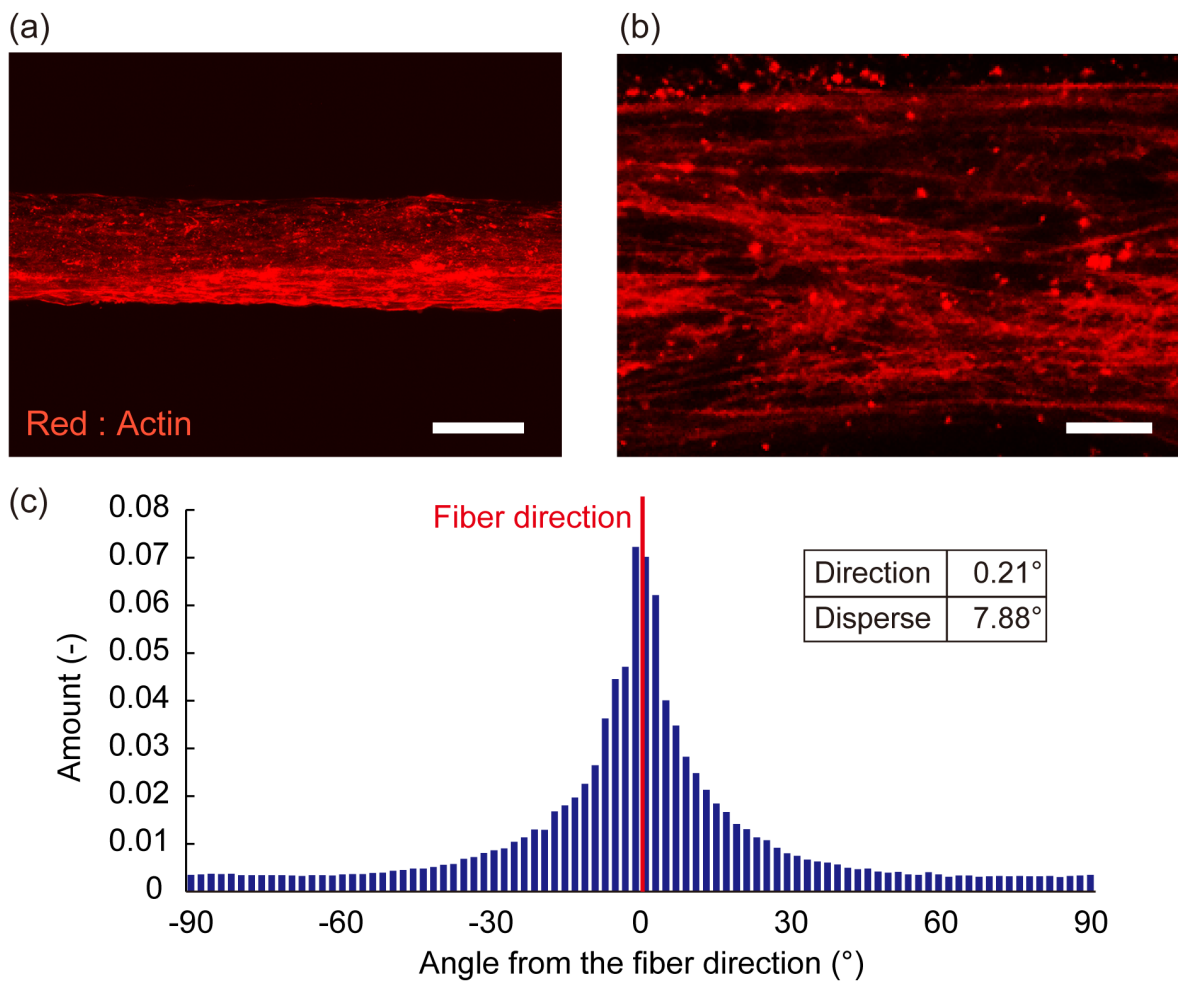


Figure 4.9 Evaluation of the alignment of SMCs in the fiber. (a) A projection image of z-stack confocal fluorescent images of the actin filaments of HUASMCs stained with live cell actin probe. (Scale bar: 200 μm) (b) An enlarged view. The axial alignment was observed. (Scale bar: 10 μm) (c) The directionality of the actin filaments in the HUASMC fiber by image analysis.

and 7.88° (Figure 4.9(c)). The values ensured the axial alignment of SMCs by the fiber formation process.

4.4.3 Fabrication results of the SMC layer embedded collagen tube

Next, the formed fiber-shaped SMC tissue was rolled up and embedded by collagen

gel to fabricate a collagen tube device with a circumferentially aligned SMC layer inside.

The fiber of about 300 μm thickness was used for the tube device fabrication. Thus, by substituting the value to the equation (4.1), the slope angle of the rolling up mold was determined as 7° .

A rolled-up SMC-embedded collagen tube was easily and stably fabricated (Figure 4.10(a)). A phase-contrast image revealed the existence of the rolled-up SMC fiber inside the collagen tube (Figure 4.10(b)). The actin filaments of the rolled-up SMCs were observed by live imaging of actin, and circumferential alignment was confirmed visibly (Figure 4.10(c)). Again, the directionality of the actin filaments was analyzed by extracting the lines of actin from the fluorescent images with image analysis software. The histogram of the ratio of the actin filaments for each direction showed alignment for the vertical direction from the tube direction. Note that 0° was defined as the tube direction. The average direction and dispersion were 80.8° and 9.82° (Figure 4.10(d)) in a sample, and the mean of the average direction of SMCs in 5 fabricated tubes was calculated as $78.95 \pm 1.79^\circ$. Since the rolling up mold gave a 7° slope for the tungsten wire, the direction of the actin in rolled-up SMCs should come around 83° . Thus, the results proved the fabrication method properly achieved the circumferential alignment of SMCs in the tube device. Also, the mean of the average direction has 2.2% of the coefficient variation, ensuring the stable fabrication of the circumferentially aligned SMC layer (Figure 4.10(e)).

From the perspective of the reproductivity of *in vivo* tissue, SMCs in the native tissues are known to form a helical structure with a wide range of helical pitch angle (from 30° or less to 70° or more)^[121]. The angle differs by the kind of vessels, the thickness, the blood pressure, and other numerous conditions. Comparing to the *in vivo* value, the SMCs of the proposed models have less helical pitch angle. However, the pitch angle would be able to control by changing the fabrication condition because the results proved that the thickness of the SMC fiber and the rolling up angle could be controlled.

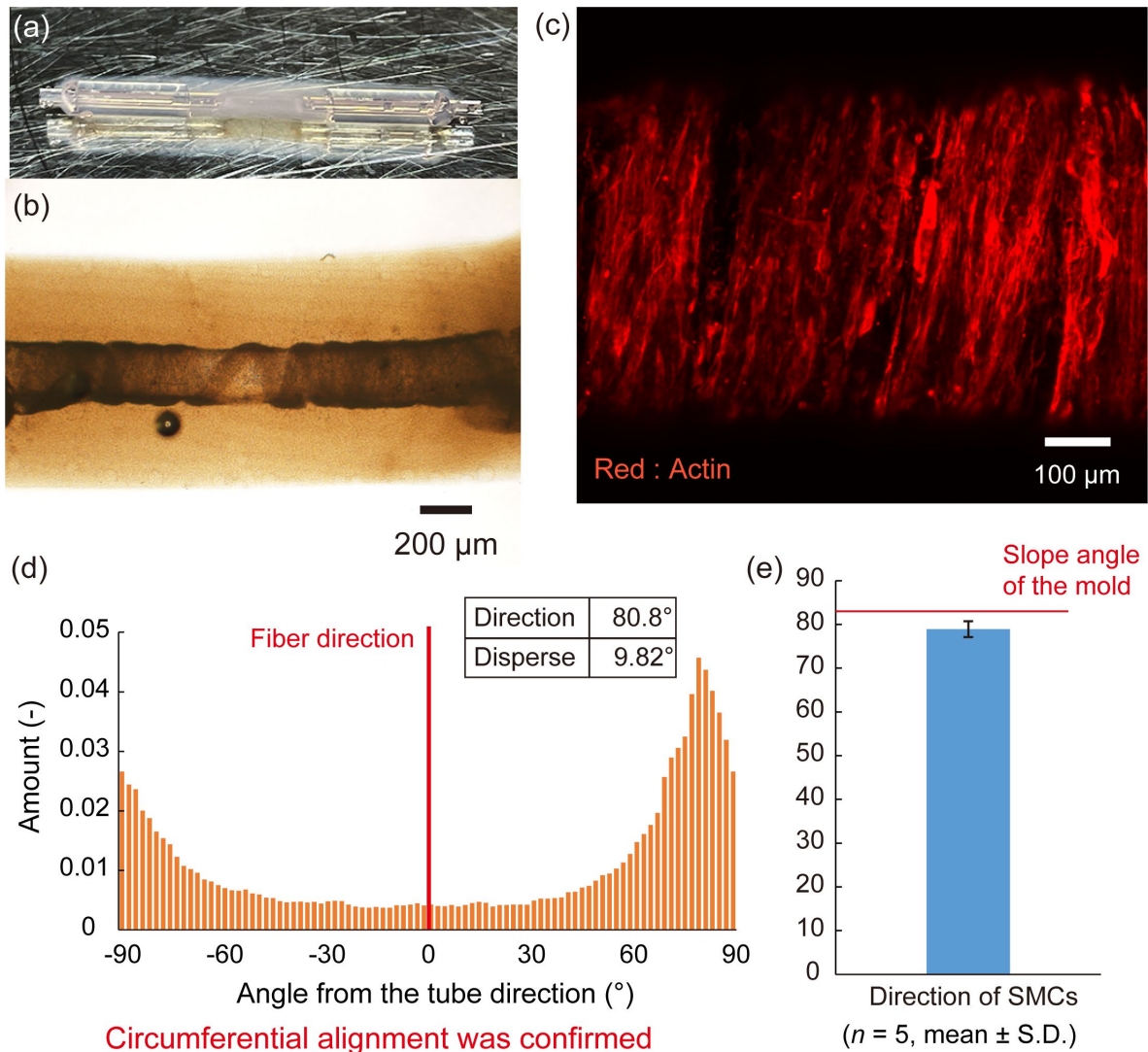


Figure 4.10 Fabrication results of the SMC layer embedded collagen tube fabricated with HUASMC fiber. (a) An overall image of the tube. (b) A phase-contrast image of the tube. (Scale bar: 200 μm) (c) A projection image of z-stack confocal fluorescent images of the stained actin of the SMCs in the tube. Circumferential alignment was observed. (Scale bar: 100 μm) (d) The directionality of the actin filaments of the HUASMCs. Red line (0°) shows the tube direction. The average direction was vertical to the tube direction, indicating the circumferential alignment of SMC tissue. (e) The mean and standard deviation of the average direction of SMCs.

4.4.4 Construction of blood vessel model by co-culture with HUVECs

HUVECs were seeded on the inner surface of the SMC layer embedded collagen tube to form a vascular model (Figure 4.11(a)). To distinguish the cells in the tube, GFP-HUVECs were used as HUVECs (Figure 4.11(b)). Also, HUASMCs were stained with the live-cell actin probe (red) continuously (Figure 4.11(c)). A merged image of the phase-contrast image and the fluorescent images were generated to observe the location of the cells in the tube (Figure 4.11(d)). These images revealed the formation of the HUVEC layer inside the HUASMC layer in 2 days of co-culture.

The thickness of the fabricated device was measured from phase-contrast images. The diameter of the outer surface, border of SMC-collagen, and inner surface were $2511 \pm 105 \mu\text{m}$, $668 \pm 24 \mu\text{m}$, and $462 \pm 20 \mu\text{m}$, respectively (Figure 4.12(a)). The coefficient variation was smaller than 5% for every diameter, ensuring the precisely controlled fabrication of the blood vessel model by the proposed method. Also, a projection image of the z-stack confocal fluorescent images was obtained by a confocal microscope (Figure 4.12(b)). From the z-stack images, a cross-sectional image was generated (Figure 4.12(c)). The image certifies the co-axial layer formation of circumferentially aligned SMCs and ECs. Moreover, elastin was detected around the SMC layer by immunostaining, especially strong on the edge of the SMC layer (Figure 4.13(a,b)) (Details of antibodies are shown in Appendix B). Elastin appears around the SMC layer as elastic lamina in the tunica media (a middle layer of arteries and veins) *in vivo*. Despite the importance of the elastic lamina on the elasticity of the blood vessel, no previous research achieved the formation of the elastic lamina *in vitro*. The locally observed elastin would have the potential to be developed as an elastic lamina, providing another advantage of the proposed tube device as a functional blood vessel model.

4.4.5 Immunological contraction demonstration of the SMC layer

As a proof of concept of the RuM-M method, the immunological deformation

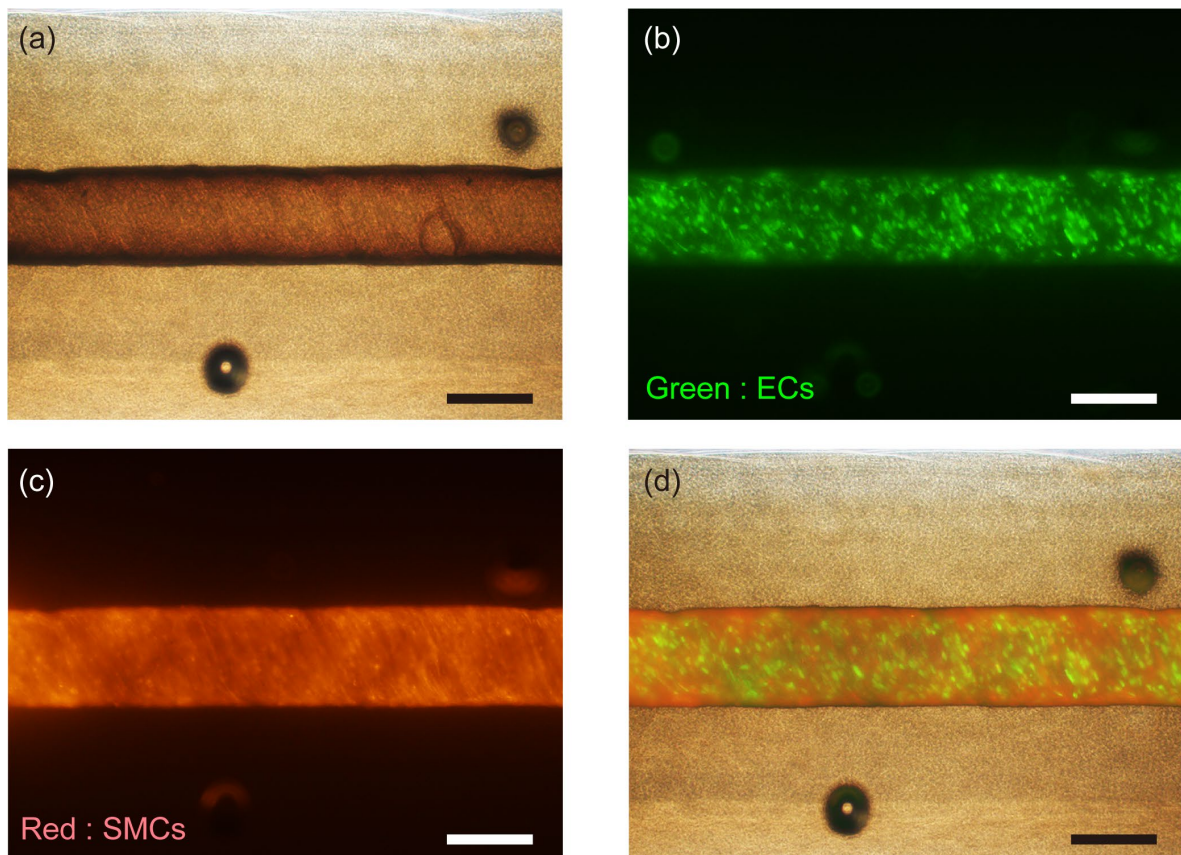


Figure 4.11 Co-culture with HUVECs for the construction of multi-layered blood vessel model. (a) A phase-contrast image of the model. (b) A fluorescent image of the GFP-HUVECs (green fluorescence) in the tube. (c) A fluorescent image of the actin fibers of HUASMCs in the tube (red fluorescence). (d) A merged image of (a-c). HUVEC layer was observed inside the HUASMC layer. (Scale bars: 500 μm)

reaction behavior of the circumferentially aligned SMC layer was demonstrated with histamine, an inflammatory mediator in allergy.

Firstly, histamine was exposed to the SMC layer in the tube device without HUVECs. The direct exposure of the histamine induces contraction of SMCs, as mentioned in section 1.4. To reproduce the behavior, the collagen tube with the SMC layer inside was immersed in a medium with 0.2 mg/mL of histamine. Note that a collagen tube that embedded not-aligned SMCs inside was prepared as a control to compare the contractility. As shown in

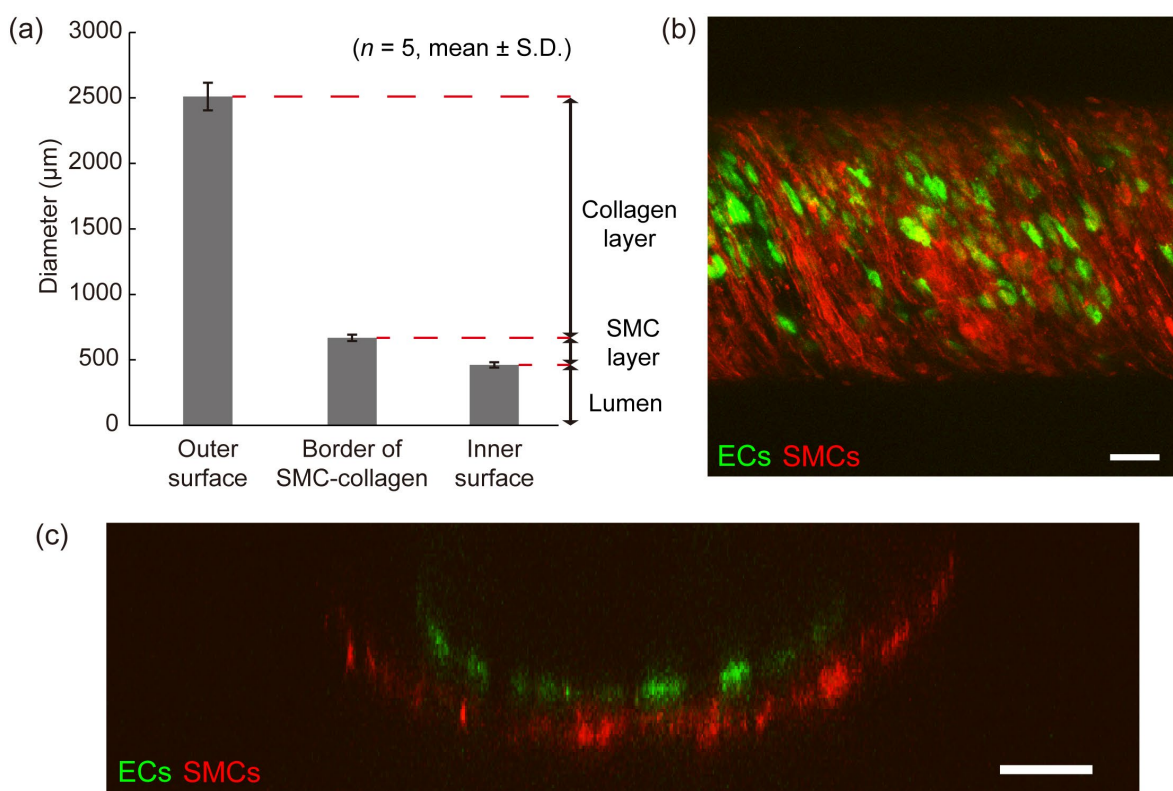


Figure 4.12 Evaluation of the co-cultured multi-layered blood vessel model. (a) Diameters of the fabricated model. Coefficient variations were less than 5% for all diameters. (b) A projection image of z-stack confocal fluorescent images of the tube. ECs were observed in the circumferentially aligned SMC layer. (Scale bar: 100 μm) (c) A cross-sectional image of the tube. The formation of the co-axial layers was confirmed. (Scale bar: 100 μm)

the deformation scheme (Figure 4.14(a)), the fabricated model with a circumferentially aligned SMC layer could circumferentially contract about 5% with slight contraction on length, while the control model could not contract circumferentially (Figure 4.14(b,c)). The contraction ratio for the axial and circumferential direction on the fabricated model was 1.15% and 4.81%, respectively, while those of the control was 7.12% and -3.68%, respectively. The results proved the ability of the fabricated SMC layer to contract circumferentially like the *in vivo* tissue.

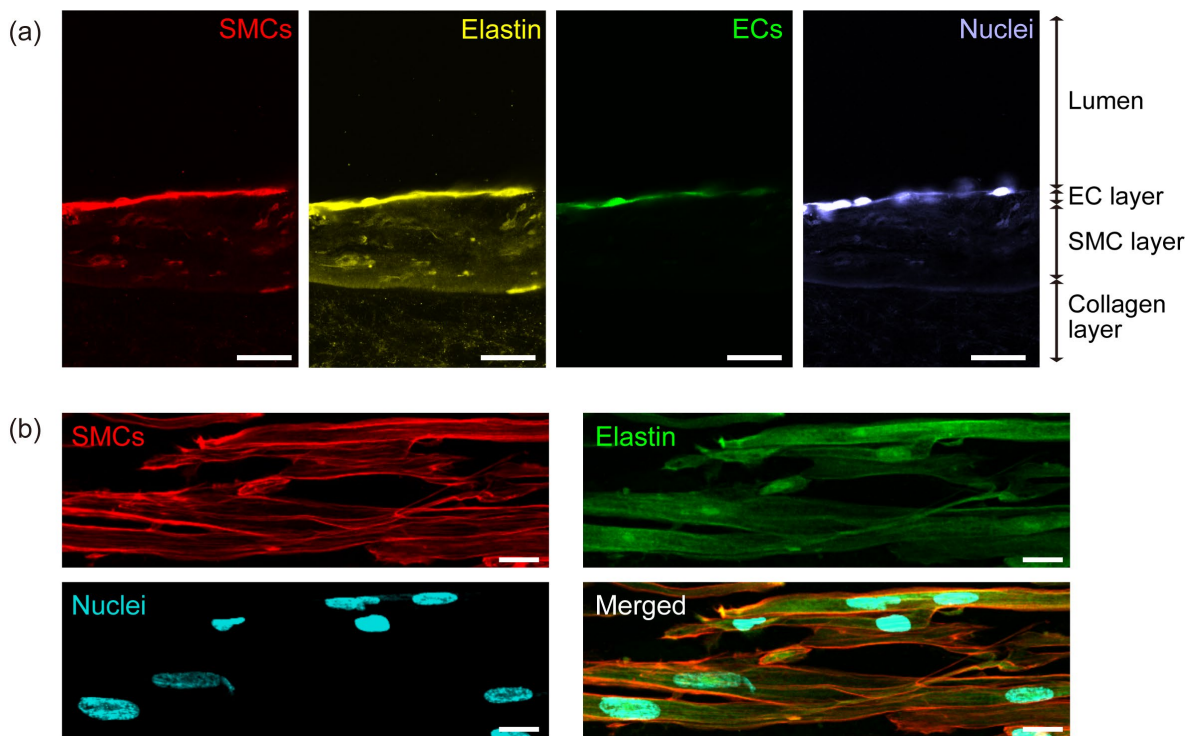


Figure 4.13 Evaluation of the elastin expression in co-cultured multi-layered blood vessel model. (a) Enlarged cross-sectional images of the tube after immunostaining. Elastin (stained yellow fluorescence) was observed around the SMC layer. (Scale bars: 50 μm) (b) Cellular level image. SMCs and elastin were distinguished. (Scale bars: 20 μm)

4.4.6 Immunological deformation on the blood vessel model

Finally, as another proof of concept, the immunological reaction of the proposed co-culture model of SMCs and ECs was performed. In arteries and veins, which contain both smooth muscle and endothelial layers, the histamine reaction leads to vasodilation as an indirect reaction other than the direct contraction behavior, as mentioned in section 1.4. Therefore, the exposure of the histamine to the co-cultured model leads to the relaxation of the SMC layer after the contraction reaction (Figure 4.15(a)). The fabricated co-culture model was immersed into a medium with 0.2 mg/mL of histamine.

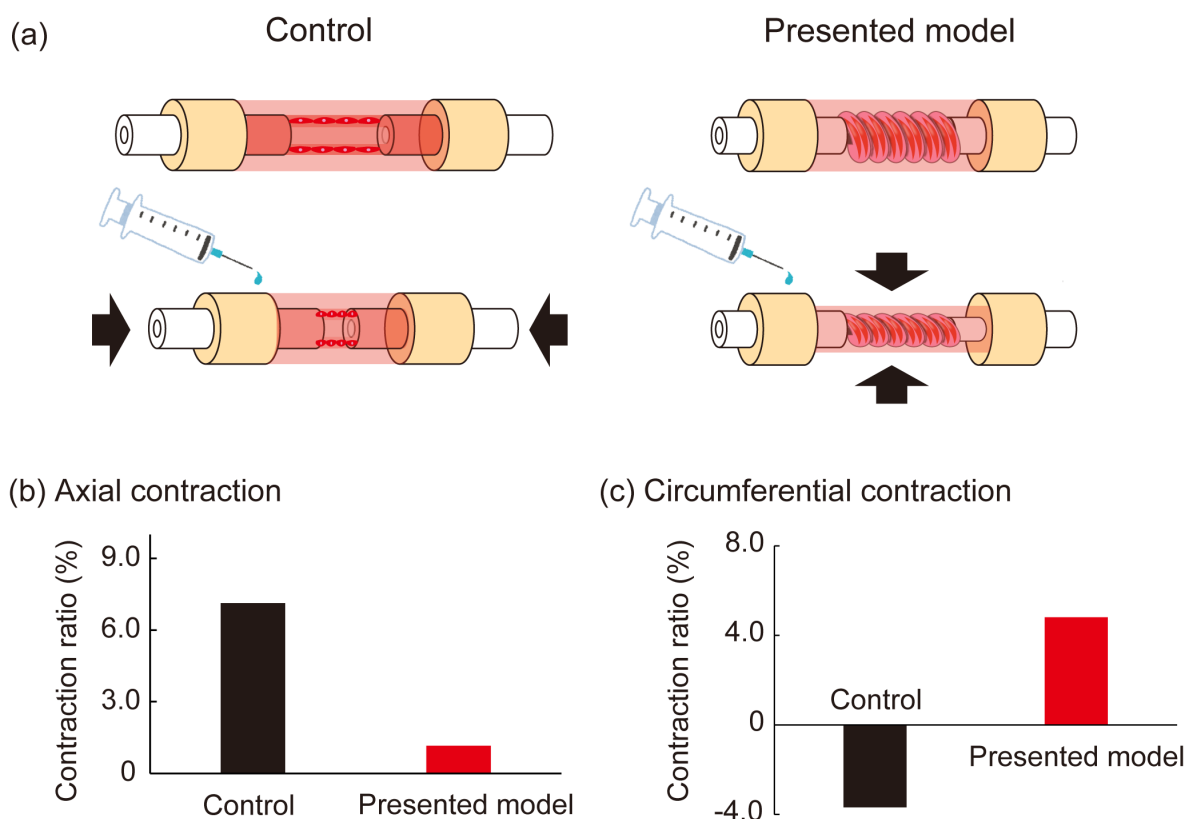


Figure 4.14 Immunological contraction reaction of the SMC layer in the tube without HUVECs by exposure to histamine. (a) A schematic image of the difference of the deformation reaction of the SMC layer between the fabricated device and the control. (b) The contraction ratio of the SMC layer for the axial direction. The fabricated model with circumferentially aligned SMC layer showed less contraction than the control model. (c) The contraction ratio of the SMC layer for the circumferential direction. Thanks to the circumferential alignment of the SMC layer in the tube, the fabricated model could contract circumferentially.

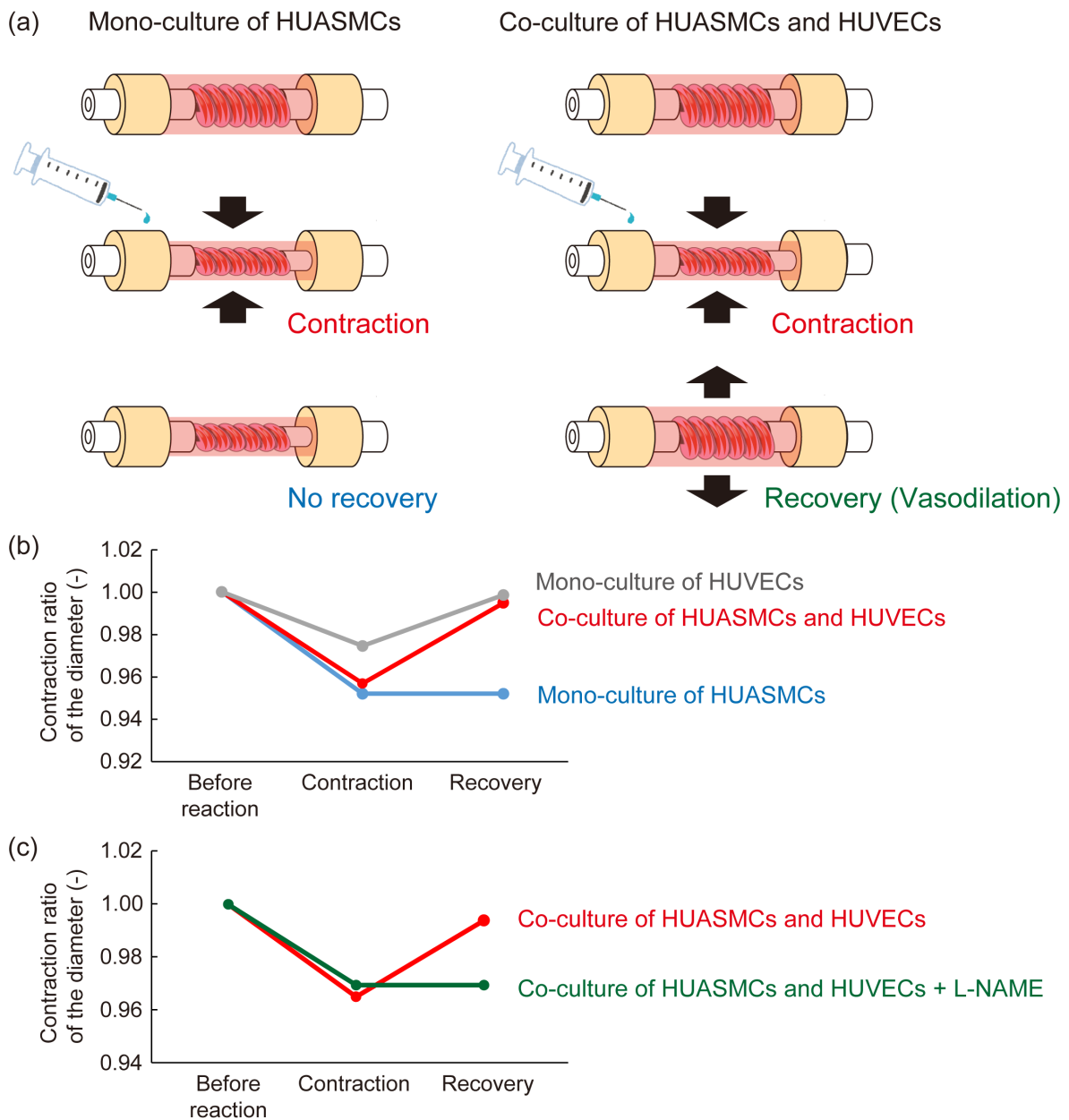


Figure 4.15 Immunological deformation reaction of the co-culture model by exposure to histamine. (a) A schematic image of the difference of the deformation reaction of the SMC layer between the mono-culture and the co-culture with ECs. (b) The contraction and recovery behavior of the model during the exposure to histamine. The co-culture model showed the recovery behavior unlike the mono-culture. Also, the shrinking ratio of the co-culture model was higher than the mono-culture model of HUVECs. (c) L-NAME exposure to the co-culture model along with histamine. L-NAME inhibited the recovering behavior comparing to the model exposed only to histamine.

The contraction ratio of the vessel model during the reaction was almost the same on the mono-culture model and the co-culture model. However, after about 10 minutes, the vessel model co-cultured with HUVECs recovered the diameter, while the mono-culture model of HUASMCs could not recover the diameter (Figure 4.15(b)). The results indicate that the indirect reaction of HUASMCs through HUVECs occurred. Moreover, the contraction ratio was 1.69 times higher than the mono-culture of HUVECs, performed in chapter 2, while these two conditions show the same shrinking and recovering behavior. The difference may be caused by the contraction of the SMC layer, ensuring the response of both ECs and SMCs to the immunological stimulation.

To prove the interaction between SMCs and ECs in the reaction, L-NAME (NOS inhibitor) was exposed to the co-culture model with histamine. The indirect relaxation reaction of SMCs is known to be induced by NO released from ECs. Thus, the inhibition of NOS of ECs is predicted to suppress the indirect reaction. As a result, the NOS-inhibited model could not recover the diameter as expected, while the contraction ratio was almost the same with the model exposed only to histamine (Figure 4.15(c)).

From the results, the shrinking ability of the proposed blood vessel model on both EC and SMC layers was confirmed. Also, the relaxation behavior of the vessel model was proved to be induced by NO-related reaction between ECs and SMCs, ensuring the ability of the proposed model to implement functional cellular interaction.

4.5 Conclusion

In this chapter, the rolling up maturation molding method (RuM-M method) was proposed to fabricate a multi-layered blood vessel model with a circumferentially aligned smooth muscle layer inside to reproduce the immunological deformation reaction of the co-culture of smooth muscle and endothelium.

The prepared SMC fiber showed axial alignment by a live fluorescent image of the actin of SMCs. By rolling up an axially aligned smooth muscle fiber, a circumferential

alignment was easily formed in a self-standing collagen tube. The alignment direction was $78.95 \pm 1.79^\circ$ with 2.2% of the coefficient variation (0° is determined as the tube direction). The fabrication results proved that the proposed method could control the alignment angle of the SMC tissue by changing the fabrication condition to mimic *in vivo* blood vessel tissues with various helical angles. After fabrication of the circumferential alignment, HUVECs were seeded on the inner surface and achieved the co-culture of SMCs and ECs.

In demonstration experiments of immunological deformation reaction, the fabricated blood vessel model showed circumferential contraction behavior in the mono-culture of SMCs by exposure to histamine due to the alignment of the SMCs and flexibility of the device. Also, the co-cultured model recovered from the contraction by the NO-related EC-SMC interaction under histamine reaction similar as *in vivo*.

These results proved that the proposed blood vessel model could reproduce the immunological deformation reaction similar to *in vivo*, ensuring the high ability of the model for various biomedical research fields.

CHAPTER 5. Concluding remarks

5.1 Conclusion

The objective in this dissertation was to fabricate an *in vitro* blood vessel model reproducing immunological deformation reaction.

To achieve the objective, the author firstly developed a double-layered collagen hydrogel tube device to form an endothelial tissue on a flexibly deformable scaffold. The device was simply made by the repetition of a molding process. The thicknesses of the collagen layers in the tube device could be flexibly designed (inner diameter approximately 300–1000 μm) using different molds and successfully controlled the coefficients of variation (C.V.) to be below 5% for the diameters of each layer. Also, the device was strong enough to manipulate with tweezers and could remain stable for more than three months in a medium. About the EC layer formation, HUVECs seeded on the inner layer properly migrated, and the immunostaining and permeability experiment revealed the formation of tight junctions with the permeability coefficient of 0.39×10^5 cm/s. Also, the ECs interacted with vascular pericytes by co-culture, resulting in the angiogenesis of the endothelial layer.

Next, using the developed flexibly deformable collagen hydrogel tube device, an inflammatory mediator-induced deformation reaction of ECs was reproduced. A self-standing collagen tube enabled the tissue to deform flexibly in biochemical reaction and achieved contraction both at tissue and cell levels. The tissue contraction relieved the stress between cells under reaction to maintain cellular junction even tight junctions were broken. Also, the drug perfusion test with the anti-histamine chemical was easily performed due to

the connector part and properly inhibited the inflammatory reaction.

Finally, the rolling up maturation molding method (RuM-M method) was proposed to fabricate a multi-layered blood vessel model with a circumferentially aligned smooth muscle layer inside to reproduce the immunological deformation reaction of smooth muscle. The prepared SMC fiber showed axial alignment by a live fluorescent image of the actin of SMCs. By rolling up an axially aligned smooth muscle fiber, a circumferential alignment was easily formed in a self-standing collagen tube. The alignment direction was $78.95 \pm 1.79^\circ$ with 2.2% of the coefficient variation (0° is determined as the tube direction). After fabrication of the circumferential alignment, HUVECs were seeded on the inner surface and achieved the co-culture of SMCs and ECs. In a demonstration of immunological deformation reaction, the fabricated blood vessel model showed circumferential contraction behavior in the mono-culture of SMCs by exposure to histamine due to the alignment of the SMCs and flexibility of the device. Also, the co-cultured model recovered from the contraction by the EC-SMC interaction under histamine reaction similar as *in vivo*.

The results proved the ability of the model to reproduce the immunological deformation reaction of the capillary and large blood vessels. The author believes that the proposed self-standing *in vitro* blood vessel model with proper alignment structure and cellular function would contribute to the fabrication of vascular tissue models mimicking *in vivo* in high similarity as a platform for biomedical researches and pharmacokinetic testing.

5.2 Future perspectives

In this research, the author successfully reproduced immunological deformation reactions of blood vessels in a self-standing collagen hydrogel tube device. The research has mainly two noteworthy points:

- (i) Reproduction of the immunological deformation reaction both at tissue and cell level.
- (ii) Construction of a circumferentially aligned smooth muscle tissue within a flexibly

deformable condition.

In vitro vascular models have high demand as drug and pharmacokinetic testing devices since blood vessels relate highly to drug absorption and various serious diseases such as cerebral infarction or myocardial infarction^{[122], [123]}. The great attention on this research topic led to the development of quite many vascular models and fabrication methods in recent decades^[90]. Still, no model could have been reproduced the biochemical reaction of blood vessels *in vivo* correctly because of the inflexibility of scaffolds and substrates. On this point, the proposed self-standing flexible collagen tube device would have a higher potential than previous models to develop as an *in vitro* vascular model for biomedical researches.

In addition, the traction force analysis serves us an essential sight on the design of *in vitro* vascular models. The numerical analysis showed that the traction force that occurred on each cell under biochemical reaction was the same; even the stiffness of the scaffolds was different. It means, the deformation behavior strongly relates to the property of the scaffold. Therefore, designing deformability of the scaffold same as *in vivo* would be a crucial criterion to reproduce biochemical reaction. As shown in the result, the author could numerically relate the young's modulus, deformation value, and tube design with traction force. Thus, the proposed device would be capable of being designed the material or concentration to mimic targeted *in vivo* tissue in tissue engineering. Since some tissues are known to change the stiffness in diseases^{[124]–[126]}, the author's device may also have the potential to mimic the property of disease models in high similarity.

Moreover, the flexible collagen tube can encapsulate cells into the collagen layer to fabricate complicated tissue models. To reproduce inflammatory reactions, histamine was added directly to the culture medium in the experiments. However, in the actual inflammatory reaction, allergy for example, histamine is released from mast cells in connective tissue^[113]. Further, mast cells have to be activated by Th2 cells, B cells, and other immune cells to react against allergen in the inflammatory reaction^{[127], [128]}. By encapsulating these cells into the collagen layer, this complicated reaction pathway could be constructed in the collagen tube device. Then, the whole allergic reaction started from the allergen invasion could be reproduced, and it would contribute to the more detailed biomedical analysis of diseases. Of

Concluding remarks

course, other various disease models have the possibility to construct on the proposed model. From this point, the model has a high potential to contribute to the development of detailed biomedical and pharmacokinetic research.

Acknowledgments

My research activities had been received great cooperation from countless people. At the last of my dissertation, I would like to state appreciation for it.

First of all, I wish to thank Professor Hiroaki Onoe, my supervisor for six years since I joined the laboratory as an undergraduate. I received assistance from him to perform all of the bachelor, the master, and the doctoral research. He was always so kind and provided me with an excellent research environment. Also, he gave me numerous critical pieces of advice to improve my research. I really admire and respect him and am proud of the precious time researched with Prof. Onoe.

Yuta Kurashina, an assistant professor of the Tokyo Institute of Technology, advised me not only on research but also on the plan as a researcher. He also gave me many chances to be involved in exciting research topics.

Takafumi Toyohara, an assistant professor of the Graduate school of Biomedical Engineering, Tohoku University, kindly spent time discussing many times and gave me valuable advice from the medical background.

Cellab members from Takemura Lab., Miyata Lab., Komotori Lab., Sudo Lab., and Funahashi Lab. gave me a great time to discuss from a variety of perspectives on biological research.

Onoe Lab. members made me have a wonderful and comfortable research life. All members are my implacable colleagues.

My best friends from junior and senior high school always supported me and cheered me up to proceed with my research.

And last, I would like to emphasize many thanks to my family. Regardless of the quite long student life, they are always by my side and back me up. They were really happy about my works and looking forward to my achievements. They made me think of striving more on research.

Acknowledgements

I cannot list all people who have been kind and supported me, but I'm grateful for all my dears.

February 2022

Shun Itai

References

- [1] L. Brewster, E. M. Brey, and H. P. Greisler, “Blood Vessels,” *Princ. Tissue Eng. Fourth Ed.*, pp. 793–812, 2013.
- [2] S. Li, D. Sengupta, and S. Chien, “Vascular tissue engineering: from in vitro to in situ,” *Wiley Interdiscip. Rev. Syst. Biol. Med.*, vol. 6, no. 1, pp. 61–76, Jan. 2014.
- [3] Z. Wang, S. M. Mithieux, and A. S. Weiss, “Fabrication Techniques for Vascular and Vascularized Tissue Engineering,” *Adv. Healthc. Mater.*, vol. 8, no. 19, Oct. 2019.
- [4] M. Potente and T. Mäkinen, “Vascular heterogeneity and specialization in development and disease,” *Nat. Rev. Mol. Cell Biol.*, vol. 18, no. 8, pp. 477–494, 2017.
- [5] J. Schöneberg *et al.*, “Engineering biofunctional in vitro vessel models using a multilayer bioprinting technique,” *Sci. Reports 2018 81*, vol. 8, no. 1, pp. 1–13, Jul. 2018.
- [6] J. E. Wagenseil and R. P. Mecham, “Vascular extracellular matrix and arterial mechanics,” *Physiol. Rev.*, vol. 89, no. 3, pp. 957–989, Jul. 2009.
- [7] H. Ardalani, A. H. Assadi, and W. L. Murphy, “Structure, function, and development of blood vessels: Lessons for tissue engineering,” *Eng. Transl. Med.*, vol. 9781447143, pp. 155–182, May 2014.
- [8] F. Wolf, F. Vogt, T. Schmitz-Rode, S. Jockenhoewel, and P. Mela, “Bioengineered vascular constructs as living models for in vitro cardiovascular research,” *Drug Discov. Today*, vol. 21, no. 9, pp. 1446–1455, Sep. 2016.
- [9] W. J. Zhang, W. Liu, L. Cui, and Y. Cao, “Tissue engineering of blood vessel,” *J. Cell. Mol. Med.*, vol. 11, no. 5, pp. 945–957, Sep. 2007.
- [10] Y. Li *et al.*, “Engineering cell alignment in vitro,” *Biotechnol. Adv.*, vol. 32, no. 2, pp. 347–365, Mar. 2014.

References

- [11] M. Tennant and J. K. McGeachie, "BLOOD VESSEL STRUCTURE AND FUNCTION: A BRIEF UPDATE ON RECENT ADVANCES," *Aust. N. Z. J. Surg.*, vol. 60, no. 10, pp. 747–753, 1990.
- [12] J. Frösen and A. Joutel, "Smooth muscle cells of intracranial vessels: from development to disease," *Cardiovasc. Res.*, vol. 114, no. 4, pp. 501–512, Mar. 2018.
- [13] S. Moosmang *et al.*, "Dominant role of smooth muscle L-type calcium channel Cav1.2 for blood pressure regulation," *EMBO J.*, vol. 22, no. 22, pp. 6027–6034, Nov. 2003.
- [14] D. G. Johns, R. C. Webb, and J. R. Charpie, "Impaired ceramide signalling in spontaneously hypertensive rat vascular smooth muscle: A possible mechanism for augmented cell proliferation," *J. Hypertens.*, vol. 19, no. 1, pp. 63–70, 2001.
- [15] F. V. Brozovich, C. J. Nicholson, C. V. Degen, Y. Z. Gao, M. Aggarwal, and K. G. Morgan, "Mechanisms of Vascular Smooth Muscle Contraction and the Basis for Pharmacologic Treatment of Smooth Muscle Disorders," *Pharmacol. Rev.*, vol. 68, no. 2, p. 476, Apr. 2016.
- [16] J. Eble and S. Niland, "The Extracellular Matrix of Blood Vessels," *Curr. Pharm. Des.*, vol. 15, no. 12, pp. 1385–1400, Mar. 2009.
- [17] G. Bergers and S. Song, "The role of pericytes in blood-vessel formation and maintenance," *Neuro. Oncol.*, vol. 7, no. 4, pp. 452–464, Oct. 2005.
- [18] L. Claesson-Welsh, "Vascular permeability - The essentials," *Ups. J. Med. Sci.*, vol. 120, no. 3, pp. 135–143, 2015.
- [19] S. Azzi, J. K. Hebda, and J. Gavard, "Vascular Permeability and Drug Delivery in Cancers," *Front. Oncol.*, vol. 3, 2013.
- [20] A. M. Dvorak, S. Kohn, E. S. Morgan, P. Fox, J. A. Nagy, and H. F. Dvorak, "The vesiculo-vacuolar organelle (VVO): a distinct endothelial cell structure that provides a transcellular pathway for macromolecular extravasation," *J. Leukoc. Biol.*, vol. 59, no. 1, pp. 100–115, Jan. 1996.
- [21] V. Pade and S. Stavchansky, "Estimation of the relative contribution of the transcellular and paracellular pathway to the transport of passively absorbed drugs

- in the Caco-2 cell culture model,” *Pharmaceutical Research*, vol. 14, no. 9. pp. 1210–1215, 1997.
- [22] Y. Komarova and A. B. Malik, “Regulation of Endothelial Permeability via Paracellular and Transcellular Transport Pathways,” *Annu. Rev. Physiol.*, vol. 72, no. 1, pp. 463–493, Mar. 2010.
- [23] E. Vandenbroucke, D. Mehta, R. Minshall, and A. B. Malik, “Regulation of endothelial junctional permeability,” *Ann. N. Y. Acad. Sci.*, vol. 1123, pp. 134–145, 2008.
- [24] D. Radke *et al.*, “Tissue Engineering at the Blood-Contacting Surface: A Review of Challenges and Strategies in Vascular Graft Development,” *Adv. Healthc. Mater.*, vol. 7, no. 15, p. 1701461, Aug. 2018.
- [25] D. Kugelmann, L. T. Rotkopf, M. Y. Radeva, A. Garcia-Ponce, E. Walter, and J. Waschke, “Histamine causes endothelial barrier disruption via Ca²⁺-mediated RhoA activation and tension at adherens junctions,” *Sci. Reports 2018 81*, vol. 8, no. 1, pp. 1–14, Sep. 2018.
- [26] L. Duluc and B. Wojciak-Stothard, “Rho GTPases in the regulation of pulmonary vascular barrier function,” *Cell Tissue Res.*, vol. 355, no. 3, pp. 675–685, 2014.
- [27] A. Nusrat, J. R. Turner, and J. L. Madara, “IV. Regulation of tight junctions by extracellular stimuli: nutrients, cytokines, and immune cells,” *Am. J. Physiol. Liver Physiol.*, vol. 279, no. 5, pp. G851–G857, Nov. 2000.
- [28] A. B. Moy *et al.*, “Histamine and thrombin modulate endothelial focal adhesion through centripetal and centrifugal forces,” *J. Clin. Invest.*, vol. 97, no. 4, pp. 1020–1027, Feb. 1996.
- [29] G. Majno, S. M. Shea, and M. Leventhal, “Endothelial contraction induced by histamine-type mediators: an electron microscopic study,” *J. Cell Biol.*, vol. 42, no. 3, pp. 647–672, 1969.
- [30] J. Silberman, A. Jha, H. Ryan, T. Abbate, and E. Moore, “Modeled vascular microenvironments: immune-endothelial cell interactions in vitro,” *Drug Deliv. Transl. Res.*, vol. 11, no. 6, pp. 2482–2495, Apr. 2021.

References

- [31] S. Huveneers *et al.*, “Vinculin associates with endothelial VE-cadherin junctions to control force-dependent remodeling,” *J. Cell Biol.*, vol. 196, no. 5, pp. 641–652, 2012.
- [32] K. Ashina *et al.*, “Histamine induces vascular hyperpermeability by increasing blood flow and endothelial barrier disruption in vivo,” *PLoS One*, vol. 10, no. 7, pp. 1–16, 2015.
- [33] D. Mehta and A. B. Malik, “Signaling mechanisms regulating endothelial permeability,” *Physiol Rev*, vol. 86, no. 1, pp. 279–367, 2006.
- [34] H. Suzuki and K. Kou, “Direct and indirect effects of histamine on the smooth muscle cells of the guinea-pig main pulmonary artery,” *Pflügers Arch. 1983 3991*, vol. 399, no. 1, pp. 46–53, Sep. 1983.
- [35] J. R. Burgoyne and P. Eaton, “Oxidant Sensing by Protein Kinases A and G Enables Integration of Cell Redox State with Phosphoregulation,” *Sensors 2010, Vol. 10, Pages 2731-2751*, vol. 10, no. 4, pp. 2731–2751, Mar. 2010.
- [36] L. J. Ignarro, “Endothelium-Derived Nitric Oxide: Pharmacology and Relationship to the Actions of Organic Nitrate Esters,” *Pharm. Res. 1989 68*, vol. 6, no. 8, pp. 651–659, 1989.
- [37] C. R. Triggle, S. M. Samuel, S. Ravishankar, I. Marei, G. Arunachalam, and H. Ding, “The endothelium: Influencing vascular smooth muscle in many ways,” *Can. J. Physiol. Pharmacol.*, vol. 90, no. 6, pp. 713–718, 2012.
- [38] D. M. Dudzinski, J. Igarashi, D. Greif, and T. Michel, “The regulation and pharmacology of endothelial nitric oxide synthase,” *Annu. Rev. Pharmacol. Toxicol.*, vol. 46, pp. 235–276, 2006.
- [39] H. J. Knot and M. T. Nelson, “Regulation of arterial diameter and wall [Ca²⁺] in cerebral arteries of rat by membrane potential and intravascular pressure,” *J. Physiol.*, vol. 508, no. 1, pp. 199–209, Apr. 1998.
- [40] L. Bacakova *et al.*, “The Role of Vascular Smooth Muscle Cells in the Physiology and Pathophysiology of Blood Vessels,” *Muscle Cell Tissue - Curr. Status Res. F.*, Oct. 2018.

-
- [41] B. J. Van Varik, R. J. M. W. Rennenberg, C. P. Reutelingsperger, A. A. Kroon, P. W. De Leeuw, and L. J. Schurgers, "Mechanisms of arterial remodeling: Lessons from genetic diseases," *Front. Genet.*, vol. 3, no. DEC, 2012.
- [42] S. T. Lust, C. M. Shanahan, R. J. Shipley, P. Lamata, and E. Gentleman, "Design considerations for engineering 3D models to study vascular pathologies in vitro," *Acta Biomater.*, vol. 132, pp. 114–128, Sep. 2021.
- [43] R. M. Nerem and D. Seliktar, "Vascular Tissue Engineering," <http://dx.doi.org/10.1146/annurev.bioeng.3.1.225>, vol. 3, pp. 225–243, Nov. 2003.
- [44] T. Hartung, "Food for Thought Look Back in Anger – What Clinical Studies Tell Us About Preclinical Work," *ALTEX*, vol. 30, pp. 275–291, 2013.
- [45] R. Mangipudy, J. Burkhardt, and V. J. Kadambi, "Use of animals for toxicology testing is necessary to ensure patient safety in pharmaceutical development," *Regul. Toxicol. Pharmacol.*, vol. 70, no. 2, pp. 439–441, 2014.
- [46] L. J. Marshall and A. N. Rowan, "Advances in alternative non-animal testing methods represent a way to find new treatments for patients," *Eur. J. Intern. Med.*, vol. letter, pp. 1–2, 2017.
- [47] S. S. Sparrow *et al.*, "Opportunities to minimise animal use in pharmaceutical regulatory general toxicology : A cross-company review," *Regul. Toxicol. Pharmacol.*, vol. 61, no. 2, pp. 222–229, 2011.
- [48] S. K. Doke and S. C. Dhawale, "Alternatives to animal testing : A review," *Saudi Pharm. J.*, vol. 23, no. 3, pp. 223–229, 2015.
- [49] S. Garattini and G. Grignaschi, "Animal testing is still the best way to find new treatments for patients," *Eur. J. Intern. Med.*, vol. 39, pp. 32–35, 2017.
- [50] S. Scholz *et al.*, "A European perspective on alternatives to animal testing for environmental hazard identification and risk assessment," *Regul. Toxicol. Pharmacol.*, vol. 67, no. 3, pp. 506–530, 2013.
- [51] M. Balls, "Future Improvements : Replacement In Vitro Methods," *ILAR J.*, vol. 43, pp. 69–73, 2002.
- [52] K. Ziółkowska, R. Kwapiszewski, and Z. Brzózka, "Microfluidic devices as tools

References

- for mimicking the in vivo environment,” *New J. Chem.*, vol. 35, no. 5, pp. 979–990, 2011.
- [53] K. Gold, A. K. Gaharwar, and A. Jain, “Emerging trends in multiscale modeling of vascular pathophysiology: Organ-on-a-chip and 3D printing,” *Biomaterials*, vol. 196, pp. 2–17, Mar. 2019.
- [54] D. G. Seifu, A. Purnama, K. Mequanint, and D. Mantovani, “Small-diameter vascular tissue engineering,” *Nat. Rev. Cardiol.*, vol. 10, no. 7, pp. 410–421, Jul. 2013.
- [55] S. Kim, W. Kim, S. Lim, and J. S. Jeon, “Vasculature-on-a-chip for in vitro disease models,” *Bioengineering*, vol. 4, no. 1, Mar. 2017.
- [56] S. Ahadian *et al.*, “Organ-On-A-Chip Platforms: A Convergence of Advanced Materials, Cells, and Microscale Technologies,” *Adv. Healthc. Mater.*, vol. 7, no. 2, Jan. 2018.
- [57] J. M. Rhodes and M. Simons, “The extracellular matrix and blood vessel formation: not just a scaffold,” *J. Cell. Mol. Med.*, vol. 11, no. 2, pp. 176–205, Mar. 2007.
- [58] V. Hosseini *et al.*, “Healthy and diseased in vitro models of vascular systems,” *Lab Chip*, vol. 21, no. 4, pp. 641–659, Feb. 2021.
- [59] K. H. Nam, A. S. T. Smith, S. Lone, S. Kwon, and D. H. Kim, “Biomimetic 3D Tissue Models for Advanced High-Throughput Drug Screening,” *J. Lab. Autom.*, vol. 20, no. 3, pp. 201–215, Jun. 2015.
- [60] J. S. Choi, Y. Piao, and T. S. Seo, “Fabrication of a circular PDMS microchannel for constructing a three-dimensional endothelial cell layer,” *Bioprocess Biosyst. Eng.*, vol. 36, no. 12, pp. 1871–1878, Nov. 2013.
- [61] J. W. Song *et al.*, “Microfluidic Endothelium for Studying the Intravascular Adhesion of Metastatic Breast Cancer Cells,” *PLoS One*, vol. 4, no. 6, p. e5756, Jun. 2009.
- [62] H. Kaji, T. Yokoi, T. Kawashima, and M. Nishizawa, “Directing the flow of medium in controlled cocultures of HeLa cells and human umbilical vein endothelial cells with a microfluidic device,” *Lab Chip*, vol. 10, no. 18, pp. 2374–

- 2379, Aug. 2010.
- [63] K. Sakaguchi *et al.*, “In vitro engineering of vascularized tissue surrogates,” *Sci. Rep.*, vol. 3, p. 1316, 2013.
- [64] M. A. Redd *et al.*, “Patterned human microvascular grafts enable rapid vascularization and increase perfusion in infarcted rat hearts,” *Nat. Commun.* 2019 101, vol. 10, no. 1, pp. 1–14, Feb. 2019.
- [65] J. Pauty *et al.*, “A Vascular Endothelial Growth Factor-Dependent Sprouting Angiogenesis Assay Based on an In Vitro Human Blood Vessel Model for the Study of Anti-Angiogenic Drugs,” *EBioMedicine*, vol. 27, pp. 225–236, Jan. 2018.
- [66] A. Tan, K. Fujisawa, Y. Yukawa, and Y. T. Matsunaga, “Bottom-up fabrication of artery-mimicking tubular co-cultures in collagen-based microchannel scaffolds,” *Biomater. Sci.*, vol. 4, no. 10, pp. 1503–1514, 2016.
- [67] F. Kabirian, B. Ditkowski, A. Zamanian, M. F. Hoylaerts, M. Mozafari, and R. Heying, “Controlled NO-Release from 3D-Printed Small-Diameter Vascular Grafts Prevents Platelet Activation and Bacterial Infectivity,” *ACS Biomater. Sci. Eng.*, vol. 5, no. 5, pp. 2284–2296, May 2019.
- [68] B. Cheng, Y. M. Xing, N. C. Shih, J. P. Weng, and H. C. Lin, “The formulation and characterization of 3D printed grafts as vascular access for potential use in hemodialysis,” *RSC Adv.*, vol. 8, no. 28, pp. 15471–15479, Apr. 2018.
- [69] K. Hoon Song *et al.*, “Complex 3D-Printed Microchannels within Cell-Degradable Hydrogels,” *Adv. Funct. Mater.*, vol. 28, no. 31, p. 1801331, Aug. 2018.
- [70] J. S. Miller *et al.*, “Rapid casting of patterned vascular networks for perfusable engineered three-dimensional tissues,” *Nat. Mater.*, vol. 11, no. 7, pp. 768–774, 2012.
- [71] X. Cao, S. Maharjan, R. Ashfaq, J. Shin, and Y. S. Zhang, “Bioprinting of Small-Diameter Blood Vessels,” *Engineering*, vol. 7, no. 6, pp. 832–844, Jun. 2021.
- [72] M. Abudupataer *et al.*, “Bioprinting a 3D vascular construct for engineering a vessel-on-a-chip,” *Biomed. Microdevices*, vol. 22, no. 1, p. 10, Mar. 2020.
- [73] Q. Pi *et al.*, “Digitally Tunable Microfluidic Bioprinting of Multilayered Cannular

References

- Tissues,” *Adv. Mater.*, vol. 30, no. 43, p. 1706913, Oct. 2018.
- [74] N. Brandenburg, M. P. Lutolf, N. Brandenburg, and M. P. Lutolf, “In Situ Patterning of Microfluidic Networks in 3D Cell-Laden Hydrogels,” *Adv. Mater.*, vol. 28, no. 34, pp. 7450–7456, Sep. 2016.
- [75] C. K. Arakawa *et al.*, “Multicellular Vascularized Engineered Tissues through User-Programmable Biomaterial Photodegradation,” *Adv. Mater.*, vol. 29, no. 37, p. 1703156, Oct. 2017.
- [76] K. A. Heintz *et al.*, “Fabrication of 3D Biomimetic Microfluidic Networks in Hydrogels,” *Adv. Healthc. Mater.*, vol. 5, no. 17, pp. 2153–2160, Sep. 2016.
- [77] C. D. Devillard and C. A. Marquette, “Vascular Tissue Engineering: Challenges and Requirements for an Ideal Large Scale Blood Vessel,” *Front. Bioeng. Biotechnol.*, vol. 9, p. 913, Oct. 2021.
- [78] E. Ercolani, C. Del Gaudio, and A. Bianco, “Vascular tissue engineering of small-diameter blood vessels: reviewing the electrospinning approach,” *J. Tissue Eng. Regen. Med.*, vol. 9, no. 8, pp. 861–888, Aug. 2015.
- [79] C. K. Hashi *et al.*, “Antithrombogenic modification of small-diameter microfibrillar vascular grafts,” *Arterioscler. Thromb. Vasc. Biol.*, vol. 30, no. 8, pp. 1621–1627, Aug. 2010.
- [80] S. A. Sell, M. J. McClure, K. Garg, P. S. Wolfe, and G. L. Bowlin, “Electrospinning of collagen/biopolymers for regenerative medicine and cardiovascular tissue engineering,” *Adv. Drug Deliv. Rev.*, vol. 61, no. 12, pp. 1007–1019, Oct. 2009.
- [81] L. Buttafoco *et al.*, “Electrospinning of collagen and elastin for tissue engineering applications,” *Biomaterials*, vol. 27, no. 5, pp. 724–734, Feb. 2006.
- [82] S. Kim, H. Lee, M. Chung, and N. L. Jeon, “Engineering of functional, perfusable 3D microvascular networks on a chip,” *Lab Chip*, vol. 13, no. 8, pp. 1489–1500, Mar. 2013.
- [83] C. Kim, J. Kasuya, J. Jeon, S. Chung, and R. D. Kamm, “A quantitative microfluidic angiogenesis screen for studying anti-angiogenic therapeutic drugs,” *Lab Chip*, vol. 15, no. 1, pp. 301–310, Dec. 2014.

- [84] P. J. Schaner *et al.*, “Decellularized vein as a potential scaffold for vascular tissue engineering,” *J. Vasc. Surg.*, vol. 40, no. 1, pp. 146–153, Jul. 2004.
- [85] M. Watanabe *et al.*, “Construction of sinusoid-scale microvessels in perfusion culture of a decellularized liver,” *Acta Biomater.*, vol. 95, pp. 307–318, Sep. 2019.
- [86] Y. Gao *et al.*, “Decellularized liver as a translucent ex vivo model for vascular embolization evaluation,” *Biomaterials*, vol. 240, p. 119855, May 2020.
- [87] S. S. Rho, K. Ando, and S. Fukuhara, “Dynamic regulation of vascular permeability by vascular endothelial cadherin-mediated endothelial cell-cell junctions,” *J. Nippon Med. Sch.*, vol. 84, no. 4, pp. 148–159, 2017.
- [88] M. Trani and E. Dejana, “New insights in the control of vascular permeability: vascular endothelial-cadherin and other players,” *Curr Opin Hematol*, vol. 22, no. 3, pp. 267–272, May 2015.
- [89] H. Schnittler, M. Taha, M. O. Schnittler, A. A. Taha, N. Lindemann, and J. Seebach, “Actin filament dynamics and endothelial cell junctions: the Ying and Yang between stabilization and motion,” *Cell Tissue Res*, vol. 355, no. 3, pp. 529–543, 2014.
- [90] V. Hosseini *et al.*, “Healthy and diseased in vitro models of vascular systems,” *Lab Chip*, vol. 21, no. 4, pp. 641–659, 2021.
- [91] P. W. Alford, A. P. Nesmith, J. N. Seywerd, A. Grosberg, and K. K. Parker, “Vascular smooth muscle contractility depends on cell shape,” *Integr. Biol.*, vol. 3, no. 11, pp. 1063–1070, Nov. 2011.
- [92] K. E. Steucke, P. V. Tracy, E. S. Hald, J. L. Hall, and P. W. Alford, “Vascular smooth muscle cell functional contractility depends on extracellular mechanical properties,” *J. Biomech.*, vol. 48, no. 12, pp. 3044–3051, Sep. 2015.
- [93] J. S. Choi, Y. Piao, and T. S. Seo, “Circumferential alignment of vascular smooth muscle cells in a circular microfluidic channel,” *Biomaterials*, vol. 35, no. 1, pp. 63–70, Jan. 2014.
- [94] A. Tijore, J. M. Behr, S. A. Irvine, V. Baisane, and S. Venkatraman, “Bioprinted gelatin hydrogel platform promotes smooth muscle cell contractile phenotype

References

- maintenance,” *Biomed. Microdevices*, vol. 20, no. 2, pp. 1–10, Jun. 2018.
- [95] P. Lacolley, V. Regnault, P. Segers, and S. Laurent, “Vascular smooth muscle cells and arterial stiffening: Relevance in development, aging, and disease,” *Physiol. Rev.*, vol. 97, no. 4, pp. 1555–1617, Oct. 2017.
- [96] S. Itai, H. Tajima, and H. Onoe, “Double-layer perfusable collagen microtube device for heterogeneous cell culture,” *Biofabrication*, vol. 11, no. 1, 2019.
- [97] S. Itai and H. Onoe, “Flexibly Deformable Collagen Hydrogel Tube Reproducing Immunological Tissue Deformation of Blood Vessels as a Pharmacokinetic Testing Model,” *Adv. Healthc. Mater.*, p. 2101509, Nov. 2021.
- [98] K. Adamiak and A. Sionkowska, “Current methods of collagen cross-linking: Review,” *Int. J. Biol. Macromol.*, vol. 161, pp. 550–560, Oct. 2020.
- [99] D. J. S. Hulmes, “Collagen diversity, synthesis and assembly,” *Collagen Struct. Mech.*, pp. 15–47, 2008.
- [100] A. Sionkowska, S. Skrzyński, K. Śmiechowski, and A. Kołodziejczak, “The review of versatile application of collagen,” *Polym. Adv. Technol.*, vol. 28, no. 1, pp. 4–9, Jan. 2017.
- [101] B. Jiang, Y. Liu, B. Bhandari, and W. Zhou, “Impact of Caramelization on the Glass Transition Temperature of Several Caramelized Sugars. Part I: Chemical Analyses,” *J. Agric. Food Chem.*, vol. 56, no. 13, pp. 5137–5147, Jul. 2008.
- [102] D. Bouř, G. A. P. Hospers, C. Meijer, G. Molema, and N. H. Mulder, “Endothelium in vitro: A review of human vascular endothelial cell lines for blood vessel-related research,” *Angiogenesis*, vol. 4, no. 2, pp. 91–102, 2001.
- [103] N. A. Rahman *et al.*, “Immortalized endothelial cell lines for in vitro blood–brain barrier models: A systematic review,” *Brain Res.*, vol. 1642, pp. 532–545, Jul. 2016.
- [104] Y. Cao *et al.*, “The use of human umbilical vein endothelial cells (HUVECs) as an in vitro model to assess the toxicity of nanoparticles to endothelium: a review,” *J. Appl. Toxicol.*, vol. 37, no. 12, pp. 1359–1369, Dec. 2017.
- [105] D. Ribatti, B. Nico, and E. Crivellato, “The role of pericytes in angiogenesis,” *Int. J. Dev. Biol.*, vol. 55, no. 3, pp. 261–268, Jun. 2011.

- [106] D. Virgintino *et al.*, “An intimate interplay between precocious, migrating pericytes and endothelial cells governs human fetal brain angiogenesis,” *Angiogenesis*, vol. 10, pp. 35–45, 2007.
- [107] L. C. D. Smyth *et al.*, “Unique and shared inflammatory profiles of human brain endothelia and pericytes,” *J. Neuroinflammation*, vol. 15, no. 1, pp. 1–18, May 2018.
- [108] S. E. Sanders, J. L. Madara, D. K. McGuirk, D. S. Gelman, and S. P. Colgan, “(PDF) Assessment of inflammatory events in epithelial permeability: A rapid screening method using fluorescein dextrans.” [Online]. Available: https://www.researchgate.net/publication/14636320_Assessment_of_inflammatory_events_in_epithelial_permeability_A_rapid_screening_method_using_fluorescein_dextrans. [Accessed: 26-Dec-2021].
- [109] D. Günzel and A. S. L. Yu, “Claudins and the modulation of tight junction permeability,” *Physiol. Rev.*, vol. 93, no. 2, pp. 525–569, 2013.
- [110] V. H. Huxley, F. E. Curry, and R. H. Adamson, “Quantitative fluorescence microscopy on single capillaries: alpha-lactalbumin transport,” *Am. J. Physiol. Circ. Physiol.*, vol. 252, no. 1, pp. H188–H197, 1987.
- [111] A. C. Burton, “Relation of Structure to Function of the Tissues of the Wall of Blood Vessels,” *Physiol. Rev.*, vol. 34, no. 4, pp. 619–642, Oct. 1954.
- [112] T. Takeda, Y. Yamashita, S. Shimazaki, and Y. Mitsui, “Histamine decreases the permeability of an endothelial cell monolayer by stimulating cyclic AMP production through the H₂-receptor,” *J. Cell Sci.*, vol. 101, no. 4, pp. 745–750, 1992.
- [113] E. B. Thangam *et al.*, “The Role of Histamine and Histamine Receptors in Mast Cell-Mediated Allergy and Inflammation: The Hunt for New Therapeutic Targets,” *Front. Immunol.*, vol. 9, Aug. 2018.
- [114] M. Shahid, T. Tripathi, F. Sobia, S. Moin, M. Siddiqui, and R. A. Khan, “Histamine, histamine receptors, and their role in immunomodulation: An updated systematic review,” *Open Immunol. J.*, vol. 2, no. 1, pp. 9–41, 2009.
- [115] K. Ohmori *et al.*, “Pharmacological, Pharmacokinetic and Clinical Properties of

References

- Olopatadine Hydrochloride, a New Antiallergic Drug,” *Jpn. J. Pharmacol.*, vol. 88, no. 4, pp. 379–397, 2002.
- [116] E. O. Meltzer *et al.*, “Safety and efficacy of olopatadine hydrochloride nasal spray for the treatment of seasonal allergic rhinitis,” *Ann. Allergy, Asthma Immunol.*, vol. 95, no. 6, pp. 600–606, Dec. 2005.
- [117] F. M. White, *FLUID MECHANICS*. McGraw-Hill Higher Education, 2010.
- [118] R. P. Franke, G. M. H. Schnittler, D. Seiffge, and C. Mittermayer, “Induction of human vascular endothelial stress fibres by fluid shear stress,” *Nature*, vol. 307, no. 16, pp. 648–649, 1984.
- [119] H. Onoe, M. Kato-negishi, A. Itou, and S. Takeuchi, “Differentiation Induction of Mouse Neural Stem Cells in Hydrogel Tubular Microenvironments with Controlled Tube Dimensions,” *Adv. Healthc. Mater.*, vol. 5, no. 9, pp. 1104–1111, 2016.
- [120] T. Hayashi *et al.*, “Endothelial cellular senescence is inhibited by nitric oxide: Implications in atherosclerosis associated with menopause and diabetes,” 2006.
- [121] H. M. Finlay, J. G. Dixon, and P. B. Canham, “Fabric Organization of the Subendothelium of the Human Brain Artery by Polarized-Light Microscopy.”
- [122] E. G. Nabel and E. Braunwald, “A Tale of Coronary Artery Disease and Myocardial Infarction,” *N. Engl. J. Med.*, vol. 366, no. 1, pp. 54–63, Jan. 2012.
- [123] L. Pantoni, “Cerebral small vessel disease: from pathogenesis and clinical characteristics to therapeutic challenges,” *Lancet Neurol.*, vol. 9, no. 7, pp. 689–701, Jul. 2010.
- [124] A. M. Handorf, Y. Zhou, M. A. Halanski, and W.-J. Li, “Tissue Stiffness Dictates Development, Homeostasis, and Disease Progression,” *Organogenesis*, vol. 11, no. 1, pp. 1–15, Jan. 2015.
- [125] M. C. Murphy *et al.*, “Decreased brain stiffness in Alzheimer’s disease determined by magnetic resonance elastography,” *J. Magn. Reson. Imaging*, vol. 34, no. 3, pp. 494–498, Sep. 2011.
- [126] M. C. Lampi and C. A. Reinhart-King, “Targeting extracellular matrix stiffness to attenuate disease: From molecular mechanisms to clinical trials,” *Sci. Transl. Med.*,

vol. 10, no. 422, p. eaao0475, Jan. 2018.

- [127] J. M. Spergel and A. S. Paller, “Atopic dermatitis and the atopic march,” *J. Allergy Clin. Immunol.*, vol. 112, no. SUPPL. 6, pp. 118–127, 2003.
- [128] D. Y. M. Leung *et al.*, “New insights into atopic dermatitis Find the latest version : Science in medicine New insights into atopic dermatitis,” *J Clin Invest.*, vol. 113, no. 7, pp. 651–657, 2004.

Appendix A License numbers

Figure number	License number
Figure 1.2	Permission is not required.
Figure 1.3	Permission is not required.
Figure 1.4	Permission is not required.
Figure 1.5(a)	Permission is not required.
Figure 1.5(b)	5186991043080
Figure 1.5(c)	Permission is not required.
Figure 1.5(d)	Permission is not required.
Figure 1.5(e)	Permission is not required.
Figure 1.6(a)	5187030000262
Figure 1.6(b)	5182521070080
Figure 1.6(c)	5187120093770
Figure 1.6(d)	5187111053308
Figure 1.7(a)	5187140266058
Figure 1.7(b)	5187140404114
Figure 1.7(c)	5215761279759
Figure 1.7(d)	5215810791834
Figure 1.8(a)	1161534-1
Figure 1.8(b)	5187530446381
Figure 1.9(a)	5182520297405
Figure 1.9(b)	5182511416354

Appendix B Antibody list

Section 2.3.1 (Figure 2.8)

	Primary antibody	Secondary antibody	Other
CD31	Anti-CD31 antibody (Mouse monoclonal)	Goat anti-Mouse IgG Antibody (Alexa fluor 488)	
Nuclei			DAPI

Section 3.2.3 (Figure 3.5)

	Primary antibody	Secondary antibody	Other
CD31	Anti-CD31 antibody (Mouse monoclonal)	Goat anti-Mouse IgG Antibody (Alexa fluor 488)	

Section 4.3.1 (Figure 4.12)

	Primary antibody	Secondary antibody	Other
Actin of SMCs			Live-cell actin probe (SPY 555)
HUVECs			GFP-transfected
Elastin	Anti-Elastin antibody (Rabbit polyclonal)	Goat anti-Rabbit IgG Antibody (Alexa fluor 647)	

関連著作リスト

1. 定期刊行誌掲載論文（主論文に関連する原著論文）

- (1) Itai, S. and Onoe, H., “Flexibly deformable collagen hydrogel tube reproducing immunological tissue deformation of blood vessels as a pharmacokinetic testing model”, *Advanced Healthcare Materials*, Vol. 11, No. 1 (9 pages) (2021).
- (2) Itai, S., Tajima, H., and Onoe, H., “Double-layer perfusable collagen microtube device for heterogeneous cell culture”, *Biofabrication*, Vol.11, 015010 (12 pages) (2019).

2. 定期刊行誌掲載論文（その他の論文）

- (1) Ando, M., Tsuchiya, M., Itai, S., Murayama, T., Kurashina, Y., Heo, Y., Onoe, H., “Janus Hydrogel Microbeads for Glucose Sensing with pH Calibration”, *Sensors*, Vol. 21, 4829 (10 pages) (2021)
- (2) Imashiro, C., Azuma, T., Itai, S., Kuribara, T., Totani, K., Onoe, H., and Takemura, K., “Travelling ultrasound promotes vasculogenesis of three-dimensional-monocultured human umbilical vein endothelial cells, *Biotechnology and Bioengineering*”, Vol. 118, No. 10, pp. 3760-3769 (2021)
- (3) Itai, S., Suzuki, K., Kurashina, Y., Kimura, H., Amemiya, T., Sato, K., Nakamura, M., and Onoe, H., “Cell-encapsulated chitosan-collagen hydrogel hybrid nerve guidance conduit for peripheral nerve regeneration”, *Biomedical Microdevices*, Vol.22, 81 (9 pages) (2020).
- (4) Shimizu, A., Goh, W., Itai, S., Hashimoto, M., Miura, S., and Onoe, H., “ECM-based microchannel for culturing in vitro vascular tissues with simultaneous perfusion and stretch”, *Lab on a chip*, Vol.20, No.11, pp.1917-1927 (2020).
- (5) Shimizu, A., Goh, W., Itai, S., Karyappa, R., Hashimoto, M., and Onoe, H., “ECM-based microfluidic gradient generator for tunable surface environment by interstitial flow”, *Biomicrofluidics*, Vol.14, 044106 (8 pages) (2020).

3. 国際会議論文（査読付きの full-length papers）

- (1) Itai, S.* and Onoe, H., “In vitro artery model with circumferentially aligned & contractible smooth muscle by unfixed molding & screwing fabrication”, *The 35th International Conference on Micro Electro Mechanical Systems (MEMS 2022, Tokyo)*, pp. 275-278 (2022).
- (2) Kawahara, M., Itai, S., and Onoe, H., “Tube-shaped in-vitro intestinal gut model with 3D isotropic medium supply for bacterial symbiosis”, *The 35th International Conference on Micro Electro Mechanical Systems (MEMS 2022, Tokyo)*, pp. 321-324 (2022).
- (3) Masuda, A., Fukada, K., Itai, S., Kurashina, Y., Akizuki, S., Tohyama, S., Fujita, J., and Onoe, H., “Fixation-free evaluation of cardiac contractile force by human iPSC-derived cardiac core-shell microfiber”, *The 35th International Conference on Micro Electro Mechanical Systems (MEMS 2022, Tokyo)*, pp. 172-175 (2022).
- (4) Itai, S.* and Onoe, H., “Endothelial chemical reaction and drug test reproduced on molded flexible collagen hydrogel tube”, *The 21st International Conference on Solid-State Sensors, Actuators and Microsystems (Transducers 2021, Online)*, pp. 283-286 (2021).
- (5) Inami, A., Iyama, E., Itai, S., and Onoe, H., “Wireless and battery-free digestible sensor for

intestinal bacteria monitoring”, The 24th International Conference on Miniaturized Systems for Chemistry and Life Sciences (MicorTAS 2020, Online), pp. 575-576 (2020).

- (6) Itai, S., Suzuki, K., Kurashina, Y., Kimura, H., Amemiya, T., Sato, K., Nakamura, M., and Onoe, H., “Cell-encapsulating chitosan-collagen hybrid hydrogel conduit for peripheral nerve regeneration”, The 23rd International Conference on Miniaturized Systems for Chemistry and Life Sciences (MicorTAS 2019, Basel), pp. 880-881 (2019).
- (7) Shimizu, A., Goh, W., Itai, S., Hashimoto, M., Miura, S., and Onoe, H., “Stretching motion-driven ECM-based pulsatile flow generator for mimicking venous blood flow in vivo”, The 23rd International Conference on Miniaturized Systems for Chemistry and Life Sciences (MicorTAS 2019, Basel), pp. 314-315 (2019).
- (8) Itai, S.* and Onoe, H., “Thin layered heterogeneous vascularized 3D tissue models constructed with separated-layer collagen microtube”, The 32nd International Conference on Micro Electro Mechanical Systems (MEMS 2019, Seoul), pp. 118-119 (2019).
- (9) Itai, S. and Onoe, H., “Double-layer collagen microtube for perfusable heterogeneous culture”, The 21st International Conference on Miniaturized Systems for Chemistry and Life Sciences (MicorTAS 2017, Georgia), pp.1137-1138, (2017).

4. 国際会議発表

- (1) Itai, S. and Onoe, H., “Perfusable double-layer collagen microtube for vascularized heterogeneous culture”, International Symposium on SSS Laser Processing (3S-LP, Yokohama, 2019), P-18.
- (2) Itai, S. and Onoe, H., “Multi-layer polymer gel tube for heterogeneous perfusion culture”, Keio University International Symposium on Advanced Technologies for Mechano-biology and Regenerative Medicine, (Yokohama, 2018), B07.
- (3) Itai, S. and Onoe, H., “Double-layer perfusable collagen microtube for heterogeneous cell culture”, International conference on BioSensors, BioElectronics, BioMedical Devices, BioMEMS/NEMS & Application, (Bio4Apps, Tokyo, 2017), Poster-14
- (4) Itai, S. and Onoe, H., “Fabrication of collagen-silicone hybrid microtube by sacrificial etching of carbohydrate film”, International Symposium on Micro-Nano Science and Technology 2016, (MNST2016, Tokyo, 2016), SaP-24.

5. 国内講演会発表

- (1) 板井駿*, 尾上弘晃, “自在に変形可能なコラーゲンゲルチューブを用いた血管組織の化学応答および薬剤反応再現”, 第 60 回日本生体医工学会大会 (日本生体医工学会, オンライン, 2021), O2-8-3-2.
- (2) 板井駿(招待講演)*, “灌流共培養可能な多層コラーゲンマイクロチューブを用いた *in vitro* 血管化組織構築”, 第 19 回日本再生医療学会総会, (日本再生医療学会, 横浜, 2020), SY-33-2
- (3) 板井駿*, 尾上弘晃, “コラーゲンゲルチューブを用いた血管内皮細胞の化学応答再現”, 第 11 回マイクロ・ナノ工学シンポジウム, (日本機械学会, オンライン, 2020), 28A3-MN3-9

- (4) 板井駿*, 鈴木果林, 倉科佑太, 木村洋朗, 雨宮剛, 佐藤和毅, 中村雅也, 尾上弘晃, “キトサン-コラーゲンゲルチューブを用いた軸索伸長誘導”, 日本機械学会 2019 年度年次大会, (日本機械学会, 秋田, 2019), J02801
- (5) 板井駿, 尾上弘晃, “分岐血管組織の構築のための多連結コラーゲンチューブ”, 第 10 回マイクロ・ナノ工学シンポジウム, (日本機械学会, 浜松, 2019), 19am3-PN3-29
- (6) 稲見文香, 井山瑛里加, 板井駿, 尾上弘晃, “生分解性材料を用いた有機電気デバイス”, 第 10 回マイクロ・ナノ工学シンポジウム, (日本機械学会, 浜松, 2019), 19am3-PN3-39
- (7) 板井駿, 鈴木果林, 倉科佑太, 木村洋朗, 雨宮剛, 佐藤和毅, 中村雅也, 尾上弘晃, “末梢神経再生のためのキトサン-コラーゲンゲルチューブ”, 第 58 回日本生体医工学会大会, (日本生体医工学会, 沖縄, 2019), OS-029 (BMS-19-017)
- (8) 板井駿*, 尾上弘晃, “共培養のための多段モールド製法による多層ゲルチューブの構築”, 日本機械学会 2018 年度年次大会, (日本機械学会, 大阪, 2018), J0220103
- (9) 板井駿, 尾上弘晃, “多段モールド製法による灌流共培養のための多層ゲルチューブ”, 化学とマイクロ・ナノシステム学会第 38 回研究会 (38th CHEMINAS), (化学とマイクロ・ナノシステム学会, 札幌, 2018), 1P05
- (10) 鈴木果林, 板井駿, 倉科佑太, 木村洋朗, 雨宮剛, 佐藤和毅, 中村雅也, 尾上弘晃, “キトサンハイドロゲルによるチューブ形状 3 次元培養デバイス”, 第 9 回マイクロ・ナノ工学シンポジウム, (日本機械学会, 札幌, 2018), 30am3-PN-49
- (11) 板井駿, 尾上弘晃, “酸性コラーゲン送液による 2 層コラーゲンマイクロチューブデバイス”, ロボティクス・メカトロニクス講演会-2017, (日本機械学会, 福島, 2017), 2A1-G01
- (12) 板井駿, 尾上弘晃, “異種細胞灌流共培養のための 2 層コラーゲンチューブデバイス”, 第 34 回「センサ・マイクロマシンと応用システム」シンポジウム, (日本電気学会, 広島, 2017), 01pm4-PS-190

6. その他

- (1) 受賞 令和 3 年度 日本生体医工学会 Young Investigator's Award 最優秀賞
- (2) 受賞 平成 30 年度 化学とマイクロ・ナノシステム学会 優秀講演賞
- (3) 受賞 平成 30 年度 日本機械学会 若手優秀講演フェロー賞
- (4) 受賞 平成 29 年度 電気学会センサ・マイクロマシン部門 優秀ポスター賞
- (5) 受賞 平成 29 年度 サイボウニクス研究会 優秀研究・オーディエンス賞